POLITECNICO DI MILANO

Facoltà di Ingegneria Industriale

Corso di Laurea in

Ingegneria Spaziale

Artificial Equilibrium Points in the Circular Restricted Three Body Problem

Relatore: Prof. Michèle Lavagna

Tesi di Laurea di:

Emanuele Piersanti Matr. 682534

Anno Accademico 2010 – 2011

“Concern for man and his fate must always form the chief interest of all technical endeavors.
Never forget this in the midst of your diagrams and equations.”
ALBERT EINSTEIN

Contents

Figure Index

Symbols and Acronyms

The most useful symbols and acronyms are here reported.

AEP	Artificial Equilibrium Point
AEPs	Artificial Equilibrium Points
CRTBP	Circular Restricted Three Body Problem
DC	Differential Corrector
NEP	Natural Equilibrium Point
TBP	Three Body Problem
x, y, z	Point coordinates in the synodic frame
$\mathbf{A}$	State space matrix of linearized system (synodic frame)
a_x, a_y, a_z	Control acceleration
$\delta_x, \delta_y, \delta_z$	Small perturbation around equilibrium point
$\boldsymbol{L_1, L_2, L_3, L_4, L_5}$	Lagrangian Libration points
Ω	Angular velocity of the synodic reference frame
$\mathbf{r}$	Position vector (synodic reference frame)
T	Orbital period of the synodic reference frame
$\mathbf{U(r)}$	Gravitational and centrifugal potential

Sommario

L'astrodinamica è lo studio del moto nello spazio di oggetti costruiti dall'uomo, soggetti a forze naturali o indotte artificialmente.
In astrodinamica il moto di un corpo non influenzato da forze aggiuntive, come quelle di un motore, è governato dall'accelerazione gravitazionale dovuta alle altre masse. Svariati modelli possono essere utilizzati per determinare le traiettorie del corpo, in tutti i casi le equazioni del moto che compaiono sono non lineari e l'unico modello che ammette soluzione in forma chiusa è il modello dei 2 corpi. Dal momento che il modello dei tre copri non può essere risolto analiticamente è conveniente semplificarlo per poterne comprendere , almeno in parte, il comportamento.

Nel problema dei tre corpi ristretto (CRTPB) ci sono cinque punti di "librazione", chiamati punti Lagrangiani. Un oggetto massivo posto in uno di questi punti si trova in equilibrio sotto l'azione della forza gravitazionale delle due masse primarie e dell'accelerazione centrifuga del sistema di riferimento sinodico.
Negli ultimi trent'anni la comunità scientifica ha sviluppato un crescente interesse per lo studio di missioni che possano avvantaggiarsi dell'impiego di posizioni di equilibrio naturali, ma è solo a partire dal decennio scorso che si è prospettata la possibilità di avviare missioni attorno a punti di equilibrio artificiali (AEPs).
Con l'aiuto di un controllo continuo, quale la propulsione a bassa (per esempio propulsione elettrica/ vele solari), è possibile manipolare le equazioni di moto così da generare punti di equilibrio artificiali laddove risulterebbero vantaggiosi.

Tra tutti i punti di equilibrio artificiali così ottenuti, alcuni consentono un moto marginalmente stabile, inoltre pochi di questi punti permettono un moto periodico. Per quei punti che non consentono questo tipo di moto è possibile modificare l'accelerazione di controllo in modo tale che si possano comunque ottenere orbite periodiche.
Il presente lavoro affronta il problema dell' identificazione di punti di equilibrio artificiali sia per via analitica che numerica, attraverso l'impiego di un controllo a spinta continua o variabile nel tempo. È stato altresì sviluppato uno strumento software per la ricerca dei punti artificiali, che

consentono moto stabile e periodico. Un ampio confronto tra modellazione analitica e approccio numerico ha permesso di evidenziare i limiti di validità dei modelli impiegati. I risultati ottenuti vengono presentati su una rosa di possibili scenari di missioni ritenuti interessanti.

Parole chiave: Punti di equilibrio artificiali (AEPs), Problema dei tre corpi, Orbite periodiche attorno a punti di librazione, bassa spinta.

Abstract

Astrodynamics is the study of the motion of man-made objects in space, subject to both natural and artificially induced forces.
In astrodynamics the motion of a body that is not influenced by additional forces, such as a thruster, is governed by the gravitational acceleration due to other masses. Several models can be used to determine the trajectories of the body, in all cases the equations of motion which appear are nonlinear and the only model that admits closed form solution is the two-body problem. Since the three body problem cannot be solved analytically, suitable simplifications are made in order to understand, at least in part, the behavior.

In the circular restricted three-body problem (CRTBP) there are five libration point, called *Lagrangian Points*. A massive object placed in one of these points is in equilibrium under the action of gravitational force of the two primary masses and the centrifugal acceleration of the synodic reference system. In the last thirty years the scientific community has developed a growing interest in the study of missions that can take advantage of the use of natural equilibrium points, but is only since last decade that the possibility of missions around artificial equilibrium points (AEP) has been proposed.
With the aid of a continuous control, such as low thrust propulsion (e.g. electric propulsion/solar sail), it's possible to manipulate the equations of motion in order to generate artificial equilibrium points where it would be advantageous.
Among all the AEPs thus obtained, some allow a marginally stable motion, furthermore few of these points permit periodic motion. For those points that don't allow this type of motion it's possible to modify the control acceleration so that periodic orbits can be achieved anyway.
The present work addresses the problem of identification of artificial equilibrium points both analytically and numerically through the use of a constant or variable thrust over time. It has also developed a software tool for detecting AEP, allowing stable periodic motion. A broad comparison between analytical modeling and numerical approach could highlight the limits of validity of models used. The results are presented on a range of missions scenarios deemed interesting .

Keywords: Artificial equilibrium points (AEPs), Three body problem, Periodic orbits around libration points, low thrust.

1 Introduction and motivations

Astrodynamics is the study of the motion of man-made objects in space, subject to both natural and artificially induced forces. In order to understand the behavior of such objects, analytical models are made. The models have a tendency to be simple if possible, in order to get some insight of more complex problem. Analytical models are generally more difficult to develop than numerical techniques, but they often lead to a better understanding of the problem. Anyway numerical simulations are necessary when real world mission are designed because the presence of perturbations substantially modify the analytical prediction.

In the last decade, thanks to the advent of low thrust propulsion, some interest on the possibility of generating artificial equilibrium points in the CRTBP was born. With the aid of a continuous thrust it's possible to manipulate the equations of motion in order to generate artificial equilibrium points where it would be advantageous. In this way a wide range of new missions could be considered.

The present work addresses the problem of identification of artificial equilibrium points both analytically and numerically through the use of a constant or variable control acceleration. Deep analysis on variable acceleration is carried on.

Since this new field is developing, it was deemed interesting study in deep, focusing on issue such as variable control acceleration, comparison between analytical models and numerical approach in order to highlight the limits of validity of the model used.
The main objective is to expand the available analytical models and to determine what are the limits, establishing whether it is possible to create real world missions.

2 State of the Art

2.1 Scientific research

In astrodynamics the model used for studying either spacecraft or natural body motion, is the restricted N+1 body problem, where N celestial bodies move under the influence of one another and the object under study moves in the field of these bodies, but its mass is considered negligible with respect to the primary bodies.
The two body problem is perhaps the simplest, integrable problem in astrodynamics. It concerns the interaction of two point masses moving under a mutual gravitational attraction described by Newton's universal law of gravitation. While the two body problem admits analytical solutions, just considering three body, makes the problem analytically unsolvable.
Simplification can help to shed more light on the problem and the behavior of motion can be understood with simple analysis.
The main simplification is the Restricted Three Body Problem in which the mass of the third body is considered small with respect to the mass of the two primaries, and starting on this, in order to get closer to more realistic situations or further simplifications, this model is modified in different ways, for example the Circular RTBP assume that the two primaries are moving with constant angular velocity, while the elliptic RTBP is a non-autonomous time-periodic perturbation in which the primaries move in an elliptic orbit instead of circular ones. The Bicircular Restricted Problem is one of the simplest restricted problem for four bodies.

Thanks to the pioneering work of Poincarè on chaos theory and through the development of dynamic systems theory, this branch of celestial mechanics has grown dramatically, and in the last few decades many works on the possibility to construct low energy transfer exploiting the three body problem were presented by Lo, M.W. and Ross (1), recent studies (2) reveled the existence of an Interplanetary Transport Network that allow spacecraft and other small bodies like comets to travel in the solar system with no costs in term of $\triangle V$.

2.1.1 Circular Restricted Three Body Problem

Generally the Circular Restricted Three Body Problem is considered since it's a simple model and can help to better understand solar system dynamics. The formal analysis will be presented in §3, in this section only the hypothesis and general motion possibility will be presented.

The main simplification of this model are:

- The primary and secondary bodies move in circular coplanar orbits about the center of mass, which lies between the two objects.
- The mass of the third body is negligible compared to that of major bodies.

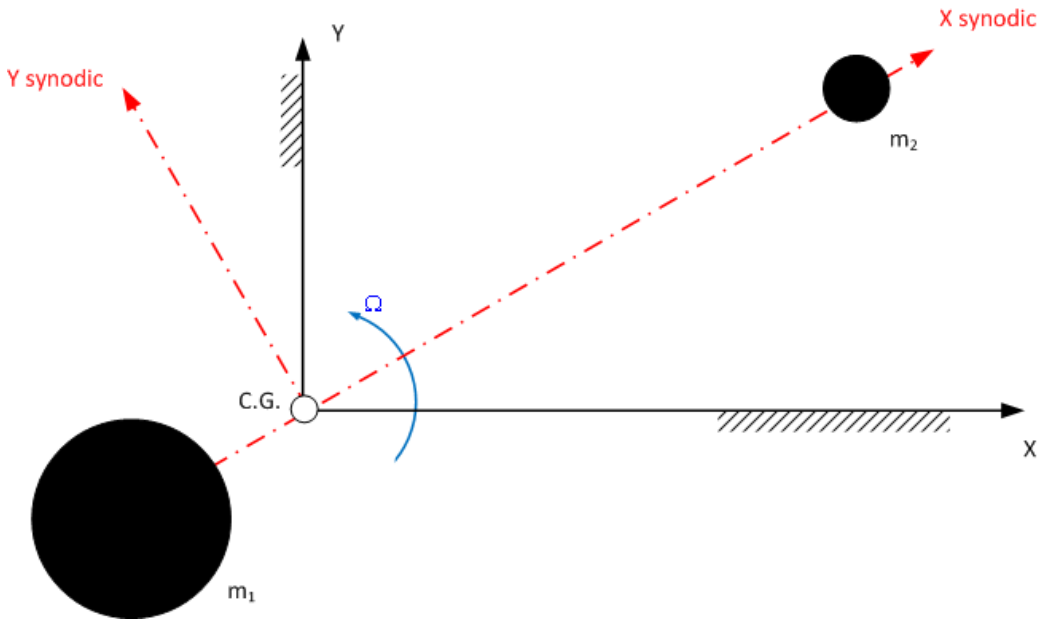

Figure 2.1 Synodic reference frame

In the case where the two primary masses move in circular orbits about their common centre of mass, their positions are stationary in a frame rotating with a constant angular velocity equal to the mean motion, this frame is called synodic (figure 2.1).
The main advantage of considering the three body problem is that is possible to satisfy mission constraints such as minimization of fuel in a better way rather than using the two body problem, furthermore some

missions that are unfeasible when analyzed with the two body model are feasible with the three body model.

In the CRTBP there is only one integral of motion, the Jacobi integral. Clearly it cannot provide an exact solution for the orbital motion but can be used to determine regions from which the particle is excluded.
The Jacobi integral is:

$$v^2 = \Omega^2\left(x^2 + y^2\right) + \frac{2\mu_1}{r_1} + \frac{2\mu_2}{r_2} + 2C_j$$

It can be interpreted as the total energy of secondary particle relative to the rotating frame. For a given value of Jacobi integral the curve of constant velocity can be determined. These curve place bounds on the motion of the particle. Since the velocity cannot be complex it turns out that

$$\Omega^2\left(x^2 + y^2\right) + \frac{2\mu_1}{r_1} + \frac{2\mu_2}{r_2} \geq 2C_j$$

Thus the zero velocity curve define the regions where the particle motion is not allowed.
Figure 2.2 shows the surface of Jacobi constant and figure 2.3 show that there are five cases of Hill's region:

- Case 1: The particle cannot move between the realms round the two primary masses (Figure 2.3a).
- Case 2: The energy is above the "neck" connecting the realms, so the particle can move between them (Figure 2.3b).
- Case 3: Both the "necks" are opened, so the particle can move close to the two primary masses or in the exterior region (Figure 2.3c).
- Case 4: In this case the particle can pass directly from the vicinity of the large primary and escape in the outer region (Figure 2.3d and e).
- Case 5: The energy level is so high that the forbidden region disappears, the particle is free to move in all the x-y space.

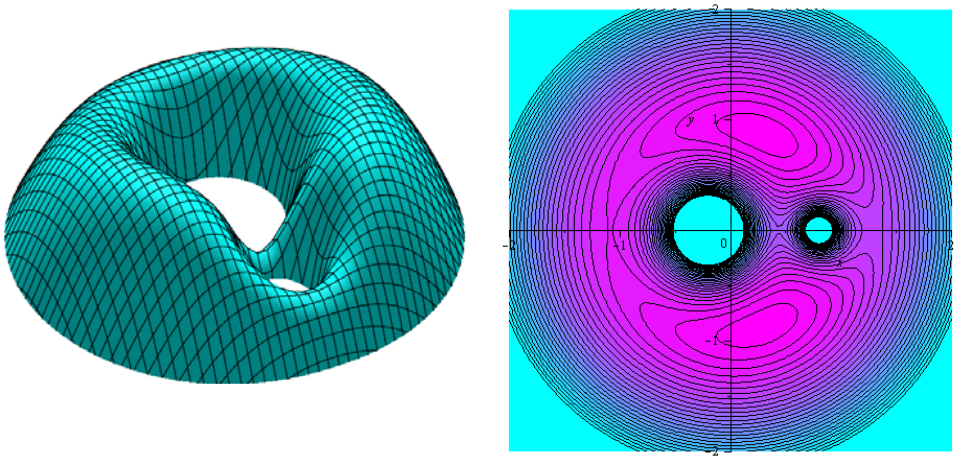

Figure 2.2 Surface and Contour of Jacobi integral (μ_1 = 0.9)

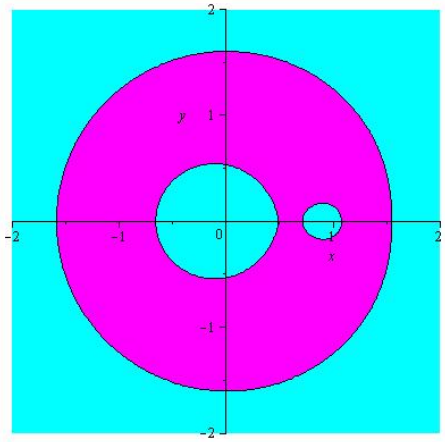

a

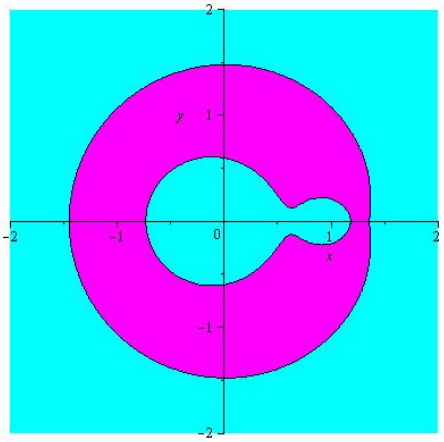

b

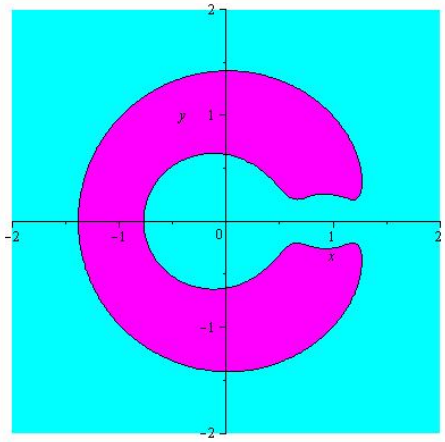

c

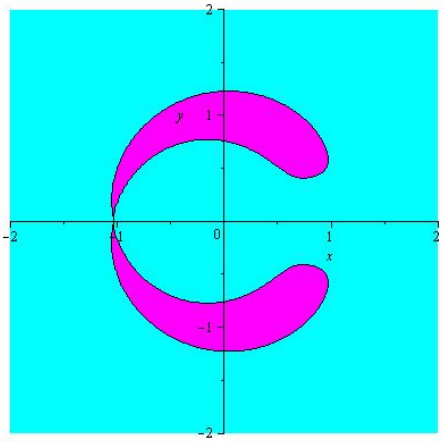

d

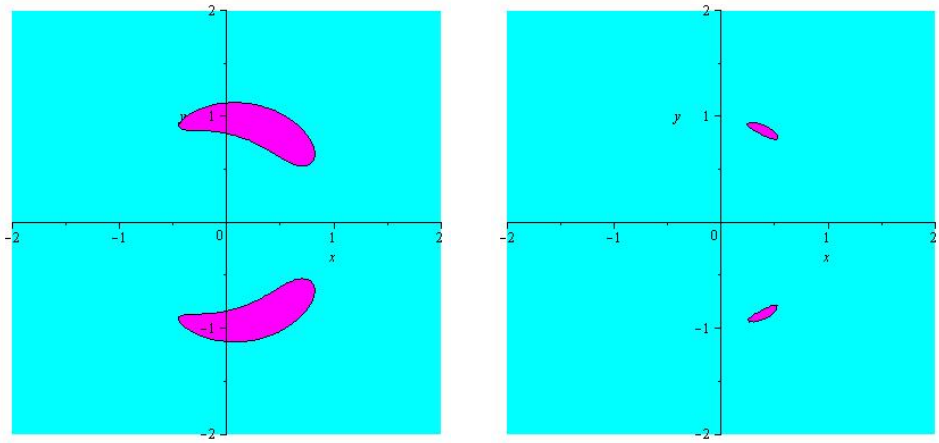

e f

Figure 2.3 Forbidden regions C = -1.8, -1.758, -1.7,-1.55,-1.458 (μ_1 = 0.9)

In 1772, J.L. Lagrange showed that there are five natural equilibrium points in the CRTBP where the combined gravitational pull of two primary is in equilibrium with the centrifugal force required to rotate with them (figure 2.4). Three of these "libration points" or Lagrangian points, are on the axis joining the primaries (collinear Lagrange points), the other two are on the vertices of equilateral triangles joining the primaries (equilateral Lagrange points). All the five point lie in the orbit plane of the two primary bodies. While the collinear points are unstable, the equilateral points are marginally stable, this implies that some form of "station keeping" is needed to maintain a spacecraft near a libration point.

Although the L_1,L_2 and L_3 points are nominally unstable, it's possible to find stable periodic orbit around this point, at least in the RTBP. These perfectly periodic orbit, referred as "halo orbits" do not exist in the full n-body problem, but quasi-periodic Lissajous orbits are possible.

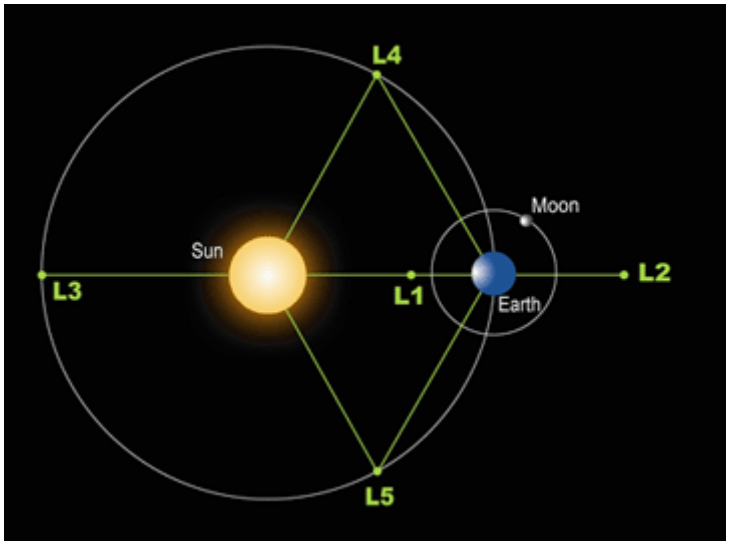

Figure 2.4 Lagrange points in the Sun-Earth system

Around libration points three main different type of orbits are possible: first, Lyapunov orbits, are curved paths that lie entirely in the plane of the two primary bodies; second, Lissajous orbits, have components in the plane and also out of plane; third, halo orbits, present not only, motion in and out of plane, but also they are periodic, while Lissajous orbits are not. It's to be noted that all these types of orbits are not centered on a focus.

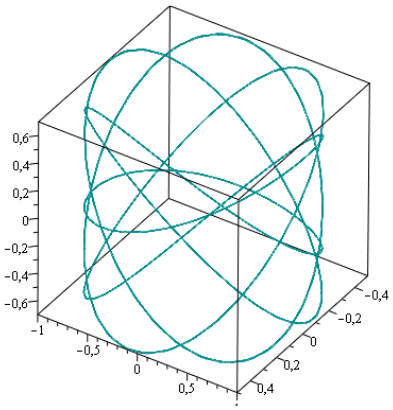

Figure 2.5 Lissajous orbit

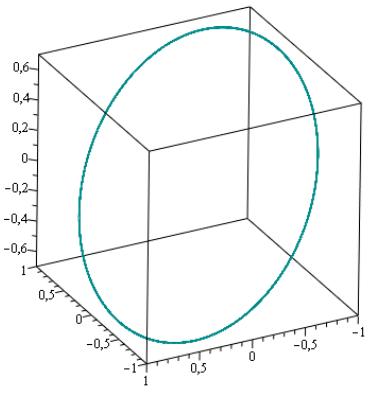

Figure 2.6 Halo orbit

Classical “halo orbits” near libration points have been extensively studied both analytically and numerically. For example Howell (3), makes a large numerical study on families of three-dimensional, periodic, halo orbits, Richardson (4) investigate an analytical solution for periodic motion of halo orbit about the collinear points, Farquhar (5) study primarily the possibility of satellite station-keeping near collinear libration points L_1 and L_2. In the last 10 years, some interest as grown around the possibility to generate “halo orbits” around Artificial Equilibrium Points (AEP). Those points can be generated if continuous acceleration is available from a low-thrust propulsion system, such solar sail or electric propulsion. Only with the advent of low-thrust engine it became possible to consider missions that previously weren’t feasible.

The acceleration given by one of these propulsion system cancels the residual acceleration at the AEP, so that a static equilibrium point can be generated. McInees (6) investigated artificial equilibrium points in three dimensional space for Sun-Earth and Earth-Moon systems using solar sails, with the limitation that the acceleration must be in the direction away from the sun. M. Morimoto (7) found AEP in the CRTBP fro solar electric low thrust propulsion system. He also found resonant periodic orbits with a constant, continuous acceleration at linear order around marginally stable AEP (8). McInnes (9) extended the analysis of low thrust periodic orbit at nonlinear order using the Lindsted Poincarè method about unstable AEPs. It is apparent that till now, few are the theoretical studies on the topic, this prevalently because, as previously stated, is only since ten years that theory on AEP was developed.

2.2 Missions

The libration points in the Earth-Moon system were known by the early pioneers of space flight, but the first who proposed a mission in one of those points was Arthur C. Clark. Clark suggested that L_2 would be an ideal site to broadcast radio signals to colonies on the back side of the Moon. But at L_2 a spacecraft would be invisible from the Earth. In 1966 Farquhar (5) proposed a Lissajous path around L_2 in order to allow Earth visibility most of the time.
There are several reasons because libration points are deemed interesting:

- Libration points in the Sun-Earth or Earth-Moon system are easy and inexpensive to reach from Earth.
- Sun-Earth L_1 provide good observation sites of the Sun.
- For missions with heat sensitive instruments, orbits near Sun-Earth L_2 provide great thermal stability, suitable for highly precise visible light telescopes.
- Earth-Moon L_2 can be used to establish a permanent communications link between Earth and the hidden side of the Moon.

The first mission designed to make use of a libration point was the International Sun-Earth Explorer spacecraft (ISEE-3). The ISEE-3 would be located on halo orbit near L1 to monitor the solar wind before it reach the magnetosphere and the other two spacecraft ISEE-1/2 that were on highly elliptical Earth orbit.

For 18 years after ISEE-3 launch, there were no further libration point missions. But in the six year period after December 1995, five libration point missions were successfully launched and operated.
Interest in the scientific advantages of the Lagrange points for space mission continued to increase and many more mission were designed to operate near this points. Table 1 lists past, present missions and proposed future missions.

Table 2.1 Past, Present and Future missions

Missions	Sun-Earth Lib. Point.	Orbit Insertion	Formation Flying	Mission Purpose
ISEE-3 (NASA)	L_1	1978	yes	Solar wind, cosmic rays, plasma studies
SOHO (ESA/NASA)	L_1	1996	no	Solar observatory
ACE (NASA)	L_1	1997	no	Solar wind, energetic particles
WIND (NASA)	L_1	1995	no	Solar-wind monitor
MAP (NASA)	L_2	2001	no	Cosmic microwave background
Genesis (NASA)	L_1	2001	no	Solar wind composition
STEREO (NASA)	L_4/L_5	2006	Yes	Solar Observatory
Herschel (ESA)	L_2	2007	no	Far infrared telescope
Planck (ESA)	L_2	2007	no	Cosmic microwave background
NGST (NASA)	L_2	2014	no	Deep space observatory
GAIA (ESA)	L_2	2012	no	Galactic structure, Astrometry
Constellation-X (NASA)	L_2	2017	no	X-ray astronomy
TPF (NASA)	L_2	n/a	no	Detection of distant planets
DARWIN (ESA)	L_2	n/a	yes	Detection of Earth-like planets

2.3 Objective of the work

Since this branch of astrodynamics is in development, it was deemed interesting to delve into the topic. In chapter 3 the analytical model is presented and the generation of AEP by means of constant and variable thrust is addressed. In chapter 4 a broad comparison between analytical and numerical solution is used in order to show the main limits of the model. In chapter 5 regions where stable AEPs can be generated are shown, furthermore a with the initial data obtained from the analytical model, a more realistic numeric analysis is carried on with STK. In chapter 6 a range of mission scenarios deemed interesting are exposed. Lastly chapter 7 presents conclusions and future developments.

3 Artificial Equilibrium Points

In this chapter equations of motion for the CRTBP in the presence of a control acceleration are derived, after which the conditions necessary to generate stable AEPs with constant thrust are discussed. Also the conditions needed to generate periodic orbit about these points are exposed. Nondimensional analysis of the problem is presented. Furthermore an analytical treatment of variable control acceleration is exposed. Lastly numerical approach to solve variable control acceleration problem is exposed, and some results are shown.

3.1 Equations of motion

A particle of negligible mass moves under the gravitational influence of two primaries, the two masses are assumed to have circular, coplanar orbits about their common center of mass. Those assumptions can easily model planetary dynamics in our solar systems, and also moons motion around their primary planet.
The primaries affect the small particle dynamics even if the converse is not true.

To write the equations of motion of the so-called CRTBP, a non-inertial rotating frame (synodic) of reference xyz whose origin lies at the center of mass of the tow body system, with the x axis directed towards m_2 as shown in Fig.1 is adopted, angular velocity of the frame is constant. The equations of motion for the CRTBP can be found in many references such as Murray and Dermott (10)

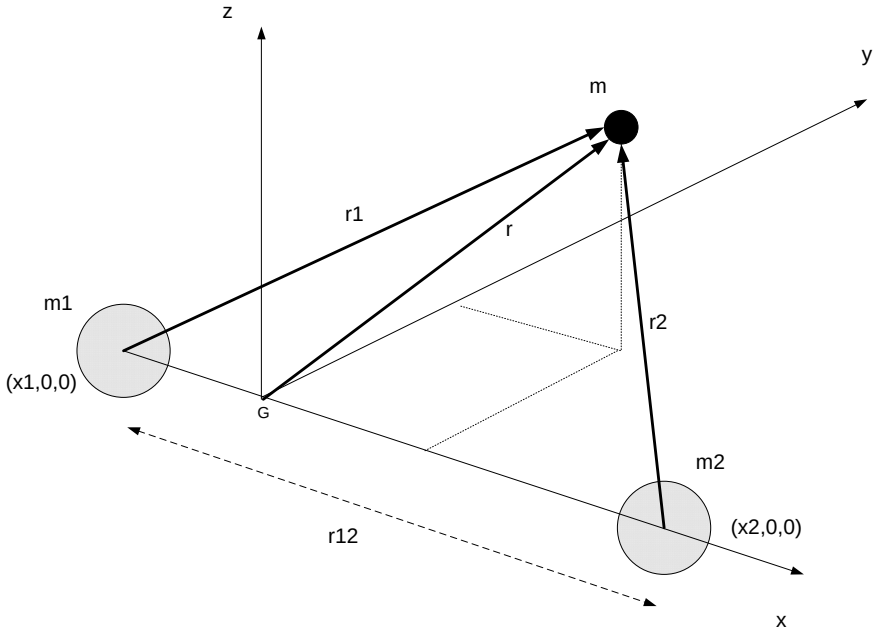

Figure 3.1 Primary bodies m_1 and m_2 in circular orbit around each other and third bodies m_3

In this frame m_1 and m_2 appear at rest. The constant inertial angular velocity is given by:

$$\mathbf{\Omega} = \omega \hat{\mathbf{k}}$$

where

$$\omega = \frac{2\pi}{T}$$

And T is the orbital period of the orbit of m_2 around m_1.

$$T = 2\pi \sqrt{\frac{r_{12}^{\ 3}}{\mu}}$$

Calling *M* the total mass of the two body system, we can write the gravitational parameter as

$$\mu = MG$$

Since

$x_1 m_1 + x_2 m_2 = 0$

$x_2 = x_1 + r_{12}$

Solving for x_1, x_2

$$x_1 = -\frac{m_2}{m_1 + m_2} r_{12}$$

$$x_2 = \frac{m_1}{m_1 + m_2} r_{12}$$

r_1, r_2 can be rewritten as:

$$r_1^2 = (x - x_1)^2 + y^2 + z^2 = (x + \Pi_2 r_{12})^2 + y^2 + z^2$$

$$r_2^2 = (x - x_2)^2 + y^2 + z^2 = (x - \Pi_1 r_{12})^2 + y^2 + z^2$$

with

$$\mathbf{r} = x\hat{\mathbf{i}} + y\hat{\mathbf{j}} + z\hat{\mathbf{k}}$$

$$\Pi_1 = \frac{m_1}{m_1 + m_2}$$

$$\Pi_2 = \frac{m_2}{m_1 + m_2}$$

The equation of motion of the small particle described in the synodic reference frame is then expressed as

$$\frac{d^2\mathbf{r}}{dt^2} + 2\boldsymbol{\Omega} \times \frac{d\mathbf{r}}{dt} + \boldsymbol{\Omega} \times (\boldsymbol{\Omega} \times \mathbf{r}) = \mathbf{a} - \nabla \mathbf{U}(\mathbf{r})^*$$

Where **a** is the control acceleration, and the potential term is

$$\nabla U(\mathbf{r})^* = -\left(\frac{\mu_1}{r_1} + \frac{\mu_2}{r_2} \right)$$

the cetrifugal term can be rewritten as

$$\nabla \boldsymbol{\Phi} = \boldsymbol{\Omega} \times (\boldsymbol{\Omega} \times \mathbf{r}) \qquad \boldsymbol{\Phi} = -\frac{1}{2} \left| \boldsymbol{\Omega} \times \mathbf{r} \right|^2 = -\frac{1}{2} \omega^2 \left(x^2 + y^2 \right)$$

$$\boxed{\frac{d^2\mathbf{r}}{dt^2} + 2\boldsymbol{\Omega} \times \frac{d\mathbf{r}}{dt} + \nabla \mathbf{U}(\mathbf{r}) - \mathbf{a} = 0} \qquad (3.1)$$

with

$$\nabla \mathbf{U}(\mathbf{r}) = \nabla \mathbf{U}(\mathbf{r})^* + \boldsymbol{\Phi}(\mathbf{r})$$

Eq. 1.1 is now expanded:

$$\begin{cases} \ddot{x} - 2\omega\dot{y} - \omega^2 x = a_x - \dfrac{\mu_1\left(x+\Pi_2 r_{12}\right)}{\left(x^2+y^2+z^2+2xr_{12}\Pi_2+\Pi_2^2 r_{12}^2\right)^{3/2}} + \\ \qquad\qquad - \dfrac{\mu_2\left(x-\Pi_1 r_{12}\right)}{\left(x^2+y^2+z^2-2xr_{12}\Pi_1+\Pi_1^2 r_{12}^2\right)^{3/2}} \\ \ddot{y} + 2\omega\dot{x} - \omega^2 y = a_y - \dfrac{\mu_1 y}{\left(x^2+y^2+z^2+2xr_{12}\Pi_2+\Pi_2^2 r_{12}^2\right)^{3/2}} + \\ \qquad\qquad - \dfrac{\mu_2 y}{\left(x^2+y^2+z^2-2xr_{12}\Pi_1+\Pi_1^2 r_{12}^2\right)^{3/2}} \\ \ddot{z} = a_z - \dfrac{\mu_1 z}{\left(x^2+y^2+z^2+2xr_{12}\Pi_2+\Pi_2^2 r_{12}^2\right)^{3/2}} - \dfrac{\mu_2 z}{\left(x^2+y^2+z^2-2xr_{12}\Pi_1+\Pi_1^2 r_{12}^2\right)^{3/2}} \end{cases} \tag{3.2}$$

These are the equations of motion for the CRTBP.

3.2 Artificial Equilibrium points: constant thrust

Given the acceleration history, System 3.2 can be solved numerically in order to obtain the trajectory of the third body in the synodic frame. In this way **a** can be considered the control parameter and the unknowns of the problem are position (x, y, z) and velocity $(\dot{x}, \dot{y}, \dot{z})$ of the particle. As can be seen, the equations are coupled by the dependence of the gravitational term $\left(\frac{1}{r_1^3}, \frac{1}{r_2^3}\right)$ since it is function of the distance. Furthermore in plane motion is also coupled by the Corioli term $(2\omega\dot{y}, 2\omega\dot{x})$ and the centrifugal term $(\omega^2 x, \omega^2 y)$.
Now, since these equations are nonlinear but are autonomous (the time is not included explicitly), it's possible to look for equilibrium points.

Equilibrium points in the synodic frame are obtained by nulling the derivative elements in the Eq. 3.1:

$$\nabla \mathbf{U}(\mathbf{r}_0) - \mathbf{a}_0 = 0 \tag{3.3}$$

The former equation includes the unknown artificial acceleration profile $\mathbf{a}_0$, this is the constant value of acceleration that must be applied at some point to turn it in an artificial equilibrium point. From now on, $\mathbf{r}_0$ will indicate a generic AEP where a constant acceleration $\mathbf{a}_0$ is applied.
Expanded in three equations reads:

$$a_{0x} = \frac{\mu_1(x+\Pi_2 r_{12})}{r_1^3} + \frac{\mu_2(x-\Pi_1 r_{12})}{r_1^3} - \omega^2 x$$
$$a_{0y} = \frac{\mu_1 y}{r_1^3} + \frac{\mu_2 y}{r_1^3} - \omega^2 y \qquad (3.4)$$
$$a_{0z} = \frac{\mu_1 z}{r_1^3} + \frac{\mu_2 z}{r_1^3}$$

In this way a non-equilibrium point $\mathbf{r_0}$ is changed in an artificial equilibrium point with an artificial acceleration profile to be defined. If **a** is set to **0** then the canonical equations of CRTBP are found. The formalism adopted till now can be found in Curtis (11) or in Morimoto (8).

3.2.1 Stability

Stability can be investigated in various way, in the present work stability is searched in a local sense, so the motion about equilibrium point in presence of small disturbance is examined, thus linearization about equilibrium point is carried on. In order to study global stability, Lyapunov second theorem could be used.
To determine whether an artificial equilibrium point is locally stable the equations of motion are linearized.
Defining $\boldsymbol{\delta}$ as a small disturbance of the equilibrium position and using the following relation

$$\mathbf{r} = \mathbf{r_0} + \boldsymbol{\delta}$$

the equations 3.1, once linearized are

$$\frac{d^2\boldsymbol{\delta}}{dt^2} + 2\boldsymbol{\Omega} \times \frac{d\boldsymbol{\delta}}{dt} + \nabla \mathbf{U}(\mathbf{r_0}) + \left[\frac{\partial}{\partial \mathbf{r}} \nabla \mathbf{U}(\mathbf{r})\right]\Big|_{\mathbf{r_0}} \boldsymbol{\delta} - \mathbf{a}(\mathbf{r_0}) - \left[\frac{\partial}{\partial \mathbf{r}} \mathbf{a}(\mathbf{r})\right]\Big|_{\mathbf{r_0}} \boldsymbol{\delta} = 0 \qquad (3.5)$$

The important assumption, later removed in §3.4, of constant artificial acceleration in time is here selected*.
This assumption is formally written as

$$\left[\frac{\partial}{\partial \mathbf{r}} \mathbf{a}(\mathbf{r})\right]\Big|_{\mathbf{r_0}} = 0$$

And the equation, considering 3.3, can be rewritten as

* The acceleration is assumed constant in magnitude and direction in the synodic reference frame.

$$\frac{d^2\boldsymbol{\delta}}{dt^2}+2\boldsymbol{\Omega}\times\frac{d\boldsymbol{\delta}}{dt}+\left[\frac{\partial}{\partial\mathbf{r}}\nabla\mathbf{U}(\mathbf{r})\right]_{\mathbf{r}_0}\boldsymbol{\delta}=0$$

To find if an AEP is stable, an eigenvalues analysis is carried on.

First of all $\left[\frac{\partial}{\partial\mathbf{r}}\nabla\mathbf{U}(\mathbf{r})\right]_{\mathbf{r}_0}$ can be expressed as:

$$\begin{bmatrix} U_{xx} & U_{xy} & U_{xz} \\ U_{yx} & U_{yy} & U_{yz} \\ U_{zx} & U_{zy} & U_{zz} \end{bmatrix}_{r_0}$$

with

$$U_x=\frac{\mu_1(x+\Pi_2 r_{12})}{r_1^3}+\frac{\mu_2(x-\Pi_1 r_{12})}{r_2^3}-\omega^2 x$$

$$U_y=\frac{\mu_1 y}{r_1^3}+\frac{\mu_2 y}{r_2^3}-\omega^2 y$$

$$U_z=\frac{\mu_1 z}{r_1^3}+\frac{\mu_2 z}{r_2^3}$$

So the derivative are:

$$U_{xx}=-\frac{3\mu_1(x+\Pi_2 r_{12})^2}{r_1^5}+\frac{\mu_1}{r_1^3}-\frac{3\mu_2(x-\Pi_1 r_{12})^2}{r_2^5}+\frac{\mu_2}{r_2^3}-\omega^2$$

$$U_{yy}=-\frac{3\mu_1 y^2}{r_1^5}+\frac{\mu_1}{r_1^3}-\frac{3\mu_2 y^2}{r_2^5}+\frac{\mu_2}{r_2^3}-\omega^2$$

$$U_{zz}=-\frac{3\mu_1 z^2}{r_1^5}+\frac{\mu_1}{r_1^3}-\frac{3\mu_2 z^2}{r_2^5}+\frac{\mu_2}{r_2^3}$$

$$U_{xy}=U_{yx}=-\frac{3\mu_1(x+\Pi_2 r_{12})y}{r_1^5}-\frac{3\mu_2(x-\Pi_1 r_{12})y}{r_2^5}$$

$$U_{xz}=U_{zx}=-\frac{3\mu_1(x+\Pi_2 r_{12})z}{r_1^5}-\frac{3\mu_2(x-\Pi_1 r_{12})z}{r_2^5}$$

$$U_{yz}=U_{zy}=-\frac{3\mu_1 yz}{r_1^5}-\frac{3\mu_2 yz}{r_2^5}$$

In matrix form, the equations are

$$\frac{d^2}{dt^2}\begin{bmatrix}\delta_x\\ \delta_y\\ \delta_z\end{bmatrix}+\frac{d}{dt}\begin{bmatrix}-2\delta_y\\ 2\delta_x\\ 0\end{bmatrix}\omega+\begin{bmatrix}U_{xx} & U_{yx} & U_{xz}\\ U_{yx} & U_{yy} & U_{yz}\\ U_{zx} & U_{zy} & U_{zz}\end{bmatrix}\begin{bmatrix}\delta_x\\ \delta_y\\ \delta_z\end{bmatrix}=0 \tag{3.6}$$

This second order system can be tuned into two first order systems making use of the state space.

$$\begin{bmatrix}\dot{\delta}_x\\ \dot{\delta}_y\\ \dot{\delta}_z\\ \ddot{\delta}_x\\ \ddot{\delta}_y\\ \ddot{\delta}_z\end{bmatrix}=\begin{bmatrix}0 & 0 & 0 & 1 & 0 & 0\\ 0 & 0 & 0 & 0 & 1 & 0\\ 0 & 0 & 0 & 0 & 0 & 1\\ -U_{xx} & -U_{xy} & -U_{xz} & 0 & 2\omega & 0\\ -U_{yx} & -U_{yy} & -U_{yz} & -2\omega & 0 & 0\\ -U_{zx} & -U_{yz} & -U_{zz} & 0 & 0 & 0\end{bmatrix}\begin{bmatrix}\delta_x\\ \delta_y\\ \delta_z\\ \dot{\delta}_x\\ \dot{\delta}_y\\ \dot{\delta}_z\end{bmatrix} \tag{3.7}$$

Or in compact form

$\dot{\boldsymbol{\delta}} = \mathbf{A}\boldsymbol{\delta}$

The analysis of stability is reduced in this way to study the eigenvalues of the **A** matrix.

3.2.2 Analytical solution

Since, as previously told, local stability is investigated, is necessary to analyze the eigenvalues of the linearized system, bearing in mind that, as mentioned in dynamical system theory (12), if a fixed point like sink, source or saddle are found in the linearized system, they will be respectively sink, source and saddle also in the non linear system. But if a center, a star or a degenerate node is found, probably non linear system will behave differently; for example a center will probably be a spiral.

If there are real eigenvalues, the spacecraft will experience damping or divergence.
If there are purely imaginary eigenvalues, is possible to found initial conditions such that the motion is periodic.

$$\boldsymbol{\delta}=\sum_{n=1}^{6}\mathbf{C}_n e^{\sigma_n t}e^{\pm i\omega_n}=\sum_{n=1}^{6}\mathbf{C}_n e^{\sigma_n t}\left(\cos(\omega_n t)\pm i\sin(\omega_n t)\right) \tag{3.8}$$

Therefore, if at least one purely imaginary solution is part of the characteristic equation of the solution, oscillatory motions exists, defined by the initial value that sets the divergence term to zero.

$$\sigma_n = 0 \qquad n = 1..6$$

Using expansion theorem, the solution is of the form:

$$\begin{bmatrix} \delta_x \\ \delta_y \\ \delta_z \\ \dot{\delta}_x \\ \dot{\delta}_y \\ \dot{\delta}_z \end{bmatrix} = \mathbf{V} \begin{bmatrix} K_1 e^{\lambda_1 t} \\ K_2 e^{\lambda_2 t} \\ K_3 e^{\lambda_3 t} \\ K_4 e^{\lambda_4 t} \\ K_5 e^{\lambda_5 t} \\ K_6 e^{\lambda_6 t} \end{bmatrix}$$

where **V** is the right eigenvector of matrix **A**, λ_j are the eigenvalues and K_j are constants.

As soon as the initial conditions are fixed, the six constants are easily quantified.

3.2.3 Periodic motion

The search for periodic orbits could be interesting from the point of view of mission design, since a satellite in an orbit of this type could be used in various way, obviously a periodic orbits is better than a complex chaotic orbit.

Expressing the solution of 3.6 with divergence term set to 0:

$$\delta_x = A_1 \cos(\omega_1 t) + A_2 \sin(\omega_1 t) + A_3 \cos(\omega_2 t) + A_4 \sin(\omega_2 t) + A_5 \cos(\omega_3 t) + A_6 \sin(\omega_3 t)$$
$$\delta_y = B_1 \cos(\omega_1 t) + B_2 \sin(\omega_1 t) + B_3 \cos(\omega_2 t) + B_4 \sin(\omega_2 t) + B_5 \cos(\omega_3 t) + B_6 \sin(\omega_3 t)$$
$$\delta_z = C_1 \cos(\omega_1 t) + C_2 \sin(\omega_1 t) + C_3 \cos(\omega_2 t) + C_4 \sin(\omega_2 t) + C_5 \cos(\omega_3 t) + C_6 \sin(\omega_3 t)$$

where

$$\lambda_j = -\lambda_{j+1} = i\omega_j \quad j = 1,3,5$$

Whenever frequencies of either (δ_x, δ_y), (δ_x, δ_z) or (δ_z, δ_y) slightly differ, the projection of the trajectory on the x-y, x-z, y-z plane become Lissajous

curves (13). If frequencies are the same or in simple integer ratio, then the particle will achieves a periodic orbit.
It's pointed out that the constants are not independent, this is easily seen:

$$\delta_x = \sum_i A_i e^{\lambda_i t} \quad \dot{\delta}_x = \sum_i A_i \lambda_i e^{\lambda_i t}$$
$$\delta_y = \sum_i B_i e^{\lambda_i t} \quad \dot{\delta}_y = \sum_i B_i \lambda_i e^{\lambda_i t}$$
$$\delta_z = \sum_i C_i e^{\lambda_i t} \quad \dot{\delta}_z = \sum_i C_i \lambda_i e^{\lambda_i t}$$

It's possible to set the constants to turn the oscillatory* motion of the particle in a periodic orbit; by fixing the initial position, the initial velocity to gain a periodic motion can be identified; similarly, whenever the problem fixes the initial velocity, the right position in space to ensure a periodic motion can be obtained. By forcing those constants which associated frequencies aren't in integer ratio to be 0, and for example, taking the case of *x:z* periodic orbit (the same procedure can be used for *y:z*), let's assume that ω_1 is in simple integer ratio with ω_3, forcing the following constants to be 0

$$A_i = 0 \quad i = 3..6$$
$$B_i = 0 \quad i = 3..6$$
$$C_i = 0 \quad i = 1..4$$

The desired solution can be expressed as†

$$\delta_x = A_1 \cos\omega_1 t + A_2 \sin\omega_1 t$$
$$\delta_y = B_1 \cos\omega_1 t + B_2 \sin\omega_1 t$$
$$\delta_z = C_5 \cos\omega_3 t + C_6 \sin\omega_3 t$$

---

* Oscillatory motion alone is not enough to obtain periodic motion, since as said, if the frequencies aren't in integer ratio, the trajectory in three dimensional space won't be closed.

† If the frequencies in simple integer ratio were ω_2 and ω_3 ,then the desired equations would have been:

$$\delta_x = A_3 \cos(\omega_2 t) + A_4 \sin(\omega_2 t)$$
$$\delta_y = B_3 \cos(\omega_2 t) + B_4 \sin(\omega_2 t)$$
$$\delta_z = C_5 \cos(\omega_3 t) + C_6 \sin(\omega_3 t)$$

By substituting expression for $\delta_x, \delta_y, \delta_z$ in one of the first two equations of 3.6 the following relationship are obtained:

$$(U_{xx} - \omega_1^2)A_1 - 2B_2\omega_1\Omega + U_{xy}B_1 + U_{xz}C_5 = 0$$
$$(U_{yy} - \omega_1^2)B_1 + 2A_2\omega_1\Omega + U_{xy}A_1 + U_{yz}C_5 = 0$$

Noting that

$$\left.\begin{aligned} A_1 &= \delta_{x0} \\ B_1 &= \delta_{y0} \\ C_5 &= \delta_{z0} \end{aligned}\right\} \Rightarrow \begin{aligned} A_2 &= -\frac{(U_{yy} - \omega_1^2)\delta_{y0} + U_{zy}\delta_{z0} + U_{xy}\delta_{x0}}{2\omega_1\Omega} \\ B_2 &= \frac{(U_{xx} - \omega_1^2)\delta_{x0} + U_{xz}\delta_{z0} + U_{xy}\delta_{y0}}{2\omega_1\Omega} \end{aligned}$$

Expanding the solution in term of eigenvector, the relationship between constants A_i, B_i, C_i and K_i are obtained from:

$$\begin{bmatrix} V_{11}K_1 + V_{12}K_2 = A_1 \\ i(V_{11}K_1 - V_{12}K_2) = A_2 \\ V_{13}K_3 + V_{14}K_4 = A_3 \\ i(V_{13}K_3 - V_{14}K_4) = A_4 \\ V_{15}K_5 + V_{16}K_6 = A_5 \\ i(V_{15}K_5 - V_{16}K_6) = A_6 \end{bmatrix} \quad \begin{bmatrix} V_{21}K_1 + V_{22}K_2 = B_1 \\ i(V_{21}K_1 - V_{22}K_2) = B_2 \\ V_{23}K_3 + V_{24}K_4 = B_3 \\ i(V_{23}K_3 - V_{24}K_4) = B_4 \\ V_{25}K_5 + V_{26}K_6 = B_5 \\ i(V_{25}K_5 - V_{26}K_6) = B_6 \end{bmatrix} \quad \begin{bmatrix} V_{31}K_1 + V_{32}K_2 = C_1 \\ i(V_{31}K_1 - V_{32}K_2) = C_2 \\ V_{33}K_3 + V_{34}K_4 = C_3 \\ i(V_{33}K_3 - V_{34}K_4) = C_4 \\ V_{35}K_5 + V_{36}K_6 = C_5 \\ i(V_{35}K_5 - V_{36}K_6) = C_6 \end{bmatrix}$$

Constant C_6 is still to be determined, but that constant can be forced to be 0 so that the initial velocity in the z direction is 0. This can be done since the system that must be solved is overdetermined. In some cases can be useful to set the initial velocity in z direction equal to some specified value, for example if the transfer orbit brings the spacecraft at the injection point of the halo orbit with some fixed value. For the same reason all the procedure can be modified so as to have initial velocity fixed.

The previous system is made of 18 equations in six unknown (K_i), this system is solved with the least square method.

Define

$$\boldsymbol{\delta}_0 = \{A_1 \quad \cdots \quad A_6 \quad B_1 \quad \cdots \quad B_6 \quad C_1 \quad \cdots \quad C_6\}^T$$

$$\mathbf{K} = \{K_1 \quad \cdots \quad K_6\}^T$$

So the system can be rewritten in the following way:

$$\mathbf{UK} = \boldsymbol{\delta}_0$$

by defining

$$\boldsymbol{\varepsilon} = \boldsymbol{\delta}_0 - \mathbf{UK}$$

And seeking the value of K that minimizes the error

$$E = \boldsymbol{\varepsilon}^T \boldsymbol{\varepsilon}$$

a compact expression can be written

$$\mathbf{K} = \left(\mathbf{U}^T\mathbf{U}\right)^{-1}\mathbf{U}^T\boldsymbol{\delta}_0$$

The solution of this system gives the looked for six **K** constants .
Afterwards, that the initial conditions vector can be found by

$$\boldsymbol{\delta}_0 = \mathbf{VK}$$

3.2.4 Discussion

Till now, all the procedure is strongly constrained by the first assumption of constant thrust, as can be seen in all this work, with such a control, the only thing that can be done is to turn a generic point into an AEP, but nor stability nor periodicity are influenced.

3.3 Nondimensional problem

Because of the great difference in magnitude of most values in the problem, nondimensional problem should be formalized. The great advantage of this approach is that a more easy analytical treatment is possible and the elements of the **A** matrix (3.6) of the state space have the same order of magnitude.

Computing an eigenvector when there are eigenvalues “very close” can be an ill-conditioned procedure (14), an index of this ill-conditiong is

$$\kappa = \frac{1}{\min_{j \neq k} \left| \lambda_k - \lambda_j \right|}$$

Higher κ correspond to ill-conditioned process.
For example in the dimensional case of Sun-Earth problem, the linearization about L_1 bring to the following **A** matrix:

$$A=\begin{bmatrix} 0 & 0 & 0 & 1 & 0 & 0 \\ 0 & 0 & 0 & 0 & 1 & 0 \\ 0 & 0 & 0 & 0 & 0 & 1 \\ 3.6158\cdot 10^{-13} & 0 & 0 & 0 & 3.982\cdot 10^{-7} & 0 \\ 0 & -1.2133\cdot 10^{-13} & 0 & -3.982\cdot 10^{-7} & 0 & 0 \\ 0 & 0 & -1.6097\cdot 10^{-13} & 0 & 0 & 0 \end{bmatrix}$$

At first sight it's apparent that any computation made with this matrix where the terms have so different magnitude, will be subject to computational errors. In this case particular case turns out to be

$\kappa = 7.0499\cdot 10^{7}$

Whereas if nondimensional units are adopted the state matrix is:

$$A=\begin{bmatrix} 0 & 0 & 0 & 1 & 0 & 0 \\ 0 & 0 & 0 & 0 & 1 & 0 \\ 0 & 0 & 0 & 0 & 0 & 1 \\ 9.1216 & 0 & 0 & 0 & 2 & 0 \\ 0 & -3.068 & 0 & -2 & 0 & 0 \\ 0 & 0 & -4.0608 & 0 & 0 & 0 \end{bmatrix}$$

And

$\kappa = 14.0362$

Clearly the nondimensionalization has increased the separation between the eigenvalues.

In order to nondimensionalize equations of motion, let's divide the spatial coordinate with respect to the distance between the two primaries (figure 3.1 is reported below for convenience)

$$\bar{x}=\frac{x}{r_{12}} \quad \bar{y}=\frac{y}{r_{12}} \quad \bar{z}=\frac{z}{r_{12}}$$

Also let the gravitational parameter, and thus the masses be nondimensianlaized as:

$$\bar{\mu}_1=\frac{\mu_1}{\mu} \quad \bar{\mu}_2=\frac{\mu_2}{\mu}$$

with

$\mu = G(m_1 + m_2)$

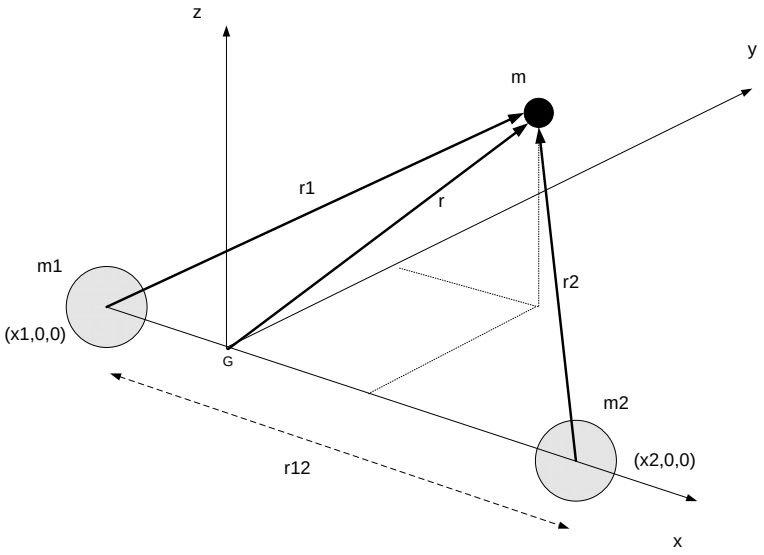

Figure 3.1 Primary bodies m_1 and m_2 in circular orbit around each other and third bodies m_3

Lastly setting the nondimensional time to be:

$$\bar{t} = 2\pi \frac{t}{T}$$

where

$$T = \frac{2\pi}{\sqrt{\mu}} r_{12}^{\frac{3}{2}}$$

It is found that the nondimensional mean motion must be 1.

$$\bar{\omega} = \omega \frac{T}{2\pi} = 1$$

Calculating the derivative

$$\frac{dx}{dt} = \frac{d(\bar{x} r_{12})}{d\bar{t}} \frac{d\bar{t}}{dt} = 2\pi \frac{r_{12}}{T} \frac{d\bar{x}}{d\bar{t}}$$

$$\frac{d^2x}{dt^2} = \frac{d}{dt}\frac{dx}{dt} = \frac{d}{dt}\left(2\pi \frac{r_{12}}{T}\frac{d\bar{x}}{d\bar{t}}\right) = \frac{d}{d\bar{t}}\left(2\pi \frac{r_{12}}{T}\frac{d\bar{x}}{d\bar{t}}\right)\frac{d\bar{t}}{dt} = 4\pi^2 \frac{r_{12}}{T^2}\frac{d^2\bar{x}}{d\bar{t}^2}$$

The exploitation of the former into the equations of motion (3.2) leads to:

$$
\begin{cases}
4\pi^2\left(\ddot{\bar{x}}\dfrac{r_{12}}{T^2}-2\dfrac{\bar{\omega}}{T}\dfrac{r_{12}}{T}\dot{\bar{y}}-\bar{x}\dfrac{\bar{\omega}^2}{T^2}r_{12}\right)=a_x-\dfrac{\bar{\mu}_1\mu\left(\bar{x}r_{12}+\Pi_2 r_{12}\right)}{\left(\bar{x}^2{r_{12}}^2+\bar{y}^2{r_{12}}^2+\bar{z}^2{r_{12}}^2+2\bar{x}{r_{12}}^2\Pi_2+{\Pi_2}^2{r_{12}}^2\right)^{3/2}} \\
\qquad\qquad -\dfrac{\bar{\mu}_2\mu\left(\bar{x}r_{12}-\Pi_1 r_{12}\right)}{\left(\bar{x}^2{r_{12}}^2+\bar{y}^2{r_{12}}^2+\bar{z}^2{r_{12}}^2-2\bar{x}{r_{12}}^2\Pi_1+{\Pi_1}^2{r_{12}}^2\right)^{3/2}} \\
4\pi^2\left(\ddot{\bar{y}}\dfrac{r_{12}}{T^2}+2\dfrac{\bar{\omega}}{T}\dfrac{r_{12}}{T}\dot{\bar{x}}-\bar{y}\dfrac{\bar{\omega}^2}{T^2}r_{12}\right)=a_y-\dfrac{\mu\bar{\mu}_1\bar{y}r_{12}}{\left(\bar{x}^2{r_{12}}^2+\bar{y}^2{r_{12}}^2+\bar{z}^2{r_{12}}^2+2\bar{x}{r_{12}}^2\Pi_2+{\Pi_2}^2{r_{12}}^2\right)^{3/2}} \\
\qquad\qquad -\dfrac{\mu\bar{\mu}_2\bar{y}r_{12}}{\left(\bar{x}^2{r_{12}}^2+\bar{y}^2{r_{12}}^2+\bar{z}^2{r_{12}}^2-2\bar{x}{r_{12}}^2\Pi_1+{\Pi_1}^2{r_{12}}^2\right)^{3/2}} \\
4\pi^2\dfrac{r_{12}}{T^2}\ddot{\bar{z}}=a_z-\dfrac{\mu\bar{\mu}_1\bar{z}r_{12}}{\left(\bar{x}^2{r_{12}}^2+\bar{y}^2{r_{12}}^2+\bar{z}^2{r_{12}}^2+2\bar{x}{r_{12}}^2\Pi_2+{\Pi_2}^2{r_{12}}^2\right)^{3/2}} \\
\qquad\qquad -\dfrac{\mu\bar{\mu}_2\bar{z}r_{12}}{\left(\bar{x}^2{r_{12}}^2+\bar{y}^2{r_{12}}^2+\bar{z}^2{r_{12}}^2-2\bar{x}{r_{12}}^2\Pi_1+{\Pi_1}^2{r_{12}}^2\right)^{3/2}}
\end{cases}
$$

Rearranging, introducing acceleration term and using $\bar{\omega}=1$

$$
\begin{cases}
\ddot{\bar{x}}-2\dot{\bar{y}}-\bar{x}=a_x\dfrac{T^2}{4\pi^2 r_{12}}-\dfrac{\bar{\mu}_1\left(\bar{x}+\Pi_2\right)}{\left(\bar{x}^2+\bar{y}^2+\bar{z}^2+2\bar{x}\Pi_2+{\Pi_2}^2\right)^{3/2}}\dfrac{\mu T^2}{4\pi^2{r_{12}}^3} \\
\qquad\qquad -\dfrac{\bar{\mu}_2\left(\bar{x}-\Pi_1\right)}{\left(\bar{x}^2+\bar{y}^2+\bar{z}^2-2\bar{x}\Pi_1+{\Pi_1}^2\right)^{3/2}}\dfrac{\mu T^2}{4\pi^2{r_{12}}^3} \\
\ddot{\bar{y}}+2\dot{\bar{x}}-\bar{y}=a_y\dfrac{T^2}{4\pi^2 r_{12}}-\dfrac{\bar{\mu}_1\bar{y}}{\left(\bar{x}^2+\bar{y}^2+\bar{z}^2+2\bar{x}\Pi_2+{\Pi_2}^2\right)^{3/2}}\dfrac{\mu T^2}{4\pi^2{r_{12}}^3} \\
\qquad\qquad -\dfrac{\bar{\mu}_2\bar{y}}{\left(\bar{x}^2+\bar{y}^2+\bar{z}^2-2\bar{x}\Pi_1+{\Pi_1}^2\right)^{3/2}}\dfrac{\mu T^2}{4\pi^2{r_{12}}^3} \\
\ddot{\bar{z}}=a_z\dfrac{T^2}{4\pi^2 r_{12}}-\dfrac{\bar{\mu}_1\bar{z}}{\left(\bar{x}^2+\bar{y}^2+\bar{z}^2+2\bar{x}\Pi_2+{\Pi_2}^2\right)^{3/2}}\dfrac{\mu T^2}{4\pi^2{r_{12}}^3} \\
\qquad -\dfrac{\bar{\mu}_2\bar{z}}{\left(\bar{x}^2+\bar{y}^2+\bar{z}^2-2\bar{x}\Pi_1+{\Pi_1}^2\right)^{3/2}}\dfrac{\mu T^2}{4\pi^2{r_{12}}^3}
\end{cases}
$$

Now

$$T = \frac{2\pi}{\sqrt{\mu}} r_{12}^{\frac{3}{2}}$$

so

$$\frac{T^2 \mu}{4\pi^2 r_{12}^{\ 3}} = 1$$

Lastly, noting that

$$\Pi_1 = \bar{\mu}_1$$
$$\Pi_2 = \bar{\mu}_2$$

Equations are rewritten as:

$$\begin{cases} \ddot{\bar{x}} - 2\dot{\bar{y}} - \bar{x} = \bar{a}_x - \dfrac{\bar{\mu}_1\left(\bar{x} + \bar{\mu}_2\right)}{\left(\bar{x}^2 + \bar{y}^2 + \bar{z}^2 + 2\bar{x}\bar{\mu}_2 + \bar{\mu}_2^{\ 2}\right)^{3/2}} \\ \qquad\qquad - \dfrac{\bar{\mu}_2\left(\bar{x} - \bar{\mu}_1\right)}{\left(\bar{x}^2 + \bar{y}^2 + \bar{z}^2 - 2\bar{x}\bar{\mu}_1 + \bar{\mu}_1^{\ 2}\right)^{3/2}} \\ \ddot{\bar{y}} + 2\dot{\bar{x}} - \bar{y} = \bar{a}_y - \dfrac{\bar{\mu}_1 \bar{y}}{\left(\bar{x}^2 + \bar{y}^2 + \bar{z}^2 + 2\bar{x}\bar{\mu}_2 + \bar{\mu}_2^{\ 2}\right)^{3/2}} \\ \qquad\qquad - \dfrac{\bar{\mu}_2 \bar{y}}{\left(\bar{x}^2 + \bar{y}^2 + \bar{z}^2 - 2\bar{x}\bar{\mu}_1 + \bar{\mu}_1^{\ 2}\right)^{3/2}} \\ \ddot{\bar{z}} = \bar{a}_z - \dfrac{\bar{\mu}_1 \bar{z}}{\left(\bar{x}^2 + \bar{y}^2 + \bar{z}^2 + 2\bar{x}\bar{\mu}_2 + \bar{\mu}_2^{\ 2}\right)^{3/2}} \\ \qquad - \dfrac{\bar{\mu}_2 \bar{z}}{\left(\bar{x}^2 + \bar{y}^2 + \bar{z}^2 - 2\bar{x}\bar{\mu}_1 + \bar{\mu}_1^{\ 2}\right)^{3/2}} \end{cases} \tag{3.9}$$

with $\bar{a}_x = a_x \dfrac{T^2}{4\pi^2 r_{12}}$, $\bar{a}_y = a_y \dfrac{T^2}{4\pi^2 r_{12}}$, $\bar{a}_z = a_z \dfrac{T^2}{4\pi^2 r_{12}}$

The state matrix is now:

$$\mathbf{A}=\begin{bmatrix} 0 & 0 & 0 & 1 & 0 & 0 \\ 0 & 0 & 0 & 0 & 1 & 0 \\ 0 & 0 & 0 & 0 & 0 & 1 \\ -U_{xx} & -U_{xy} & -U_{xz} & 0 & 2 & 0 \\ -U_{yx} & -U_{yy} & -U_{yz} & -2 & 0 & 0 \\ -U_{zx} & -U_{yz} & -U_{zz} & 0 & 0 & 0 \end{bmatrix} \tag{3.10}$$

Dropping the over bar the derivative are:

$$U_{xx}=-\frac{3\mu_1\left(x+\mu_2\right)^2}{\left(x^2+y^2+z^2+2x\mu_2+\mu_2^2\right)^{5/2}}+\frac{\mu_1}{\left(x^2+y^2+z^2+2x\mu_2+\mu_2^2\right)^{3/2}}+$$
$$-\frac{3\mu_2\left(x-\mu_1\right)^2}{\left(x^2+y^2+z^2-2x\mu_1+\mu_1^2\right)^{5/2}}+\frac{\mu_2}{\left(x^2+y^2+z^2-2x\mu_1+\mu_1^2\right)^{3/2}}-1$$

$$U_{yy}=-\frac{3\mu_1y^2}{\left(x^2+y^2+z^2+2x\mu_2+\mu_2^2\right)^{5/2}}+\frac{\mu_1}{\left(x^2+y^2+z^2+2x\mu_2+\mu_2^2\right)^{3/2}}+$$
$$-\frac{3\mu_2y^2}{\left(x^2+y^2+z^2-2x\mu_1+\mu_1^2\right)^{5/2}}+\frac{\mu_2}{\left(x^2+y^2+z^2-2x\mu_1+\mu_1^2\right)^{3/2}}-1$$

$$U_{z}=-\frac{3\mu_1z^2}{\left(x^2+y^2+z^2+2x\mu_2+\mu_2^2\right)^{5/2}}+\frac{\mu_1}{\left(x^2+y^2+z^2+2x\mu_2+\mu_2^2\right)^{3/2}}+$$
$$-\frac{3\mu_2z^2}{\left(x^2+y^2+z^2-2x\mu_1+\mu_1^2\right)^{5/2}}+\frac{\mu_2}{\left(x^2+y^2+z^2-2x\mu_1+\mu_1^2\right)^{3/2}}$$

$$U_{xy}=-\frac{3\mu_1\left(x+\mu_2\right)y}{\left(x^2+y^2+z^2+2x\mu_2+\mu_2^2\right)^{5/2}}-\frac{3\mu_2\left(x-\mu_1\right)y}{\left(x^2+y^2+z^2-2x\mu_1+\mu_1^2\right)^{5/2}}$$

$$U_{xz}=-\frac{3\mu_1\left(x+\mu_2\right)z}{\left(x^2+y^2+z^2+2x\mu_2+\mu_2^2\right)^{5/2}}-\frac{3\mu_2\left(x-\mu_1\right)z}{\left(x^2+y^2+z^2-2x\mu_1+\mu_1^2\right)^{5/2}}$$

$$U_{yz}=-\frac{3\mu_1zy}{\left(x^2+y^2+z^2+2x\mu_2+\mu_2^2\right)^{5/2}}-\frac{3\mu_2zy}{\left(x^2+y^2+z^2-2x\mu_1+\mu_1^2\right)^{5/2}}$$

In order to view the benefic effect of nondimensinalization, the following pictures (from Figure 3.2 to Figure 3.4) show the values of U_{xx}, U_{yy}, U_{xy} in

function of *x* and *y* (with *z=0)* for various TBP in both case dimensional and nondimensional.

Earth-Sun System

$\omega = 1.991 \cdot 10^{-7}$

Dimensional Nondimensional

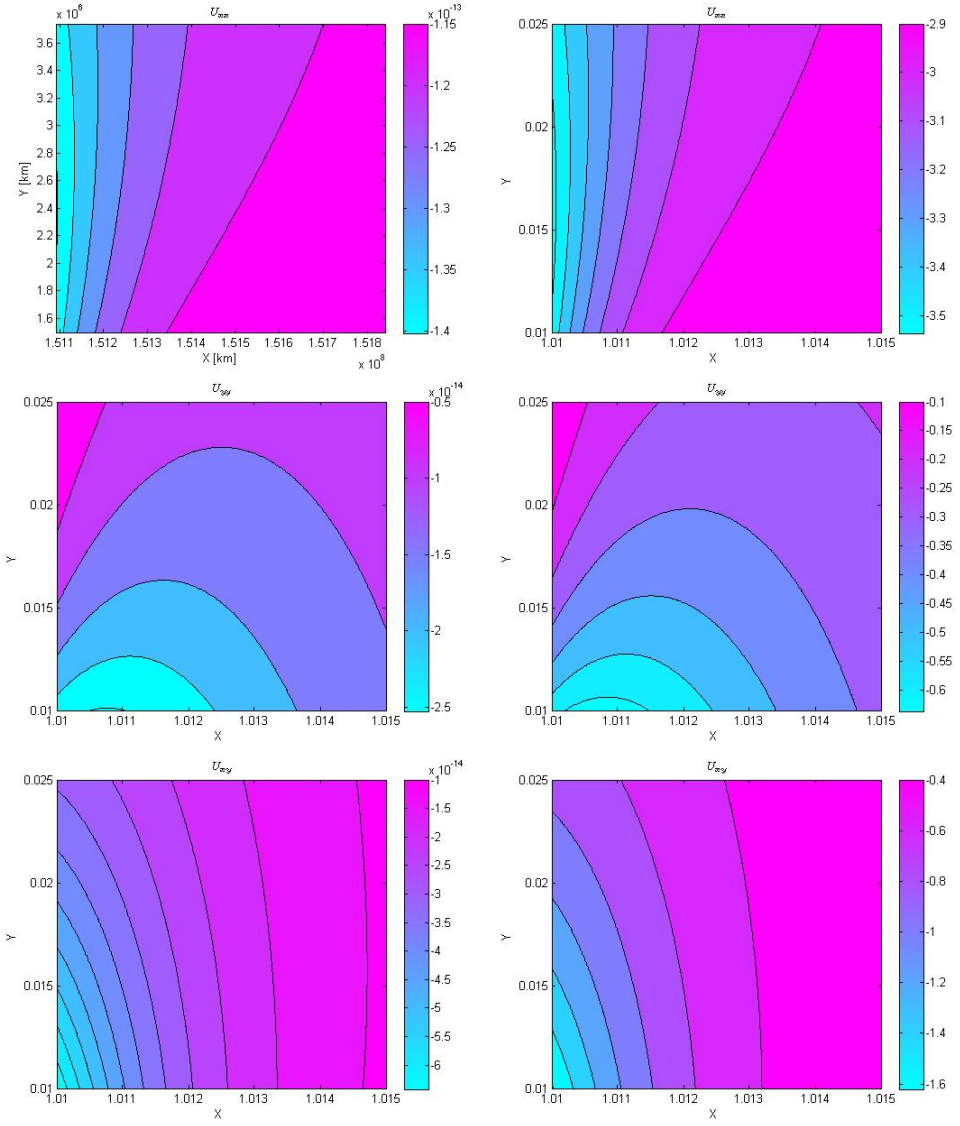

Figure 3.2 U_{xx}, U_{yy} and U_{xy} values for dimensional and nondimensional cases (Sun-Earth System)

Sun-Jupiter System

$\omega = 1.6776 \cdot 10^{-8}$

Dimensional Nondimensional

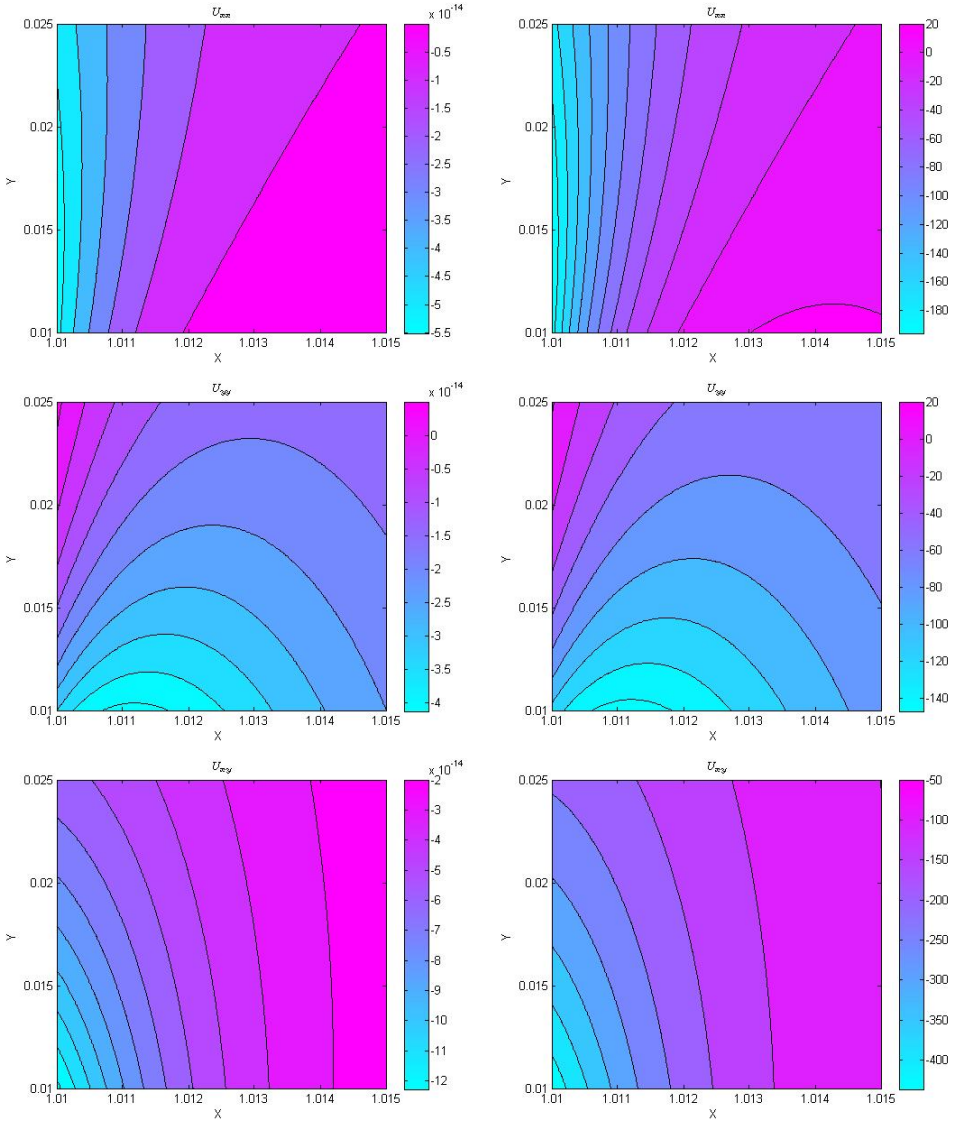

Figure 3.3 U_{xx}, U_{yy} and U_{xy} values for dimensional and nondimensional cases (Sun-Jupiter System)

Jupiter-Europa System

$\omega = 2.0483 \cdot 10^{-5}$

Dimensional Nondimensional

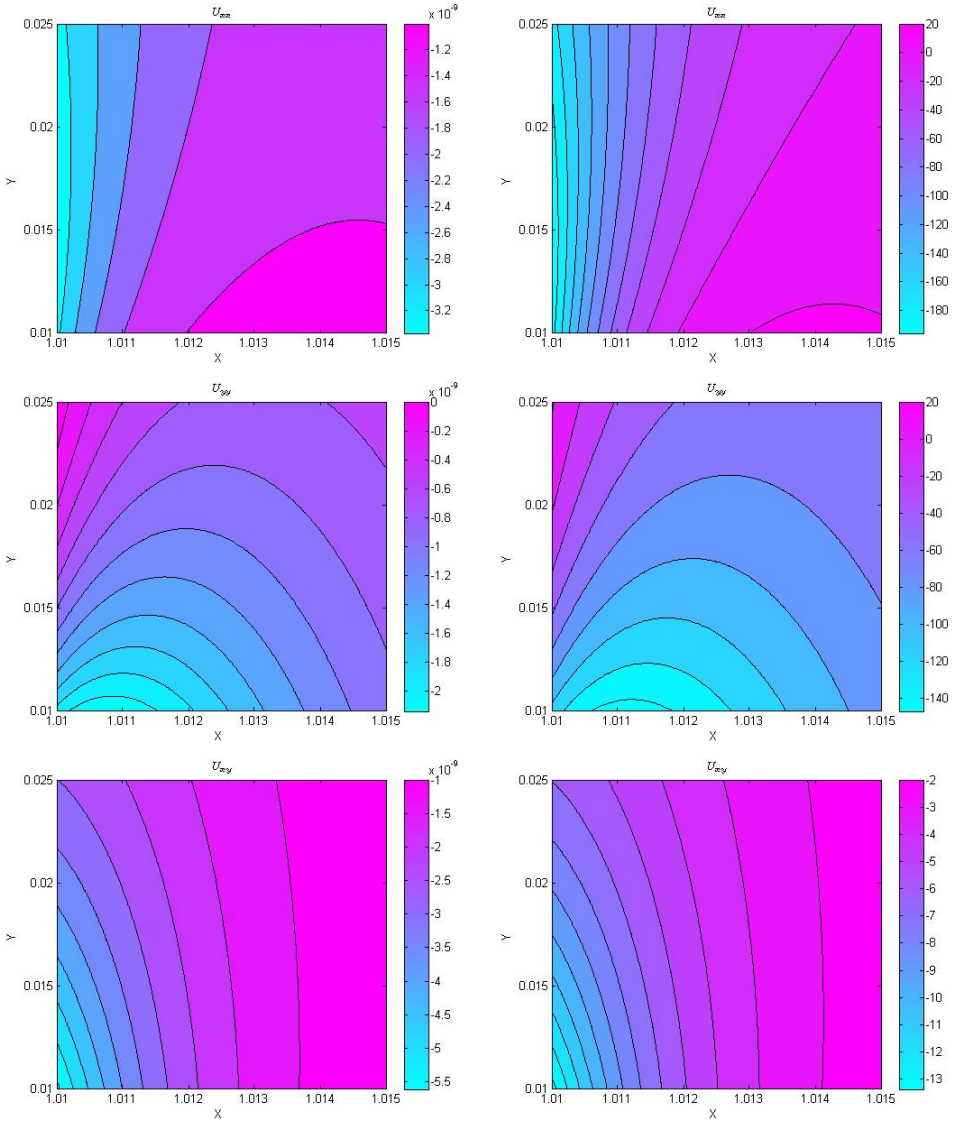

Figure 3.4 U_{xx}, U_{yy} and U_{xy} values for dimensional and nondimensional cases (Jupiter-Europa System)

In all this pictures, the x and y axis have a range near the less massive primary; for each systems the angular velocity is also provided (this since in the dimensional case ω is a term of the **A** matrix) .
Clearly the coefficients in the dimensional case have a larger magnitude differences as can be seen from the following graph.

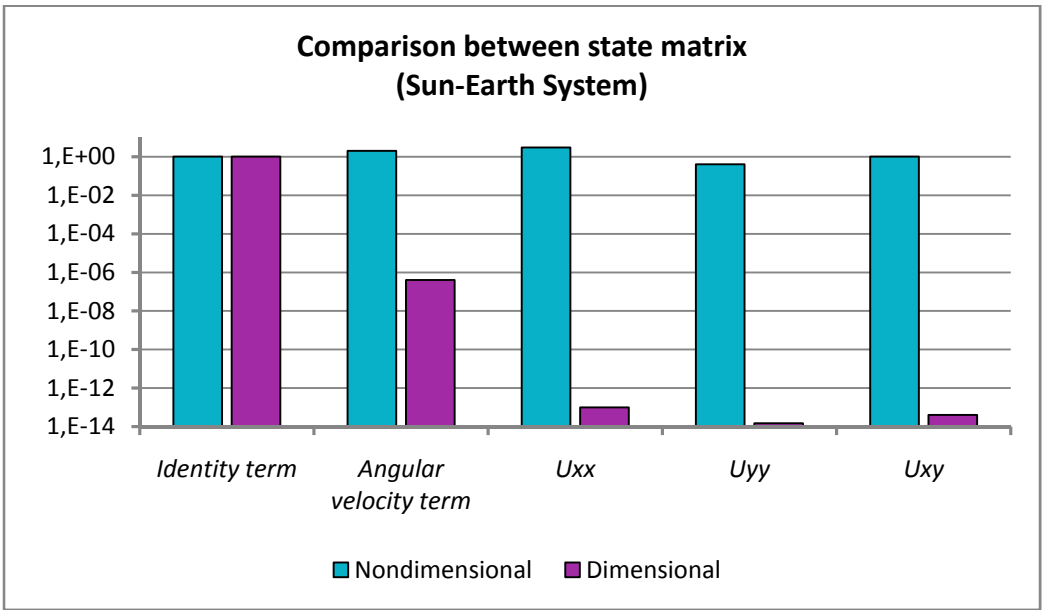

3.4 Artificial equilibrium points: Variable thrust

A further degree of freedom is available in the context of the control acceleration. Up to now a constant acceleration has been considered, but the current propulsion technology allows considering variable acceleration profiles too. All the available references, including (7) (8) (9) (15) (16), had considered only constant thrust, sometime with also directional limits (15). This aspect is the added value of this work.
From the analytical point of view in Eq. (3.6), while the dynamic system is linearized, the acceleration derivative is no more null.

$$\left[\frac{\partial}{\partial \mathbf{r}}\mathbf{a}(\mathbf{r})\right]\Big|_{\mathbf{r}_0} \neq 0$$

The hope is that adding degree of freedom will give more control. While, as stated in 3.2.4, with constant acceleration, points are turned into equilibrium points, but stability is not influenced in any way, variable

acceleration will probably allow to modify stability and periodicity of the orbit.
To get a deeper understanding of the problem and to get the implications of a variable acceleration, an analytical approach is adopted, with specific assumptions and simplifications highlighted in the followings.

3.4.1 Variable acceleration on AEP lying on the two primaries direction

In order to verify that using variable acceleration can lead to benefits such as to stabilize and also make periodic the motion, some simplification must be made, otherwise the problem wouldn't be analytically solvable.
Consider linearized orbits about $r_0=(X_0,Y_0,Z_0)$ with $Y_0=Z_0=0$*, and variable control acceleration of the type:
$a_x=a_0+a_1\,\bar{x}$.
This profile is needed in order to modify the equations of motion, obviously many type of polynomials could be used, but to keep the analysis simple, a linear acceleration is chosen.
Nondimensional, linearized equations are:

$$\begin{bmatrix}\ddot{\delta}_x\\ \ddot{\delta}_y\\ \ddot{\delta}_z\end{bmatrix}+2\begin{bmatrix}-\dot{\delta}_y\\ \dot{\delta}_x\\ 0\end{bmatrix}+\begin{bmatrix}U_{xx}-a_1 & 0 & 0\\ 0 & U_{yy} & 0\\ 0 & 0 & U_{zz}\end{bmatrix}\begin{bmatrix}\delta_x\\ \delta_y\\ \delta_z\end{bmatrix}=\begin{bmatrix}0\\ 0\\ 0\end{bmatrix} \tag{3.11}$$

The out of the plane is decoupled from the in plane motion. The former matrix equation can be rewritten in the state space, as follows:

$$\begin{bmatrix}\dot{\delta}_x\\ \dot{\delta}_y\\ \ddot{\delta}_x\\ \ddot{\delta}_y\end{bmatrix}=\begin{bmatrix}0 & 0 & 1 & 0\\ 0 & 0 & 0 & 1\\ a_1-U_{xx} & 0 & 0 & 2\\ 0 & -U_{yy} & -2 & 0\end{bmatrix}\begin{bmatrix}\delta_x\\ \delta_y\\ \dot{\delta}_x\\ \dot{\delta}_y\end{bmatrix} \tag{3.12}$$

* These assumption are not so restrictive as they seem, since once it has been shown that variable acceleration can modify an unstable AEP that lie on the line joining the two primaries, into a stable one, so adding further degree of freedom on the acceleration can lead to the same results for a point that isn't constrained to lie on the direction of the two primaries.

$$\begin{bmatrix} \dot{\delta}_z \\ \ddot{\delta}_z \end{bmatrix} = \begin{bmatrix} 0 & 1 \\ -U_{zz} & 0 \end{bmatrix} \begin{bmatrix} \delta_z \\ \dot{\delta}_z \end{bmatrix}$$

with

$$U_{xx} = -\frac{3\bar{\mu}_1(x+\bar{\mu}_2)^2}{(x^2+2\bar{\mu}_2 x+\bar{\mu}_2{}^2)^{5/2}} + \frac{\bar{\mu}_1}{(x^2+2\bar{\mu}_2 x+\bar{\mu}_2{}^2)^{3/2}} - \frac{3\bar{\mu}_2(x-\bar{\mu}_1)^2}{(x^2-2\bar{\mu}_1 x+\bar{\mu}_1{}^2)^{5/2}} + \frac{\bar{\mu}_2}{(x^2-2\bar{\mu}_1 x+\bar{\mu}_1{}^2)^{3/2}} - 1$$

$$U_{yy} = \frac{\bar{\mu}_1}{(x^2+2\bar{\mu}_2 x+\bar{\mu}_2{}^2)^{3/2}} + \frac{\bar{\mu}_2}{(x^2-2\bar{\mu}_1 x+\bar{\mu}_1{}^2)^{3/2}} - 1$$

$$U_{zz} = \frac{\bar{\mu}_1}{(x^2+2\bar{\mu}_2 x+\bar{\mu}_2{}^2)^{3/2}} + \frac{\bar{\mu}_2}{(x^2-2\bar{\mu}_1 x+\bar{\mu}_1{}^2)^{3/2}}$$

The following substitutions are applied:

$$P = \frac{\bar{\mu}_1}{(x^2+2\bar{\mu}_2 x+\bar{\mu}_2{}^2)^{3/2}} + \frac{\bar{\mu}_2}{(x^2-2\bar{\mu}_1 x+\bar{\mu}_1{}^2)^{3/2}} = \frac{\bar{\mu}_1}{r_1{}^3} + \frac{\bar{\mu}_2}{r_2{}^3}$$

$$U_{xx} = -2P - 1$$

$$U_{yy} = P - 1$$

$$U_{zz} = P$$

For the out of plane motion, the stability condition is P>0, while for in plane motion, the eigenvalues analysis must be carried on by solving the characteristic equation:

$$s^4 + \left(-P+2-a_1\right)s^2 + \left(\left(2P+1+a_1\right)\left(1-P\right)\right) = 0$$

calling $k = s^2$ and solving for k

$$k_{1,2} = \frac{P+a_1-2}{2} \pm \frac{1}{2}\sqrt{\Delta}$$

$$\Delta = 9P^2 - 8P + 6a_1P - 8a_1 + a_1{}^2$$

Whenever k is real and negative, eigenvalues are purely imaginary and an oscillatory motion is obtained. So oscillations ask for:

$$9P^2 - 8P + 6a_1P - 8a_1 + a_1{}^2 \geq 0 \rightarrow \text{k real} \qquad (3.13)$$

and

$$P + a_1 - 2 \pm \sqrt{9P^2 - 8P + 6a_1P - 8a_1 + a_1{}^2} < 0 \rightarrow \text{k negative}$$

The solution of the first inequalities is

$$a_1{}^2 + (6P - 8)a_1 + (9P^2 - 8P) \geq 0$$

$$a_{1I,II} = \frac{8 - 6P \pm \sqrt{36P^2 + 64 - 96P - 36P^2 + 32P}}{2} = -3P + 4 \pm 4\sqrt{1 - P}$$

since P>1 would imply that acceleration could be imaginary, the solution is considered in the region $P \leq 1$ and is

$$\boxed{a_1 \leq -3P + 4 - 4\sqrt{1 - P} \quad a_1 \geq -3P + 4 + 4\sqrt{1 - P}}$$

(3.14)

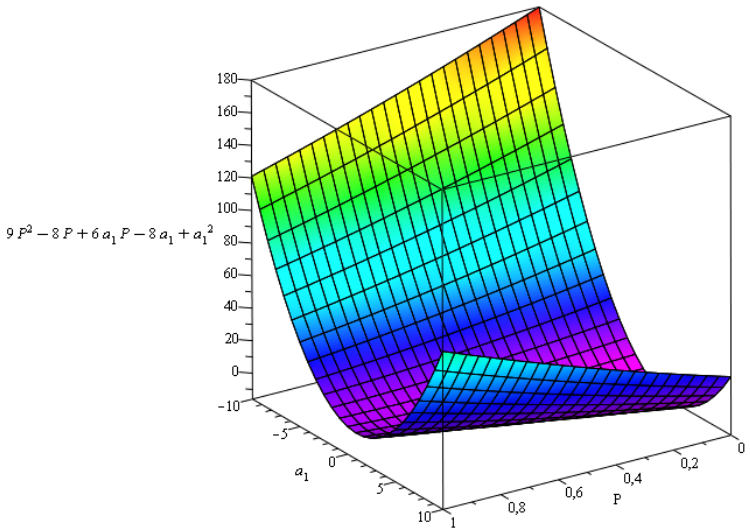

Figure 3.5 Surface $\Delta = 9P^2 - 8P + 6a_1P - 8a_1 + a_1^2$

In figure 3.5 the surface Δ is shown for $0 < P \leq 1$, and $-10 \leq a_1 \leq 10$. The limit on P is due to the limit of stability (P>0) and as stated before, that P should be less or equal than 1 in order to have real value for the acceleration. In figure 3.6 is highlighted the constrain (3.13). Figure 3.7 show the contour of since this view will be helpful in understanding the behavior of stability in function of the position (*P* axis) and the value of a_1. The limit of a1 can be arbitrarily chosen, in the specific case $-3 \leq a_1 \leq 3$ is a good choice in order to better visualize regions where the inequalities hold (figure3.8).

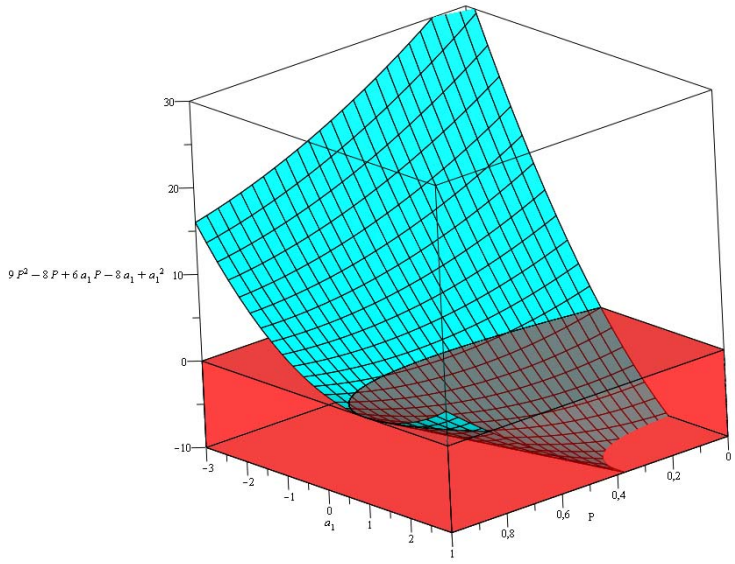

Figure 3.6 Crossing of Δ with x-y plane (marked with black line), and region (red) where (3.10) don't hold.

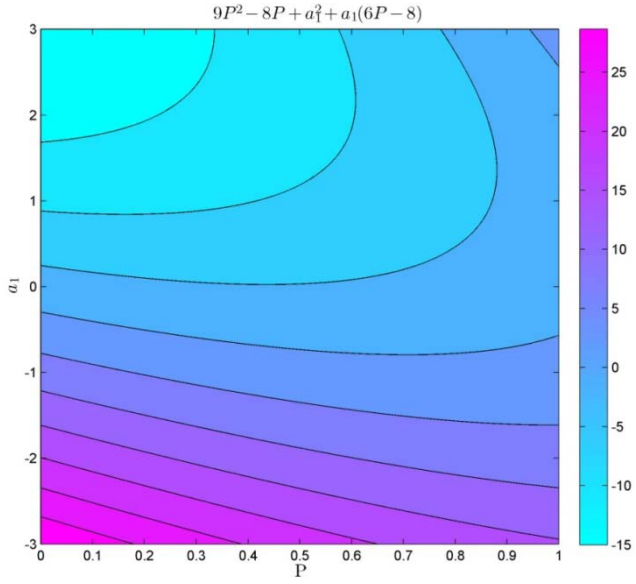

Figure 3.7 Contour of Δ

Also if the first inequalities hold, to have imaginary eigenvalues is necessary that:

$$P+a_1-2\pm\sqrt{9P^2-8P+a_1{}^2+a_1\left(6P-8\right)}<0$$

(3.15)

This two inequalities (3.15) can be viewed as

$$\boxed{\begin{array}{l} C(a_1,P) > \sqrt{\Delta\left(a_1,P\right)} \\ \text{the solution is} \\ \begin{cases} \Delta(a_1,P) \geq 0 \\ C(a_1,P) > 0 \\ \left|C(a_1,P)\right|^2 > \Delta(a_1,P) \end{cases} \end{array}}$$

(3.16)

$$\boxed{\begin{array}{l} C(a_1,P) < \sqrt{\Delta\left(a_1,P\right)} \\ \text{the solution is} \\ \begin{cases} \Delta(a_1,P) \geq 0 \\ C(a_1,P) < 0 \end{cases} \cup \begin{cases} \Delta(a_1,P) \geq 0 \\ \left|C(a_1,P)\right|^2 < \Delta(a_1,P) \end{cases} \end{array}}$$

(3.17)

Now, the condition $\Delta(a_1,P) \geq 0$ is precisely the same condition that is necessary to have real k (3.13), and is always present, so solving (3.13) and (3.14), and requiring that both are satisfied, will give the solutions of the problem.

- Starting with the first,

$$P + a_1 - 2 + \sqrt{9P^2 - 8P + {a_1}^2 + a_1\left(6P-8\right)} < 0$$

$$\underbrace{-P - a_1 + 2}_{C} > \sqrt{\underbrace{9P^2 - 8P + {a_1}^2 + a_1\left(6P-8\right)}_{\Delta}}$$

$$\begin{cases} \Delta \geq 0 \rightarrow a_1 \leq -3P + 4\left(1 - \sqrt{1-P}\right) \cup a_1 \geq -3P + 4\left(1 + \sqrt{1-P}\right) \\ C > 0 \rightarrow a_1 < 2 - P \\ \left|C(a_1,P)\right|^2 > \Delta(a_1,P) \rightarrow 4 + P^2 + {a_1}^2 + 2a_1P - 4P - 4a_1 > 9P^2 - 8P + {a_1}^2 \\ \qquad\qquad + a_1\left(6P-8\right) \end{cases}$$

The third equation need to be slightly rearranged

$$0 > 8P^2 - 4P + a_1(4P-4) - 4$$
$$2P^2 - P - a_1 - 1 + a_1 P < 0$$
$$(P-1)(2P+1+a_1) < 0$$

now, since $P \le 1$

$$(2P+1+a_1) > 0$$
$$a_1 > -2P-1$$

In compact form the solution is

$$\left[a_1 \le -3P + 4\left(1-\sqrt{1-P}\right) \cup a_1 \ge -3P + 4\left(1+\sqrt{1-P}\right)\right] \wedge a_1 < 2-P \wedge a_1 > -2P-1 \tag{3.18}$$

- The second is

$$P + a_1 - 2 - \sqrt{9P^2 - 8P + a_1^{\,2} + a_1(6P-8)} < 0$$
$$\underbrace{P + a_1 - 2}_{C} < \sqrt{\underbrace{9P^2 - 8P + a_1^{\,2} + a_1(6P-8)}_{\Delta}}$$
$$\begin{cases} \Delta \ge 0 \\ C < 0 \rightarrow a_1 < 2-P \end{cases}$$

$$\begin{cases} \Delta \ge 0 \\ |C(a_1,P)|^2 < \Delta(a_1,P) \rightarrow P^2 + a_1^{\,2} + 4 - 4P - a_1 + 2a_1P < 9P^2 - 8P + a_1^{\,2} \\ \qquad\qquad + a_1(6P-8) \end{cases}$$

as before the last equation can be rearranged

$$0 < 8P^2 - 4P + 4a_1P - 4a_1$$
$$(P-1)(2P+1+a_1) > 0$$

since $P \le 1$

$$a_1 < -2P-1$$

In compact form the solution is:

$$\left[a_1 \le -3P + 4\left(1-\sqrt{1-P}\right) \cup a_1 \ge -3P + 4\left(1+\sqrt{1-P}\right)\right] \wedge \left[a_1 < 2-P \vee a_1 < -2P-1\right] \tag{3.19}$$

The following figure (3.8) may be used to get a more deep insight of the problem, purple region indicates area where the inequalities are satisfied.

Picture I in figure 3.8 shows the condition
$a_1 \le -3P+4-4\sqrt{1-P} \quad a_1 \ge -3P+4+4\sqrt{1-P}$
Picture II in figure 3.8 shows the condition
$\left[a_1 \le -3P+4\left(1-\sqrt{1-P}\right) \cup a_1 \ge -3P+4\left(1+\sqrt{1-P}\right)\right] \wedge a_1 < 2-P \wedge a_1 > -2P-1$
Picture III shows the condition
$\left[a_1 \le -3P+4\left(1-\sqrt{1-P}\right) \cup a_1 \ge -3P+4\left(1+\sqrt{1-P}\right)\right] \wedge \left[a_1 < 2-P \vee a_1 < -2P-1\right]$
Picture IV in figure 3.8 shows the total solution of all inequalities combined $\left(\text{II} \wedge \text{III}\right)$.

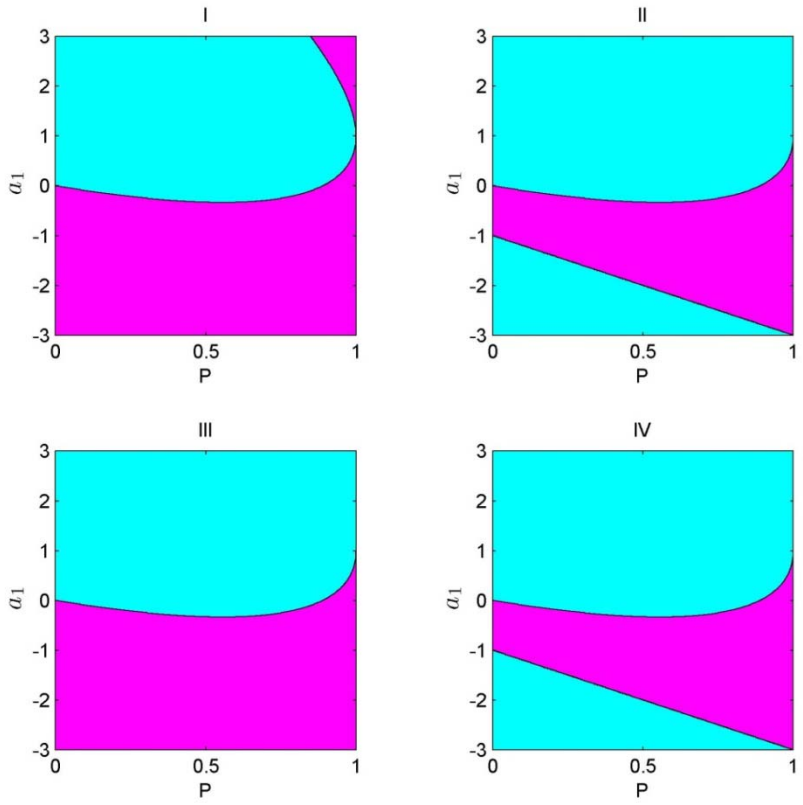

Figure 3.8 Region of stability variable control acceleration (violet).

From this figure, specifically from image IV, is clear that all the range $0 \leq P \leq 1$ (for a point that line on the line joining the two primaries) could be made stable as long a suitable acceleration (linear profile) is chosen.

In contrast, Morimoto (8) showed that for constant control acceleration, only the range $8/9 \leq P \leq 1$ is stable. Thus thanks to the additional degree of freedom the stable domain is made larger than the case of constant acceleration, this can be seen in figure 3.9; in this figure the blue line represent the value of P function of the x value (abscissa axis) in the Sun-Earth system.

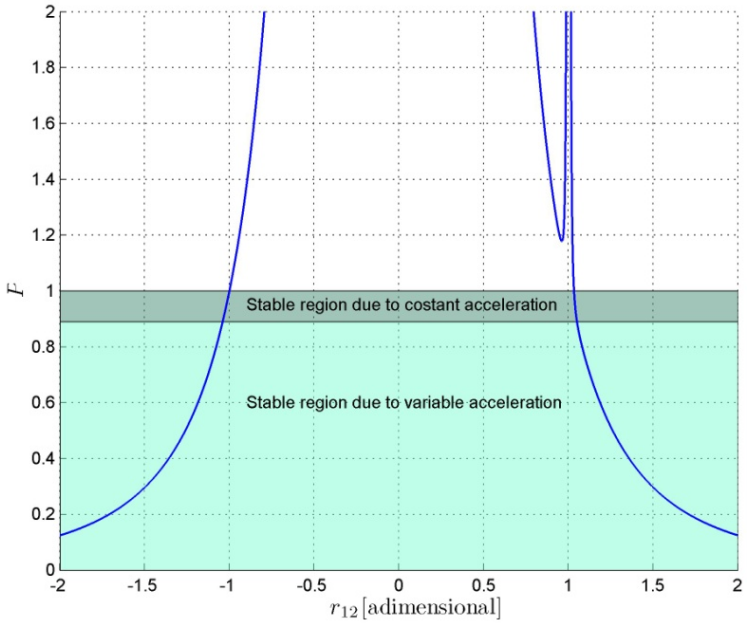

Figure 3.9 P function of r_{12} and stability region

The quantitative results obtained so far are valid only for AEPs that lies on the line joining the two primaries. Furthermore the augmented region of stability due to variable acceleration is far from the less massive secondary than the region due to constant acceleration. Anyway, as stated at the beginning, the objective is to verify that the additional degree of freedom can be used to obtain larger stable region. Thus the important thing here is the qualitative behavior of the solution.

The next step is to find out if the value of a_1 can be chosen so as to make the motion periodic.

a_1 selection

The inequalities reported in eq.(3.18) & (3.19) say that, given a value of P, a_1 must be enclosed within a specific domain to ensure the equilibrium point stability. This arbitrariness can be exploited to make the AEP not only stable, but also to allow periodic motion. Since the out of plane eigenvector cannot be modified*, the only choice, in this case, is to select a_1 such that a couple of eigenvalues of the **A** matrix in eq.(3.12) is in simple integer ratio with the out of plane frequencies.
That is:
Given $\omega_3$the value of a_1 must be chosen such that

$$\frac{\omega_1}{\omega_3} = n \quad \text{or} \quad \frac{\omega_2}{\omega_3} = n$$

With n integer.
If all the inequalities (3.18) & (3.19) are satisfied the eigenvalues are:

$$\sqrt{k_1} = \pm i\sqrt{|k_1|}$$
$$\sqrt{k_2} = \pm i\sqrt{|k_2|}$$
$$\sqrt{-P} = \pm i\sqrt{P}$$

calling

$$\omega_1 \triangleq k_1$$
$$\omega_2 \triangleq k_2$$
$$\omega_z \triangleq P$$

Necessary condition to obtain periodic motion can be
$\omega_1 = \omega_z$ or $\omega_2 = \omega_z$
With n=1.

That is

* This since the linearized equations of motion are decoupled (3.11), so a_1 can only influence in plane motion.

$$\begin{cases} k_1 = P \\ k_2 = P \end{cases} \rightarrow \begin{cases} \dfrac{P + a_1 - 2 + \sqrt{9P^2 - 8P + a_1{}^2 + a_1(6P-8)}}{2} = P \\ \dfrac{P + a_1 - 2 - \sqrt{9P^2 - 8P + a_1{}^2 + a_1(6P-8)}}{2} = P \end{cases}$$

$$\begin{cases} \sqrt{9P^2 - 8P + a_1{}^2 + a_1(6P-8)} = P - a_1 + 2 \\ -\sqrt{9P^2 - 8P + a_1{}^2 + a_1(6P-8)} = P - a_1 + 2 \end{cases}$$

Squaring both sides

$$\begin{cases} 9P^2 - 8P + a_1{}^2 + a_1(6P-8) = P^2 + a_1{}^2 + 4 - 4a_1 + 4P - 2a_1P \\ 9P^2 - 8P + a_1{}^2 + a_1(6P-8) = P^2 + a_1{}^2 + 4 - 4a_1 + 4P - 2a_1P \end{cases}$$

Since these two equations are identical only one is retained

$$8P^2 - 12P - 4 - 4a_1 + 8a_1P = 0$$

$$4a_1(2P-1) = 4(-2P^2 + 3P + 1)$$

$$a_1 = \frac{2P^2 - 3P - 1}{1 - 2P}$$

This value of a_1 function of P is shown in figure 3.10.

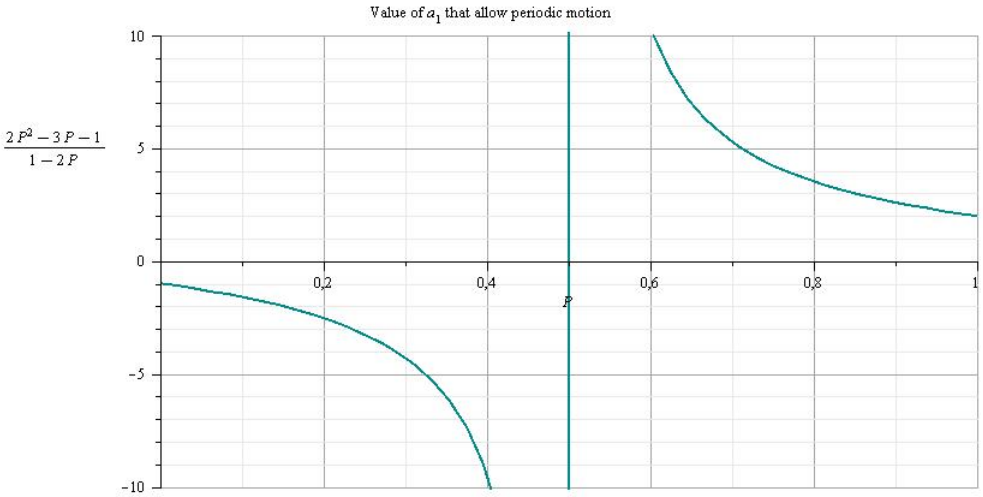

Figure 3.10 Values of a1 that allow periodic motion

Clearly the value of a_1 that allow periodic motion must satisfy all the inequalities that ensure stability. It turns out that there is no region where all this conditions are fulfilled.

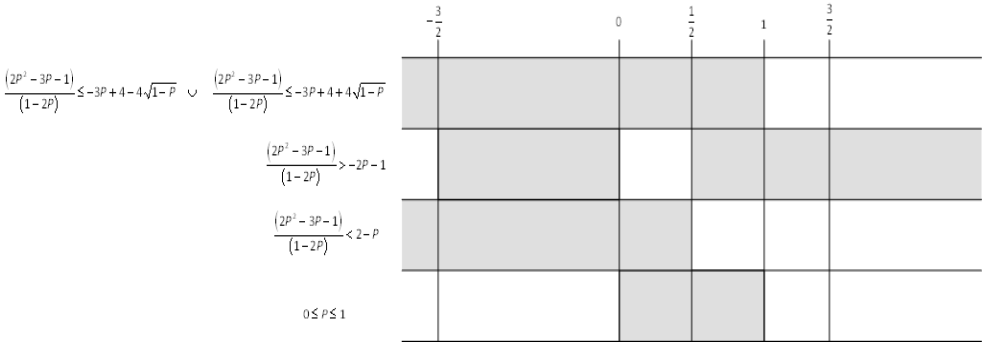

Figure 3.11 Region where inequalities hold (gray)

The presented analysis highlights that a linear profile to model the control variable accelerations increases the range of stability, but "artificial" periodic motion is unfeasible. The addition of further degrees of freedom could reveal to be the right path to force the eigenvalues to be in simple integer ratio. The next paragraph shows a way to implement this by numerical approach.
This choice is due to the fact that it would be very hard to find analytical solution to the complete coupled problem, with quadratic acceleration profile in every direction.

3.4.2 Numerical method for variable control accelerations

To confirm that the intuition of adding degree of freedom in order to make a generic point not only stable but also periodic, a numerical approach of the full coupled problem is followed.
Clearly the limitation is that not always a solution can be obtained, and with this approach there are no information about unfeasibility.

The equations of motion, with variable acceleration are reported below:

$$\frac{d^2\boldsymbol{\delta}}{dt^2} + 2\boldsymbol{\Omega} \times \frac{d\boldsymbol{\delta}}{dt} + \nabla \mathbf{U}(\mathbf{r}_0) + \left[\frac{\partial}{\partial \mathbf{r}} \nabla \mathbf{U}(\mathbf{r})\right]\Big|_{\mathbf{r}_0} \boldsymbol{\delta} - \mathbf{a}(\mathbf{r}_0) - \left[\frac{\partial}{\partial \mathbf{r}} \mathbf{a}(\mathbf{r})\right]\Big|_{\mathbf{r}_0} \boldsymbol{\delta} = 0$$

$$\frac{d^2}{dt^2}\begin{bmatrix}\delta_x\\ \delta_y\\ \delta_z\end{bmatrix}+\frac{d}{dt}\begin{bmatrix}-2\delta_y\\ 2\delta_x\\ 0\end{bmatrix}\omega+\begin{bmatrix}U_{xx}-a_{xx} & U_{yx}-a_{xy} & U_{xz}-a_{xz}\\ U_{yx}-a_{yx} & U_{yy}-a_{yy} & U_{yz}-a_{yz}\\ U_{zx}-a_{zx} & U_{zy}-a_{zy} & U_{zz}-a_{z}\end{bmatrix}\begin{bmatrix}\delta_x\\ \delta_y\\ \delta_z\end{bmatrix}=0$$

To proceed is necessary to assume some type of control acceleration. As shown throughout the analysis offered in §3.4.1, the linear model for the variable control acceleration doesn't meet the goal; therefore a higher order model, say a second order polynomium, is here tempted. To obtain reasonable value of the quadratic term, a Legendre polynomial is used.

$$\begin{cases}a_x=a_0+a_1x+\frac{a_2}{2}\left(3x^2-1\right)\\ a_y=b_0+b_1y+\frac{b_2}{2}\left(3y^2-1\right)\\ a_z=c_0+c_1z+\frac{c_2}{2}\left(3z^2-1\right)\end{cases}$$

As stated before the acceleration is now considered in all the direction, in this way 6 new degrees of freedom are added.

The linearized term can, therefore, be recasted in the following form:

$$\left[\frac{\partial}{\partial\mathbf{r}}\mathbf{a}(\mathbf{r})\right]\Big|_{\mathbf{r}_0}=\begin{bmatrix}a_{xx} & a_{xy} & a_{xz}\\ a_{yx} & a_{yy} & a_{yz}\\ a_{zx} & a_{zy} & a_{zz}\end{bmatrix}$$

where the extra-diagonal term are zero and:

$$\begin{aligned}a_{xx}&=\frac{\partial a_x}{\partial x}=a_1+3a_2x\\ a_{yy}&=\frac{\partial a_y}{\partial y}=b_1+3b_2y\\ a_{zz}&=\frac{\partial a_z}{\partial z}=c_1+3c_2z\end{aligned}\qquad(3.20)$$

The state space formalization of the equations of motion becomes:

$$\begin{bmatrix} \dot{\delta}_x \\ \dot{\delta}_y \\ \dot{\delta}_z \\ \ddot{\delta}_x \\ \ddot{\delta}_y \\ \ddot{\delta}_z \end{bmatrix} = \begin{bmatrix} 0 & 0 & 0 & 1 & 0 & 0 \\ 0 & 0 & 0 & 0 & 1 & 0 \\ 0 & 0 & 0 & 0 & 0 & 1 \\ a_{xx}-U_{xx} & -U_{xy} & -U_{xz} & 0 & 2\omega & 0 \\ -U_{yx} & a_{yy}-U_{yy} & -U_{yz} & -2\omega & 0 & 0 \\ -U_{zx} & -U_{yz} & a_{zz}-U_{zz} & 0 & 0 & 0 \end{bmatrix} \begin{bmatrix} \delta_x \\ \delta_y \\ \delta_z \\ \dot{\delta}_x \\ \dot{\delta}_y \\ \dot{\delta}_z \end{bmatrix} \tag{3.21}$$

Now it's possible to choose the coefficients $\begin{bmatrix} a_1 & a_2 & b_1 & b_2 & c_1 & c_2 \end{bmatrix}$ such that the eigenvalues of the system (3.21) experiences a zero real part, and imaginary parts in simple integer ratio. In this way the motion obtained is stable and periodic.

To this end, any numerical approach that try minimizing a functional, that is a measure of the difference between actual values and desired one, could be used.
The functional is defined as:

$$J = \sum_{i=1}^{6} \left| \mathrm{Re}\left(\lambda_i\right) \right| + k_1 + k_2 + F$$

Where the optimization variable are

$$\begin{Bmatrix} \lambda_1 & \lambda_2 & \lambda_3 & \lambda_4 & \lambda_5 & \lambda_6 & F \end{Bmatrix}$$

with

λ_i eigenvalue

$$k_1, k_2 \left| \mathrm{round}\left(\frac{\lambda_i}{\lambda_j}\right) - \frac{\lambda_i}{\lambda_j} \right| \text{ with } \lambda_i > \lambda_j \quad \begin{matrix} i=1, j=3 \\ i=2, j=3 \end{matrix}$$

$$F = \left(\left| a_0 + a_1 x + \frac{a_2}{2}(3x^2-1) \right| + \left| b_0 + b_1 y + \frac{b_2}{2}(3y^2-1) \right| + \left| c_0 + c_1 z + \frac{c_2}{2}(3z^2-1) \right| \right) \Bigg|_{x=x_0, y=y_0, z=z_0}$$

The first six terms are a "measure" of stability, and bring the real part of eigenvalues to 0. The two k_i terms are necessary to get frequency of motion in simple integer ratio, to obtain periodic motion. The last term is introduced to keep reasonable value of the control acceleration.

The coefficients $\begin{bmatrix} a_0 & b_0 & c_0 \end{bmatrix}$ are obtained by taking into account that:

$$\nabla \mathbf{U}(\mathbf{r}) - \mathbf{a_0} = 0$$

$$a_0 = \left[\frac{\mu_1 (x + \Pi_2 r_{12})}{r_1^{\,3}} + \frac{\mu_2 (x - \Pi_1 r_{12})}{r_1^{\,3}} - \omega^2 x - a_1 x - \frac{a_2}{2}\left(3x^2 - 1\right) \right]_{x_0}$$

$$b_0 = \left[\frac{\mu_1 y}{r_1^{\,3}} + \frac{\mu_2 y}{r_1^{\,3}} - \omega^2 y - b_1 y - \frac{b_2}{2}\left(3y^2 - 1\right) \right]_{y_0}$$

$$c_0 = \left[\frac{\mu_1 z}{r_1^{\,3}} + \frac{\mu_2 z}{r_1^{\,3}} - c_1 z - \frac{c_2}{2}\left(3z^2 - 1\right) \right]_{z_0}$$

In the present work the optimization is made in two separate steps, first a Multi Swarm Optimization method is adopted, to better define a restricted search space for the solution to be fed into a local optimizer as a first guess.

Numerical example

The described approach is now applied to a simple example: the second order control acceleration is computed to turn an unstable equilibrium point into a stable and periodic equilibrium point in the Sun-Earth system. The point coordinates are given in table 3.1, figure 3. shows the position of the point in the TBP considered.
The AEP is chosen taking the one presented in Morimoto (8) pg. 1137, for the first orbit analyzed, and later it was modified in order so as the distance between the point and earth was reduced by 1e5 km. Also to make the problem more realistic the point was shifted in Y direction.

Table 3.1 AEP coordinates

X_0	154306406 [*km*]
Y_0	-31100 [*km*]
Z_0	0 [*km*]

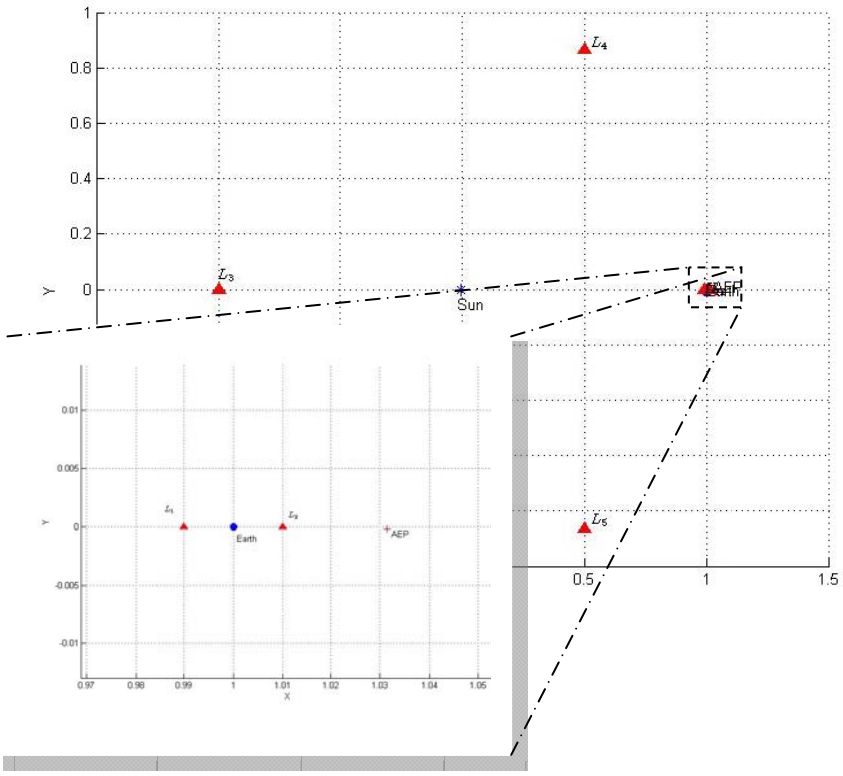

Figure 3.12 Sun – Earth system

For this point, if constant thrust is applied, the eigenvalues of the state matrix (3.10) are:

Table 3.2 AEP eigenvalues

-0.138734173159928	✗
0.138734173159928	✗
1.00636751485174 i	✓
-1.00636751485174 i	✓
1.00323057960442 i	✓
-1.00323057960442 i	✓

Since there is an eigenvalues with positive real part (λ_2), the AEP is unstable. If the previous procedure is employed the following values of polynomial acceleration (3.20) are found:

a_1	*-10.0463*	b_1	*-8.6316*	c_1	*-5.7624*
a_2	*-4.5792*	b_2	*10.2594*	c_2	*10.1655*

The convergence is checked to be sure that the optimization process has reached a minimum.

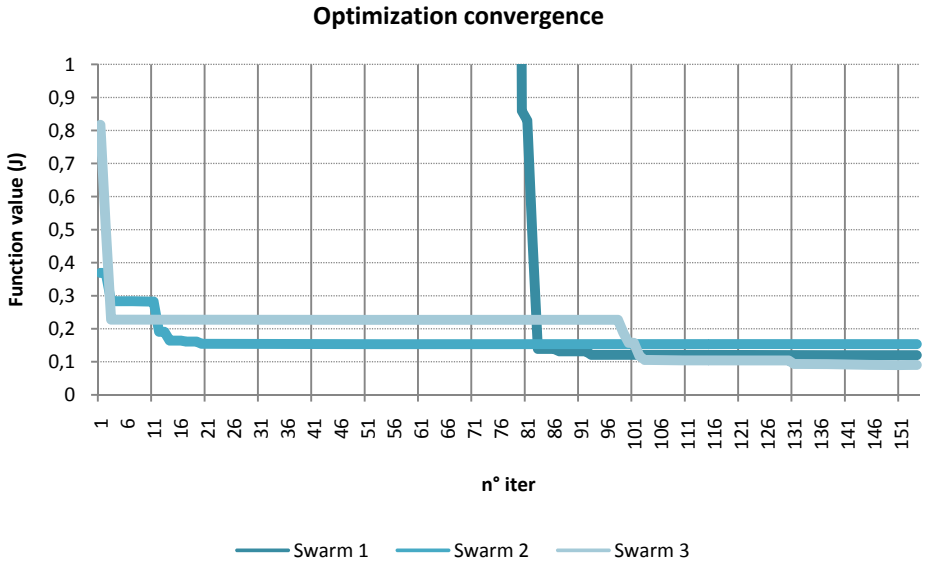

Figure 3.13 Convergence of the optimization process (15 particle per swarm)

Eigenvalues of this modified problem are:

5.20360287086428i
- 5.20360287086428i
2.60178734072275i
- 2.60178734072275i
2.60190391066737i
- 2.60190391066737i

$$\frac{\mathrm{Im}(\lambda_1)}{\mathrm{Im}(\lambda_5)} = 1.999 \simeq 2 \qquad \frac{\mathrm{Im}(\lambda_3)}{\mathrm{Im}(\lambda_5)} = 0.999 \simeq 1$$

Thus stable, periodic orbit is obtained, and the acceleration to achieve this condition must be:

$$a_x = 15.2923 - 10.0463x - \frac{4.5792}{2}\left(3x^2 - 1\right)$$

$$a_y = 5.1279 - 8.6316y + \frac{10.2594}{2}\left(3y^2 - 1\right)$$

$$a_z = 5.0827 - 5.7624z + \frac{10.1655}{2}\left(3z^2 - 1\right)$$

It's to be noted that polynomial coefficients values are given with enough significant figures needed to achieve a correct integration.

The orbit so obtained has ~70 days of period for the x direction and ~140 days for the z direction.

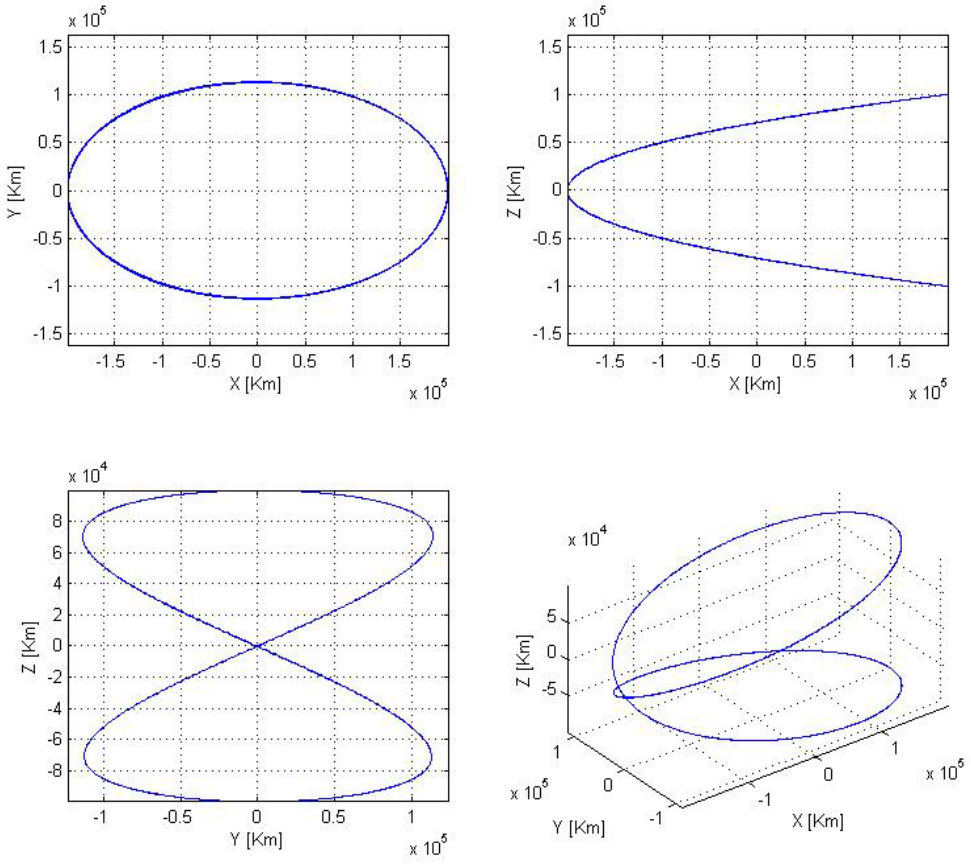

Figure 3.14 Analytic Orbit trajectory with variable control acceleration (δ_x=1e5 km, δ_y=0 km, δ_z=1e5 km)

In figure 3.15 and 3.16 the acceleration profile are shown.

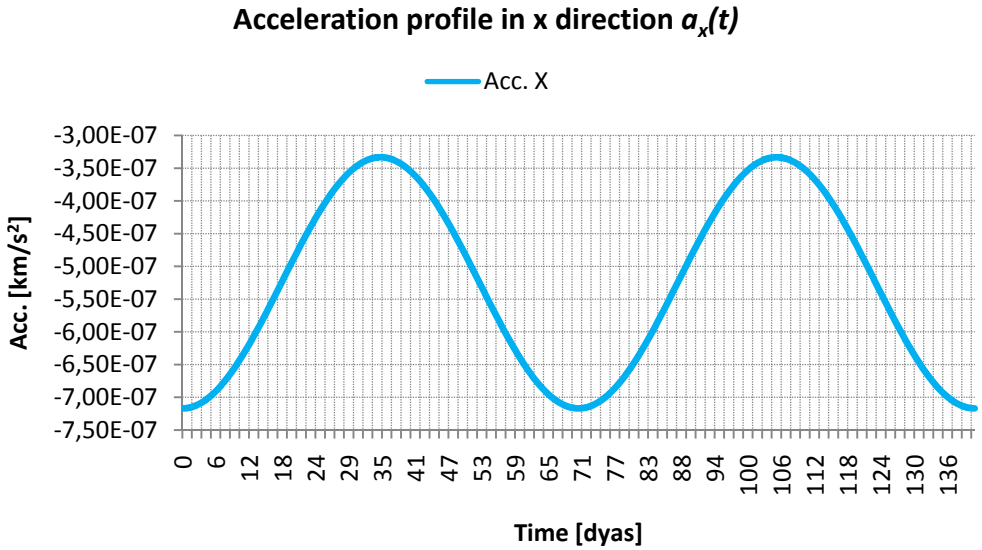

Figure 3.15 Acceleration profile in x direction.

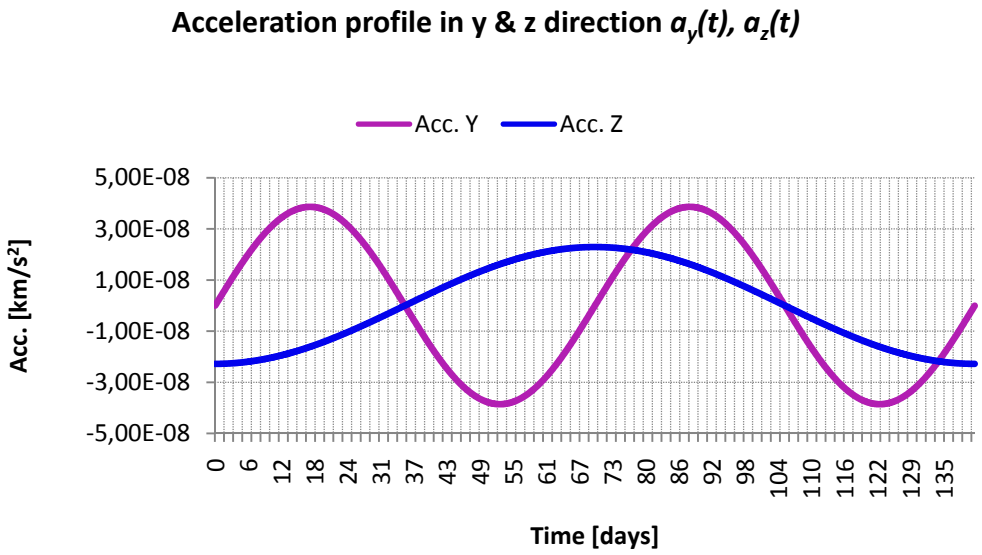

Figure 3.16 Convergence of the optimization process (15 particle per swarm)

3.4.3 Conclusion

The results obtained validate the idea that adding degrees of freedom to the system can be one way to force a generic point to be stable and periodic.
It's to be noted that anyway, the numerical approach presented, not always can bring to a satisfactory solution in term of admissible acceleration, also sometimes it's possible that no solution at all can be found.
The analytical procedure could be improved, but, probably, it would be very hard to obtain a solution to the general case of system (3.21) and a specific solution to some simplified conditions will be obtained.
However this could be a possible issue for further investigation.

Lastly, since the stability searched is local stability, and linearization of the non linear problem was made, probably it could be also possible to realize a variable control acceleration allocating the pole of system (3.10), and later adding to the control obtained the offset due to the constant value computed by (3.3).

4 Model Validity and Problematics

4.1 The selected model: benefits and limitations

The present chapter focuses on the critical discussion about the error the selected model and the imposed assumptions so far generates with respect to real motion.

Possible solutions to face the identified limitations are discussed too.

4.1.1 The linearized approach

Since all the theory developed till now is based on linearization, it is clear that if high values of initial orbit amplitude are chosen, analytical solution could be anyway obtained but once nonlinear equations of motion are integrated, great discrepancy between analytical and numerical results is found.

The limitation arising from retaining first term only is, therefore, that the motion amplitude must be small.
There isn't an "exact value" from which analytical solutions begin differing from numerical one. This because problem is strongly dependant on the parameter μ_1, and thus on the type of three body problem analyzed (e.g. Sun-Earth, Erath-Moon), also it depends on the AEP location. Some results obtained with integration of the nonlinear equations (3.9), for the Sun-Earth problem, are shown in figures from 4.1 to 4.6.Earth and Sun are aligned on the x axis. Every graph shows the trajectory of the spacecraft integrated with different initial amplitudes.
Table 4.1 show the AEP coordinates, while table 4.2 show the accelerations nondimensional values; for coordinates I a constant acceleration is applied, while for coordinates II variable acceleration is applied. Table 4.3 list the various initial amplitudes.

Table 4.1 AEP coordinates

AEP	X_0 *[km]*	Y_0 *[km]*	Z_0 *[km]*
I	154406406	0	0
II	154306406	0	0

Table 4.2 AEP nondimensional acceleration

AEP	I	II
a_x *[---]*	0.0906	$8.2982 + 2.6474x - \frac{10.1445}{2}(3x^2 - 1)$
a_y *[---]*	0	$5.034 - 9.6294y + \frac{10.0607}{2}(3y^2 - 1)$
a_z *[---]*	0	$0.7858 - 6.8657z + \frac{1.5716}{2}(3z^2 - 1)$

Table 4.3 AEP Amplitude

Amplitude	δ_x *[km]*	δ_y *[km]*	δ_z *[km]*
1	1e4	0	1e4
2	1e5	0	1e5
3	1e6	0	1e6

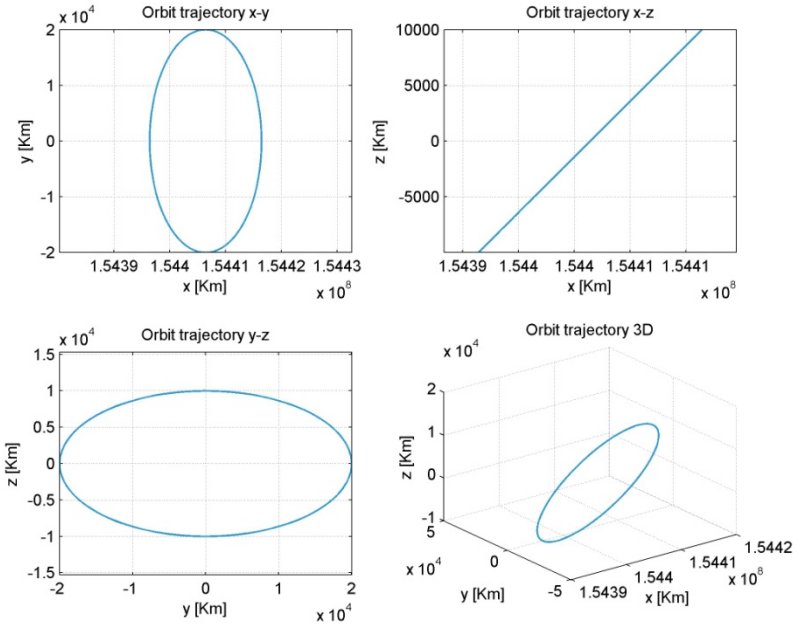

Figure 4.1 Orbit I Propagation I.C.: δ_x=δ_z=*1e4 km,* δ_y=*0 km*

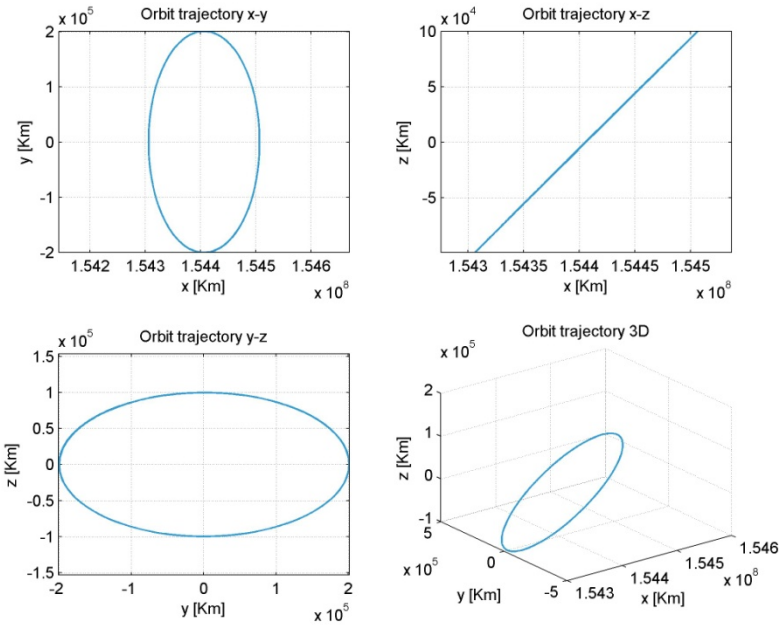

Figure 4.2 Orbit I Propagation I.C.: $\delta_x=\delta_z$=1e5 km, δ_y=0 km

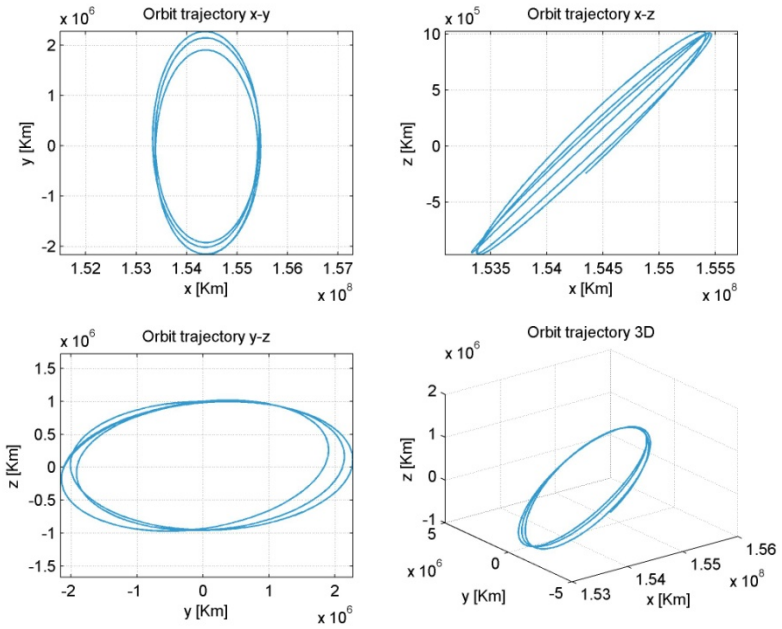

Figure 4.3 Orbit I Propagation I.C.: $\delta_x=\delta_z$=1e6 km, δ_y=0 km

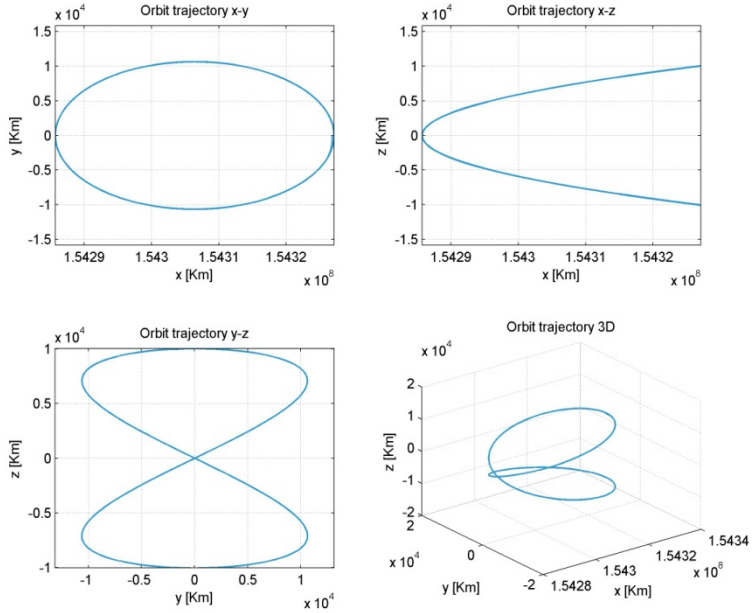

Figure 4.4 Orbit II Propagation I.C.: $\delta_x=\delta_z=1e4$ km, $\delta_y=0$ km

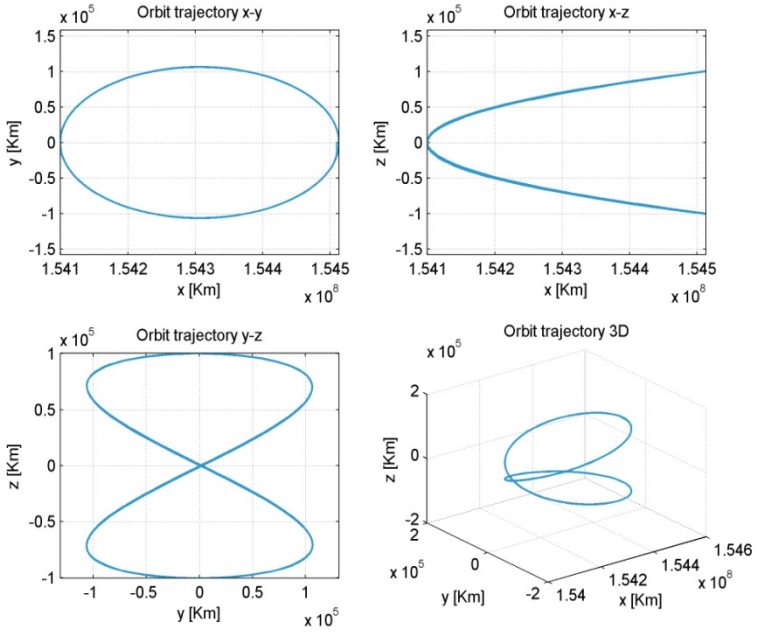

Figure 4.5 Orbit II Propagation I.C.: $\delta_x=\delta_z=1e5$ km, $\delta_y=0$ km

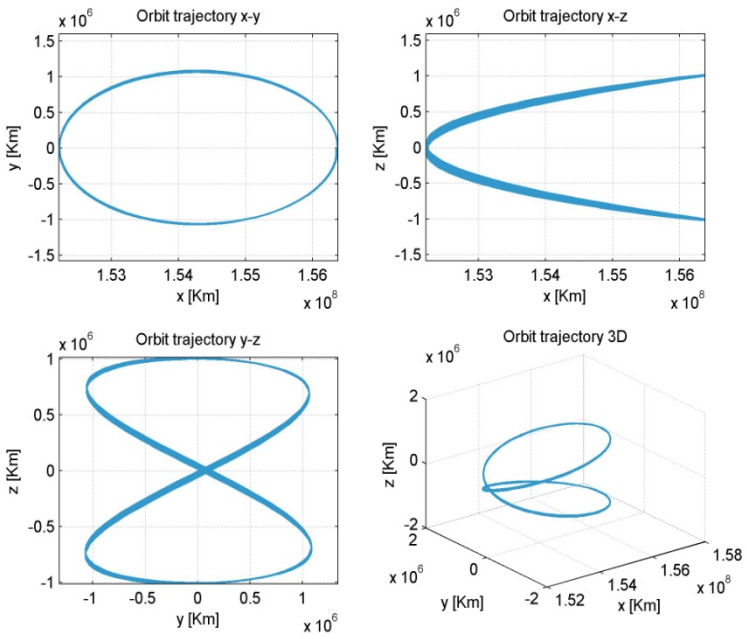

Figure 4.6 Orbit II Propagation I.C.: $\delta_x=\delta_z=1e6$ km, $\delta_y=0$ km

As it can be seen and as expected, high initial amplitudes (figure 4.3 and 4.6) prevent the spacecraft to complete more than one "revolution" in his periodic orbit. A possible solution could be to apply a sort of "station keeping" to correct the orbit similarly to the strategy exploited to make unstable L_1/L_2 orbits quasi-periodic (17) .

4.1.2 Analytical and Numerical orbit discrepancies

The comparison between orbits with small amplitude (10^3-10^4 km) obtained by the analytical and numerical approach, in the Sun-Earth system, show that if the constant control acceleration are rounded to 5 or lower floating point digits, the numerical and the analytical solutions differ. Moreover it has been observed that, neglecting an acceleration in a direction that is some order of magnitude lower than the others, e.g. z acceleration for a point slightly out of the plane, would introduce significant discrepancies between analytical and numerical solution. To take into account very small control acceleration with high resolution on its variation, means, from the technological perspective, to assure the availability of finely trhotteable thrusters, actually inexistent.

This is due to the fact that rounding or neglecting acceleration introduces a "residuum" term that is not considered in the linearized equations of motion.

Let consider the linearized equations (see eq. (3.5)) around an AEP with $r_0=(X_0,0,0)$ and using constant control acceleration, take the first one (x direction):

$$\ddot{\delta}_x = 2\dot{\delta}_y - U_{xx}\delta_x$$

Clearly, if the engine would supply an acceleration slightly different from the one required to satisfy (3.3), a residuum term would be present:

$$\mathbf{a}_{applied} \simeq \mathbf{a}_0$$

so that

$$\nabla \mathbf{U}(\mathbf{r}) - \mathbf{a}_{applied} = R \neq 0$$

In this case the equation become:

$$\ddot{\delta}_x = 2\dot{\delta}_y - U_{xx}\delta_x + R_x$$

Where R_x is the difference between acceleration truly applied and the desired one a_0. Evidently in order to neglect it, the residuum must be a small value compared to the other terms. To better understand the problem a quantitative analysis has been carried on, the graph in Figure 3.7,3.8,3.9,3.10 show how the value of instantaneous acceleration $\ddot{\delta}_x$ varies for some values of U_{xx} in the Sun-Earth system, when $R_x=0$.

$\ddot{\delta}_x$ $[km/s^2]$ is plotted as function of $\dot{\delta}_y, \delta_x$.

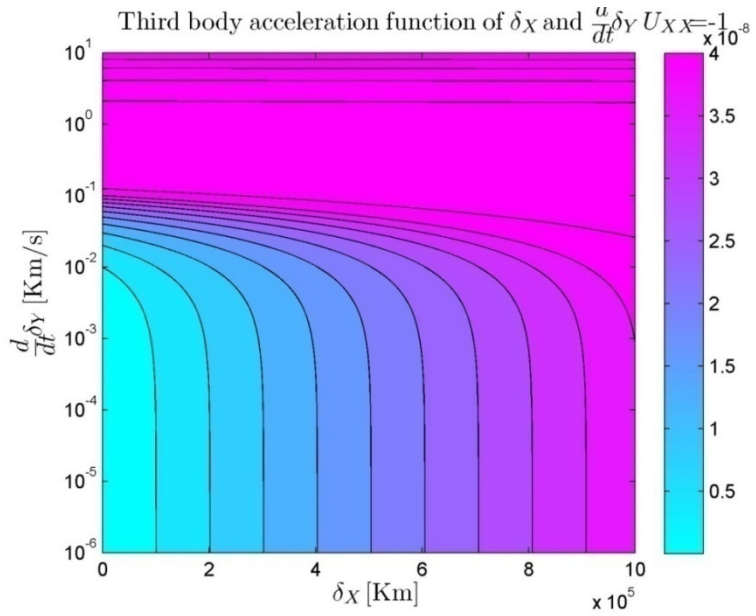

Figure 4.7 Instantaneous acceleration U_{xx}=-1

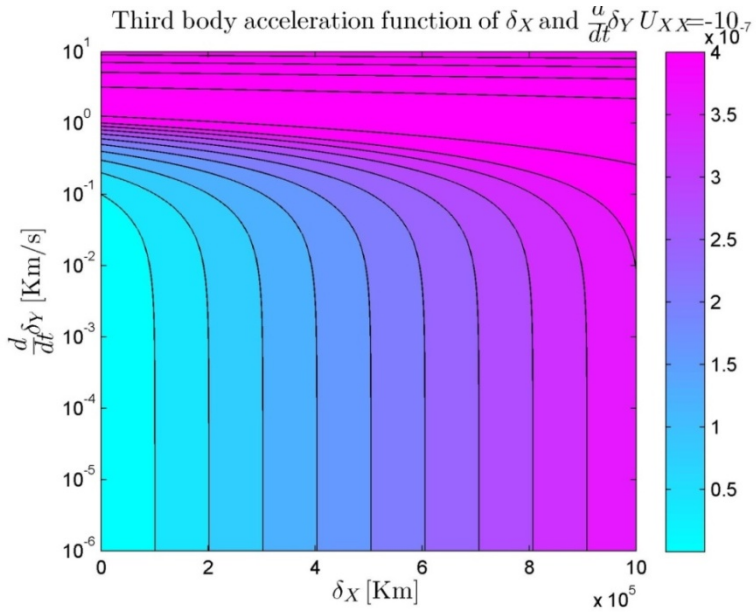

Figure 4.8 Instantaneous acceleration U_{xx}=-10

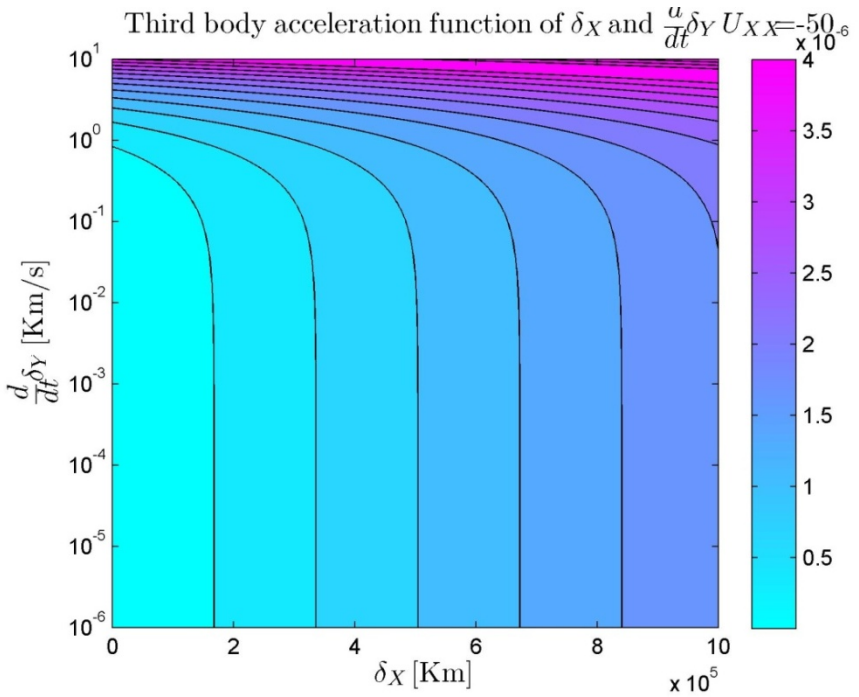

Figure 4.9 Instantaneous acceleration U_{xx}=-50

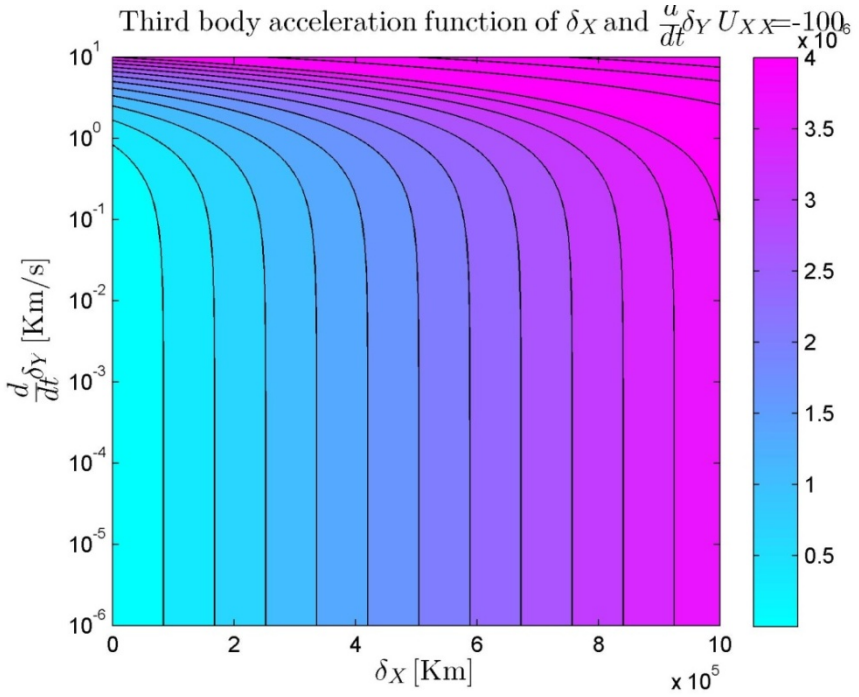

Figure 4.10 Instantaneous acceleration U_{xx}=-100

Those graphs clearly underline that $\dot{\delta}_y$ contribution to instantaneous acceleration is relevant only for high value of $\dot{\delta}_y$ itself, indeed for values of velocity in y direction less than ~1 m/s, the value of acceleration is predominantly determined by x amplitude. Moreover, by increasing the absolute value of U_{xx} (thus being nearer to the secondary as can be seen in figure 4.11) will increase the value of instantaneous particle acceleration.

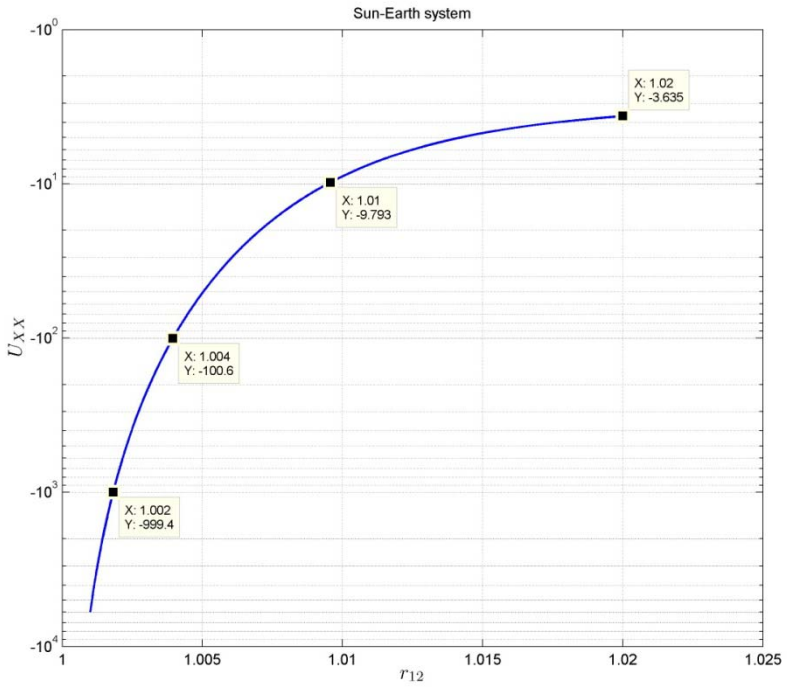

Figure 4.11 This graph show how U_{xx} varies function of r_{12} in the Sun-Earth system

Since the addition of R_x shouldn't change significantly the value of $\ddot{\delta}_x$, R_x should range from 1% to 5% of $\ddot{\delta}_x$ in the unperturbed case. Clearly, by increasing the orbit amplitude and the velocity* and being nearer to the secondary will increase the residuum magnitude and, accordingly, the allowable difference between true and required thrust.

* Since velocity and amplitude aren't independent, the increase of one also involve an augmentation of the other.

In the following tables some example are showed in order to give an idea of the magnitude of the involved quantities.
Given a generic point AEP, data relative to the control acceleration and instantaneous thrust required are presented; the allowable residuum is also computed. The value of the instantaneous acceleration is, then, calculated for various values of $\dot{\delta}_y$ and δ_x; lastly the residuum is compared to a percentage value of the instantaneous acceleration and, whenever less, the residuum is deemed tolerable and thus the model is valid.

Since the mass is variable, to analyze the worst condition, various values of spacecraft instantaneous mass are taken for the same point.

For every point, various tables are presented. In "data" table, constant control acceleration required computed. The thrust is found multiplying acceleration required by spacecraft mass. Thrust applied is determined rounding thrust required to the first integer, to take into account that the engine cannot develop exactly the computed thrust. The residuum is lastly found as the difference between the absolute values of the control acceleration.

Table 4.4 AEP data (X_0=1.01 m=300 kg)

	AEP	
X_0	1.01	[---]
Spacecraft dry mass	300	*kg*
Acc. required a_x	1.8034166E-09	*km/s²*
Thrust required T_x	0.541025	*mN*
Thrust applied $\widetilde{T_x}$	1.0	*mN*
Acc. applied $\widetilde{a_x}$	3.333333E-09	*km/s²*
Residuum order $\lvert a_x\rvert - \lvert\widetilde{a_x}\rvert$	2.E-09	*km/s²*

Table 4.5 AEP Instantaneous acceleration (X_0=1.01 m=300 kg)

Instantaneous acceleration $\ddot{\delta}_x$ [km/s²]							
		Speed $\dot{\delta}_y$ [km/s]					
		1.E-06	*1.E-05*	*1.E-04*	*1.E-03*	*1.E-02*	*1.E-01*
Orbit Amplitude δ_x [km]	*1.E+02*	3.585E-11	3.943E-11	7.527E-11	4.336E-10	4.017E-09	3.986E-08
	1.E+03	3.549E-10	3.585E-10	3.943E-10	7.527E-10	4.336E-09	4.017E-08
	1.E+04	3.545E-09	3.549E-09	3.585E-09	3.943E-09	7.527E-09	4.336E-08
	1.E+05	3.545E-08	3.545E-08	3.549E-08	3.585E-08	3.943E-08	7.527E-08
	1.E+06	3.545E-07	3.545E-07	3.545E-07	3.549E-07	3.585E-07	3.943E-07

Table 4.6 AEP 1% of instantaneous acceleration (X_0=1.01 m=300 kg)

1% Instantaneous acceleration [km/s²]							
		Speed [km/s]					
		1.E-06	1.E-05	1.E-04	1.E-03	1.E-02	1.E-01
Orbit Amplitude δ_x [km]	1.E+02	✗ 4 E-13	✗ 4 E-13	✗ 8 E-13	✗ 4 E-12	✗ 4 E-11	✗ 4 E-10
	1.E+03	✗ 4 E-12	✗ 4 E-12	✗ 4 E-12	✗ 8 E-12	✗ 4 E-11	✗ 4 E-10
	1.E+04	✗ 4 E-11	✗ 4 E-11	✗ 4 E-11	✗ 4 E-11	✗ 8 E-11	✗ 4 E-10
	1.E+05	✗ 4 E-10	✗ 4 E-10	✗ 4 E-10	✗ 4 E-10	✗ 4 E-10	✗ 8 E-10
	1.E+06	✓ 4 E-09	✓ 4 E-09	✓ 4 E-09	✓ 4 E-09	✓ 4 E-09	✓ 4 E-09

✗ the residuum is greater than 1% of instantaneous acceleration
✓ the residuum is less than 1% of instantaneous acceleration

Table 4.7 AEP data (X_0=1.01 m=3000 kg)

AEP		
X0	1.01	[---]
Spacecraft dry mass	3000	kg
Acc. required	1.8034166E-09	km/s²
Thrust required	5.41025	mN
Thrust applied	5.0	mN
Acc. applied	1.666667E-09	km/s²
Residuum order	1.E-10	km/s²

Table 4.8 AEP Instantaneous acceleration (X_0=1.01 m=3000 kg)

Instantaneous acceleration [km/s²]							
		Speed [km/s]					
		1.E-06	1.E-05	1.E-04	1.E-03	1.E-02	1.E-01
Orbit Amplitude δ_x [km]	1.E+02	3.585E-11	3.943E-11	7.527E-11	4.336E-10	4.017E-09	3.986E-08
	1.E+03	3.549E-10	3.585E-10	3.943E-10	7.527E-10	4.336E-09	4.017E-08
	1.E+04	3.545E-09	3.549E-09	3.585E-09	3.943E-09	7.527E-09	4.336E-08
	1.E+05	3.545E-08	3.545E-08	3.549E-08	3.585E-08	3.943E-08	7.527E-08
	1.E+06	3.545E-07	3.545E-07	3.545E-07	3.549E-07	3.585E-07	3.943E-07

Table 4.9 AEP 1% of instantaneous acceleration (X_0=1.01 m=3000 kg)

1% Instantaneous acceleration [km/s²]							
		Speed [km/s]					
		1.E-06	1.E-05	1.E-04	1.E-03	1.E-02	1.E-01
Orbit Amplitude δ_x [km]	1.E+02	✗ 4 E-13	✗ 4 E-13	✗ 8 E-13	✗ 4 E-12	✗ 4 E-11	✓ 4 E-10
	1.E+03	✗ 4 E-12	✗ 4 E-12	✗ 4 E-12	✗ 8 E-12	✗ 4 E-11	✓ 4 E-10
	1.E+04	✗ 4 E-11	✗ 4 E-11	✗ 4 E-11	✗ 4 E-11	✗ 8 E-11	✓ 4 E-10
	1.E+05	✓ 4 E-10	✓ 4 E-10	✓ 4 E-10	✓ 4 E-10	✓ 4 E-10	✓ 8 E-10
	1.E+06	✓ 4 E-09	✓ 4 E-09	✓ 4 E-09	✓ 4 E-09	✓ 4 E-09	✓ 4 E-09

Table 4.10 AEP data (X_0=1.032 m=300 kg)

AEP		
X0	1.032	[---]
Spacecraft dry mass	300	kg
Acc. required	-5.3447595E-07	km/s^2
Thrust required	-160.342785	mN
Thrust applied	-160.0	mN
Acc. applied	-5.333333E-07	km/s^2
Residuum order	1.E-09	km/s^2

Table 4.11 AEP Instantaneous acceleration (X_0=1.032 m=300 kg)

Instantaneous acceleration [km/s^2]							
		Speed [km/s]					
		1.E-06	1.E-05	1.E-04	1.E-03	1.E-02	1.E-01
Orbit Amplitude δ_x [km]	1.E+02	1.230E-11	1.589E-11	5.172E-11	4.101E-10	3.994E-09	3.983E-08
	1.E+03	1.194E-10	1.230E-10	1.589E-10	5.172E-10	4.101E-09	3.994E-08
	1.E+04	1.191E-09	1.194E-09	1.230E-09	1.589E-09	5.172E-09	4.101E-08
	1.E+05	1.190E-08	1.191E-08	1.194E-08	1.230E-08	1.589E-08	5.172E-08
	1.E+06	1.190E-07	1.190E-07	1.191E-07	1.194E-07	1.230E-07	1.589E-07

Table 4.12 AEP 1% of instantaneous acceleration (X_0=1.032 m=300 kg)

1% Instantaneous acceleration [km/s^2]							
		Speed [km/s]					
		1.E-06	1.E-05	1.E-04	1.E-03	1.E-02	1.E-01
Orbit Amplitude δ_x [km]	1.E+02	✗ 1 E-13	✗ 2 E-13	✗ 5 E-13	✗ 4 E-12	✗ 4 E-11	✗ 4 E-10
	1.E+03	✗ 1 E-12	✗ 1 E-12	✗ 2 E-12	✗ 5 E-12	✗ 4 E-11	✗ 4 E-10
	1.E+04	✗ 1 E-11	✗ 1 E-11	✗ 1 E-11	✗ 2 E-11	✗ 5 E-11	✗ 4 E-10
	1.E+05	✗ 1 E-10	✗ 1 E-10	✗ 1 E-10	✗ 1 E-10	✗ 2 E-10	✗ 5 E-10
	1.E+06	✓ 1 E-09	✓ 1 E-09	✓ 1 E-09	✓ 1 E-09	✓ 1 E-09	✓ 2 E-09

Table 4.13 AEP data (X_0=1.032 m=3000 kg)

AEP		
X0	1.032	[---]
Spacecraft dry mass	3000	kg
Acc. required	-5.3447595E-07	km/s^2
Thrust required	-1603.42785	mN
Thrust applied	-1603.0	mN
Acc. applied	-5.343333E-07	km/s^2
Residuum order	1.E-010	km/s^2

Table 4.14 AEP Instantaneous acceleration (X_0=1.032 m=3000 kg)

Instantaneous acceleration [km/s²]							
		Speed [km/s]					
		1.E-06	1.E-05	1.E-04	1.E-03	1.E-02	1.E-01
Orbit Amplitude δ_x [km]	1.E+02	1.230E-11	1.589E-11	5.172E-11	4.101E-10	3.994E-09	3.983E-08
	1.E+03	1.194E-10	1.230E-10	1.589E-10	5.172E-10	4.101E-09	3.994E-08
	1.E+04	1.191E-09	1.194E-09	1.230E-09	1.589E-09	5.172E-09	4.101E-08
	1.E+05	1.190E-08	1.191E-08	1.194E-08	1.230E-08	1.589E-08	5.172E-08
	1.E+06	1.190E-07	1.190E-07	1.191E-07	1.194E-07	1.230E-07	1.589E-07

Table 4.15 AEP 1% of instantaneous acceleration (X_0=1.032 m=3000 kg)

1 % Instantaneous acceleration [km/s²]							
		Speed [km/s]					
		1.E-06	1.E-05	1.E-04	1.E-03	1.E-02	1.E-01
Orbit Amplitude δ_x [km]	1.E+02	1 E-13	2 E-13	5 E-13	4 E-12	4 E-11	4 E-10
	1.E+03	1 E-12	1 E-12	2 E-12	5 E-12	4 E-11	4 E-10
	1.E+04	1 E-11	1 E-11	1 E-11	2 E-11	5 E-11	4 E-10
	1.E+05	1 E-10	1 E-10	1 E-10	1 E-10	2 E-10	5 E-10
	1.E+06	1 E-09	1 E-09	1 E-09	1 E-09	1 E-09	2 E-09

Table 4.16 AEP data (X_0=1.05 m=300 kg)

AEP		
X0	1.05	[---]
Spacecraft dry mass	300	kg
Acc. required	-8.4074883E-07	km/s²
Thrust required	-252.224648	mN
Thrust applied	-252.0	mN
Acc. applied	-8.400000E-07	km/s²
Residuum order	7E-10	km/s²

Table 4.17 AEP Instantaneous acceleration (X_0=1.05 m=300 kg)

Instantaneous acceleration [km/s²]							
		Speed [km/s]					
		1.E-06	1.E-05	1.E-04	1.E-03	1.E-02	1.E-01
Orbit Amplitude δ_x [km]	1.E+02	1.140E-11	1.498E-11	5.082E-11	4.092E-10	3.993E-09	3.983E-08
	1.E+03	1.104E-10	1.140E-10	1.498E-10	5.082E-10	4.092E-09	3.993E-08
	1.E+04	1.101E-09	1.104E-09	1.140E-09	1.498E-09	5.082E-09	4.092E-08
	1.E+05	1.100E-08	1.101E-08	1.104E-08	1.140E-08	1.498E-08	5.082E-08
	1.E+06	1.100E-07	1.100E-07	1.101E-07	1.104E-07	1.140E-07	1.498E-07

Table 4.18 AEP 1% of instantaneous acceleration (X_0=1.05 m=300 kg)

Instantaneous acceleration [km/s²]							
		Speed [km/s]					
		1.E-06	1.E-05	1.E-04	1.E-03	1.E-02	1.E-01
Orbit Amplitude δ_x [km]	1.E+02	✗ 1 E-13	✗ 1 E-13	✗ 5 E-13	✗ 4 E-12	✗ 4 E-11	✗ 4 E-10
	1.E+03	✗ 1 E-12	✗ 1 E-12	✗ 1 E-12	✗ 5 E-12	✗ 4 E-11	✗ 4 E-10
	1.E+04	✗ 1 E-11	✗ 1 E-11	✗ 1 E-11	✗ 1 E-11	✗ 5 E-11	✗ 4 E-10
	1.E+05	✗ 1 E-10	✗ 1 E-10	✗ 1 E-10	✗ 1 E-10	✗ 1 E-10	✗ 5 E-10
	1.E+06	✓ 1 E-09	✓ 1 E-09	✓ 1 E-09	✓ 1 E-09	✓ 1 E-09	✓ 1 E-09

Table 4.19 AEP data (X_0=1.05 m_{dry}=3000 kg)

AEP		
X0	1.05	[---]
Spacecraft dry mass	3000	kg
Acc. required	-8.4074883E-07	km/s²
Thrust required	-2522.24648	mN
Thrust applied	-2522	mN
Acc. applied	-8.406667E-07	km/s²
Residuum order	8E-11	km/s²

Table 4.20 AEP Instantaneous acceleration (X_0=1.05 m=3000 kg)

Instantaneous acceleration [km/s²]							
		Speed [km/s]					
		1.E-06	1.E-05	1.E-04	1.E-03	1.E-02	1.E-01
Orbit Amplitude δ_x [km]	1.E+02	1.140E-11	1.498E-11	5.082E-11	4.092E-10	3.993E-09	3.983E-08
	1.E+03	1.104E-10	1.140E-10	1.498E-10	5.082E-10	4.092E-09	3.993E-08
	1.E+04	1.101E-09	1.104E-09	1.140E-09	1.498E-09	5.082E-09	4.092E-08
	1.E+05	1.100E-08	1.101E-08	1.104E-08	1.140E-08	1.498E-08	5.082E-08
	1.E+06	1.100E-07	1.100E-07	1.101E-07	1.104E-07	1.140E-07	1.498E-07

Table 4.21 AEP 1% of instantaneous acceleration (X_0=1.05 m=3000 kg)

1% Instantaneous acceleration [km/s²]							
		Speed [km/s]					
		1.E-06	1.E-05	1.E-04	1.E-03	1.E-02	1.E-01
Orbit Amplitude δ_x [km]	1.E+02	✗ 1 E-13	✗ 1 E-13	✗ 5 E-13	✗ 4 E-12	✗ 4 E-11	✓ 4 E-10
	1.E+03	✗ 1 E-12	✗ 1 E-12	✗ 1 E-12	✗ 5 E-12	✗ 4 E-11	✓ 4 E-10
	1.E+04	✗ 1 E-11	✗ 1 E-11	✗ 1 E-11	✗ 1 E-11	✗ 5 E-11	✓ 4 E-10
	1.E+05	✓ 1 E-10	✓ 1 E-10	✓ 1 E-10	✓ 1 E-10	✓ 1 E-10	✓ 5 E-10
	1.E+06	✓ 1 E-09	✓ 1 E-09	✓ 1 E-09	✓ 1 E-09	✓ 1 E-09	✓ 1 E-09

Table 4.22 AEP data (X_0=1.2 m=300 kg)

AEP		
X0	1.2	[---]
Spacecraft dry mass	300	kg
Acc. required	-2.9975683E-06	km/s^2
Thrust required	-899.270482	mN
Thrust applied	-899.0	mN
Acc. applied	-2.9966667E-06	km/s^2
Residuum order	9E-10	km/s^2

Table 4.23 AEP Instantaneous acceleration (X_0=1.2 m=300 kg)

Instantaneous acceleration $[km/s^2]$							
		Speed [km/s]					
		1.E-06	1.E-05	1.E-04	1.E-03	1.E-02	1.E-01
Orbit Amplitude δ_x [km]	1.E+02	8.953E-12	1.254E-11	4.837E-11	4.068E-10	3.991E-09	3.983E-08
	1.E+03	8.595E-11	8.953E-11	1.254E-10	4.837E-10	4.068E-09	3.991E-08
	1.E+04	8.559E-10	8.595E-10	8.953E-10	1.254E-09	4.837E-09	4.068E-08
	1.E+05	8.555E-09	8.559E-09	8.595E-09	8.953E-09	1.254E-08	4.837E-08
	1.E+06	8.555E-08	8.555E-08	8.559E-08	8.595E-08	8.953E-08	1.254E-07

Table 4.24 AEP 1% of instantaneous acceleration (X_0=1.2 m=300 kg)

1% Instantaneous acceleration $[km/s^2]$							
		Speed [km/s]					
		1.E-06	1.E-05	1.E-04	1.E-03	1.E-02	1.E-01
Orbit Amplitude δ_x [km]	1.E+02	✗ 9 E-14	✗ 1 E-13	✗ 5 E-13	✗ 4 E-12	✗ 4 E-11	✗ 4 E-10
	1.E+03	✗ 9 E-13	✗ 9 E-13	✗ 1 E-12	✗ 5 E-12	✗ 4 E-11	✗ 4 E-10
	1.E+04	✗ 9 E-12	✗ 9 E-12	✗ 9 E-12	✗ 1 E-11	✗ 5 E-11	✗ 4 E-10
	1.E+05	✗ 9 E-11	✗ 9 E-11	✗ 9 E-11	✗ 9 E-11	✗ 1 E-10	✗ 5 E-10
	1.E+06	✓ 9 E-10	✓ 9 E-10	✓ 9 E-10	✓ 9 E-10	✓ 9 E-10	✓ 1 E-09

Table 4.25 AEP data (X_0=1.2 m=3000 kg)

AEP		
X0	1.2	[---]
Spacecraft dry mass	3000	kg
Acc. required	-2.9975683E-06	km/s^2
Thrust required	-8992.70482	mN
Thrust applied	-8992.0	mN
Acc. applied	-2.9976667E-06	km/s^2
Residuum order	1E-10	km/s^2

Table 4.26 AEP Instantaneous acceleration (X_0=1.2 m=3000 kg)

Instantaneous acceleration [km/s²]							
		Speed [km/s]					
		1.E-06	1.E-05	1.E-04	1.E-03	1.E-02	1.E-01
Orbit Amplitude δ_x [km]	1.E+02	8.953E-12	1.254E-11	4.837E-11	4.068E-10	3.991E-09	3.983E-08
	1.E+03	8.595E-11	8.953E-11	1.254E-10	4.837E-10	4.068E-09	3.991E-08
	1.E+04	8.559E-10	8.595E-10	8.953E-10	1.254E-09	4.837E-09	4.068E-08
	1.E+05	8.555E-09	8.559E-09	8.595E-09	8.953E-09	1.254E-08	4.837E-08
	1.E+06	8.555E-08	8.555E-08	8.559E-08	8.595E-08	8.953E-08	1.254E-07

Table 4.27 AEP 1% of instantaneous acceleration (X_0=1.2 m=3000 kg)

1% Instantaneous acceleration [km/s²]							
		Speed [km/s]					
		1.E-06	1.E-05	1.E-04	1.E-03	1.E-02	1.E-01
Orbit Amplitude δ_x [km]	1.E+02	✗ 9 E-14	✗ 1 E-13	✗ 5 E-13	✗ 4 E-12	✗ 4 E-11	✓ 4 E-10
	1.E+03	✗ 9 E-13	✗ 9 E-13	✗ 1 E-12	✗ 5 E-12	✗ 4 E-11	✓ 4E-10
	1.E+04	✗ 9 E-12	✗ 9 E-12	✗ 9 E-12	✗ 1 E-11	✗ 5 E-11	✓ 4 E-10
	1.E+05	✗ 9 E-11	✗ 9 E-11	✗ 9 E-11	✗ 9 E-11	✓ 1 E-10	✓ 5 E-10
	1.E+06	✓ 9 E-10	✓ 9 E-10	✓ 9 E-10	✓ 9 E-10	✓ 9 E-10	✓ 1 E-09

All those tables illustrate that, as might be expected given the form of linearized equation of motion in x direction, for large amplitudes of the orbit the tolerable residuum is greater than for orbits with small amplitudes, therefore the difference between the thrust applied is also small (it adequate to look at any table "1% Instantaneous acceleration" to notice what was just said). Note also that by increasing the spacecraft mass, the residuum tends decreasing. This suggest that fuel consumption probably will prevent the spacecraft to retain his periodic orbit with an open loop control, that is applying a constant control acceleration.

This analysis highlights that to obtain a periodic motion with constant control acceleration, is necessary that orbits amplitudes are "high enough", however all the numeric computation are made for the Sun-Earth mass ratio, thus it is possible that with smaller ratio small amplitude are achievable.

4.1.3 Numerical Propagation

The previous chapter shows, under the mentioned assumptions, that if orbit amplitudes are small, as required by the linearization approach, high precision on thrust is needed in order to achieve the correct periodic orbit. The following figures (from 4.12 to 4.24) show, the absolute error on position of the orbit, the state space ( ) and the trajectory of the

spacecraft for various values of thrust uncertainty and initial amplitudes. The AEP on which the analysis is carried on is $X_0 = 1.0321$, $Y_0 = 0$, $Z_0 = 0$.

As it can be expected and as can be seen in figures 4.12, 4.15, 4.18 and 4.21, whenever increasing uncertainty on the thrust magnitude increases the position error enlarges.

It should be noted that to vary the initial amplitude is a sort of "scaling" and since the error plotted in figures 4.12, 4.15, 4.18 and 4.21 is the absolute error, those graphs are quite identical, the only difference is in figure 4.21 since the amplitudes are high enough that nonlinear behavior is dominant even at low uncertainty.

State space representation gives an easier way to see that increasing amplitudes allow higher uncertainty values on thrust, this because the relative error is smaller. For example if a thrust has an uncertainty of 1e-3 mN, then the absolute error range between $100 - 1000\ km$ thus for an orbit with initial amplitudes of 1000 km this imply that the percent error is near 100%, while if the orbit has initial amplitudes of 100 000 km the percent error is about 1%. In the state space is apparent that whenever the orbit doesn't close on itself but instead "drifts" the orbit isn't periodic anymore. Furthermore state space for amplitudes of 1e6 km show clearly that the motion become **chaotic** (12) (18).

Lastly from the state space it seems that if uncertainty value are low, the orbit is periodic, but if a Poincarè section is made its clear that the orbit is not truly periodic (figure 4.24 & 4.25), anyway the difference in X position is about 400 km over an amplitude of 1e5 km, thus the error is about 0.4%. Thus the orbit is substantially periodic.

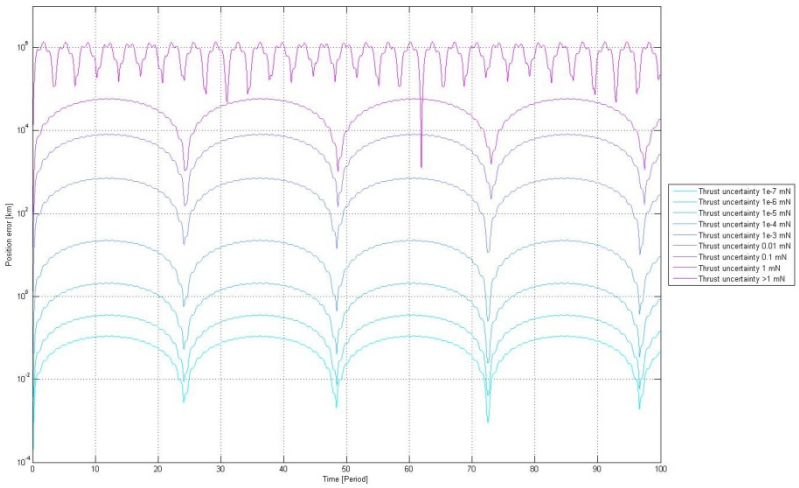

Figure 4.12 Error on Y for various values of thrust uncertainty, initial amplitudes $(\delta_x = 1e3\ km, \delta_y = 0\ km, \delta_z = 1e3\ km)$

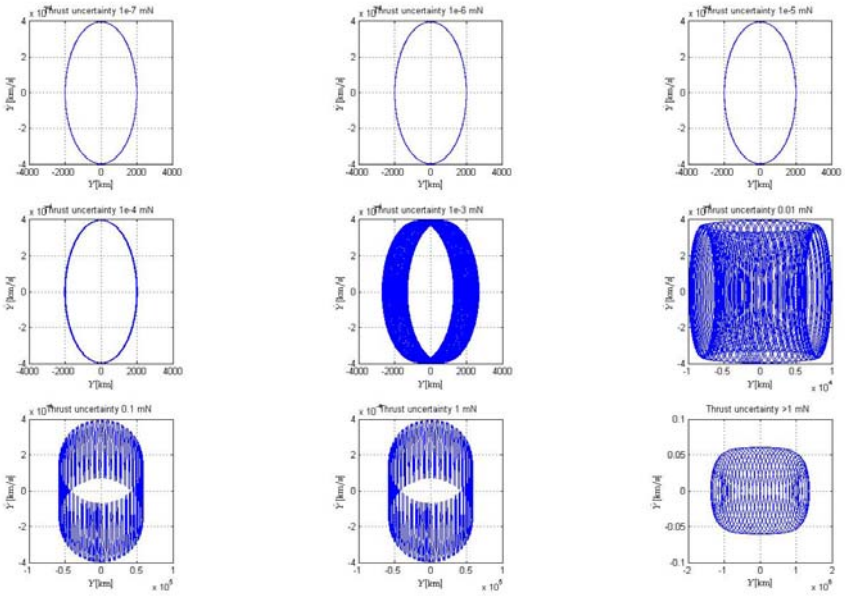

Figure 4.13 State space $(Y - \dot{Y})$ for various values of thrust uncertainty, initial amplitudes $(\delta_x = 1e3\ km, \delta_y = 0\ km, \delta_z = 1e3\ km)$

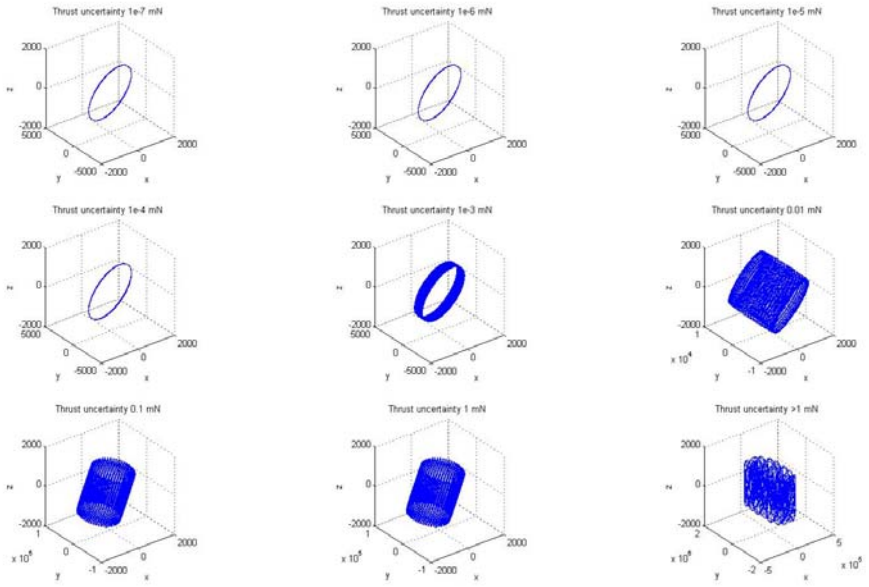

Figure 4.14 3D trajectory for various values of thrust uncertainty, initial amplitudes ($\delta_x = 1e3\ km, \delta_y = 0\ km, \delta_z = 1e3\ km$)

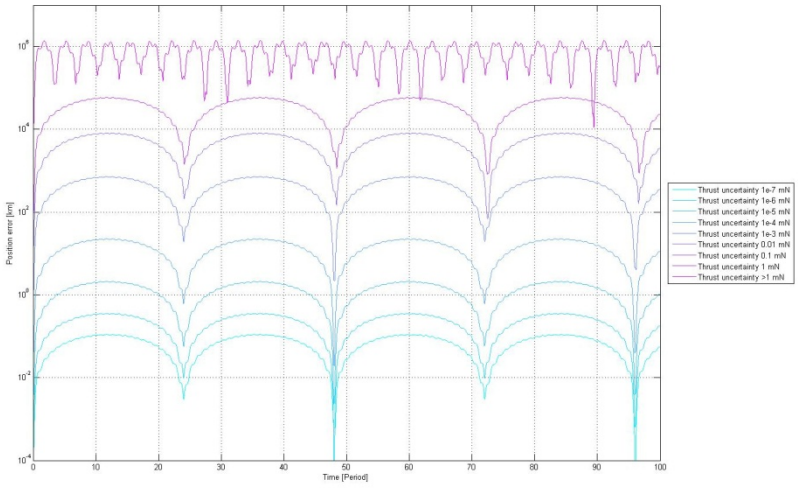

Figure 4.15 Error on Y for various values of thrust uncertainty, initial amplitudes ($\delta_x = 1e4\ km, \delta_y = 0\ km, \delta_z = 1e4\ km$)

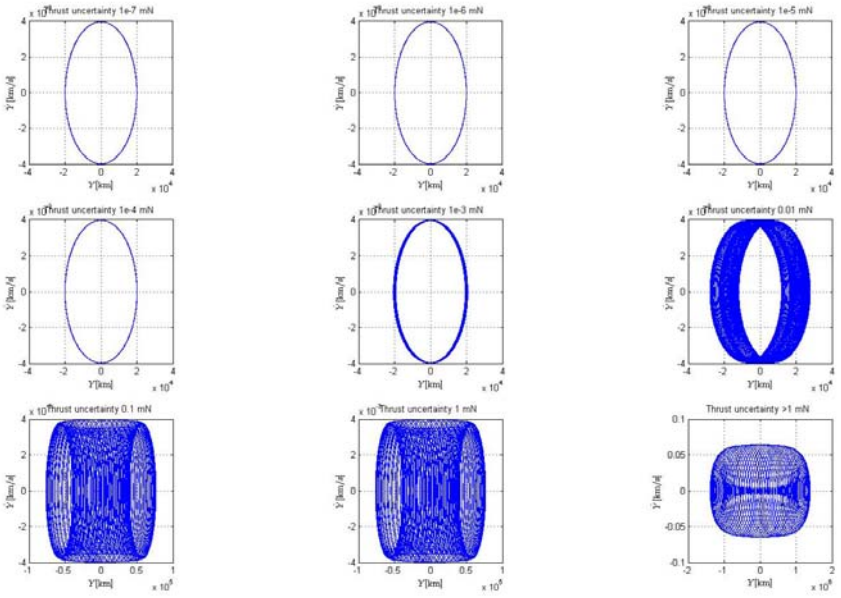

Figure 4.16 State space $(Y - \dot{Y})$ for various values of thrust uncertainty, initial amplitudes $(\delta_x = 1e4\ km, \delta_y = 0\ km, \delta_z = 1e4\ km)$

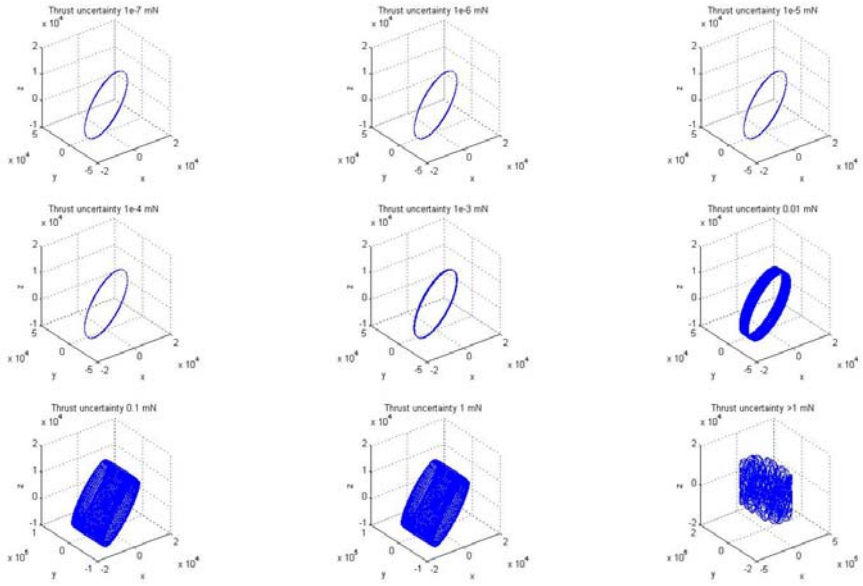

Figure 4.17 3D trajectory for various values of thrust uncertainty, initial amplitudes $(\delta_x = 1e4\ km, \delta_y = 0\ km, \delta_z = 1e4\ km)$

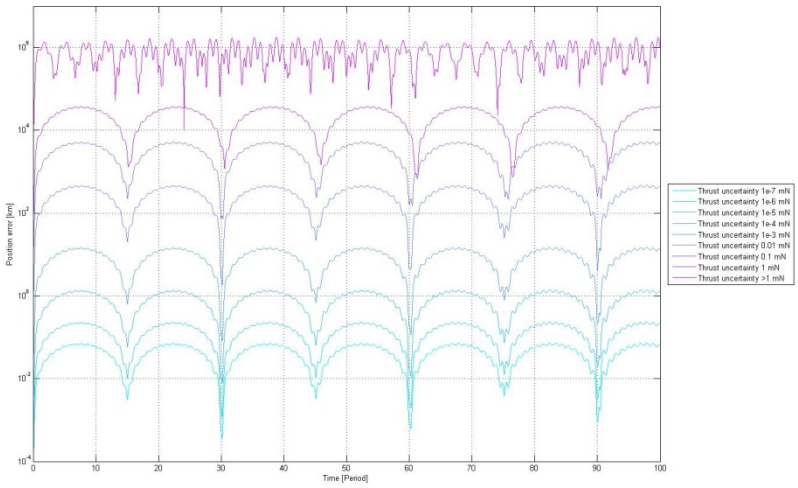

Figure 4.18 Error on Y for various values of thrust uncertainty, initial amplitudes $(\delta_x = 1e5\ km, \delta_y = 0\ km, \delta_z = 1e5\ km)$

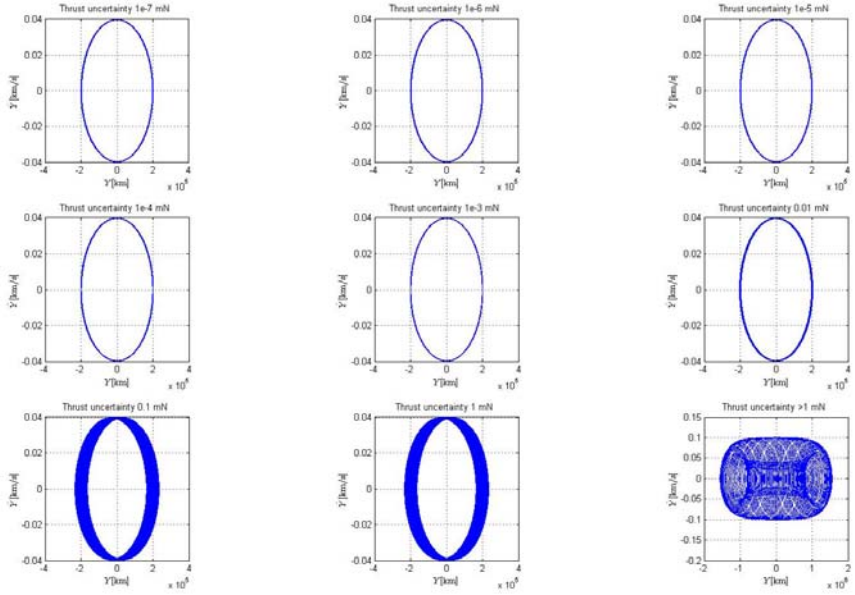

Figure 4.19 State space $(Y - \dot{Y})$ for various values of thrust uncertainty, initial amplitudes $(\delta_x = 1e5\ km, \delta_y = 0\ km, \delta_z = 1e5\ km)$

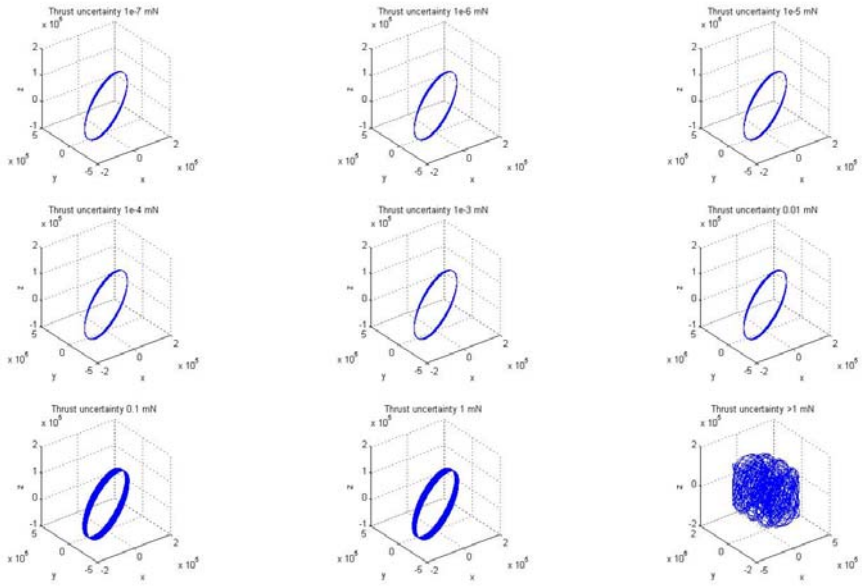

Figure 4.20 3D trajectory for various values of thrust uncertainty, initial amplitudes $(\delta_x = 1e5\ km, \delta_y = 0\ km, \delta_z = 1e5\ km)$

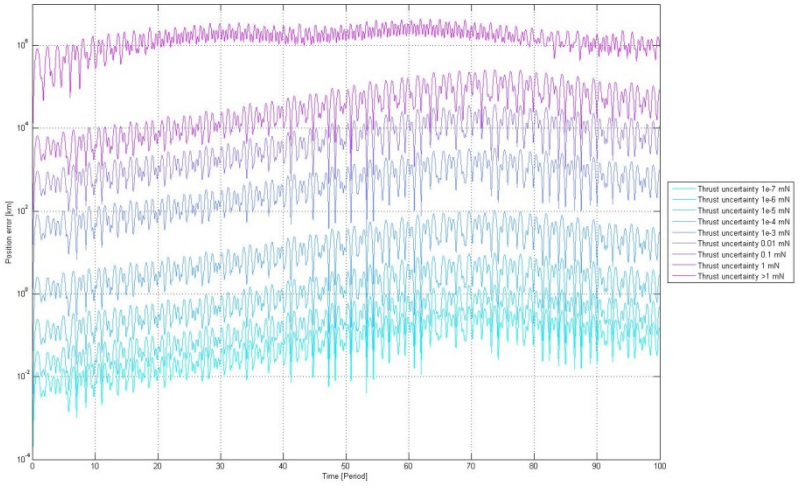

Figure 4.21 Error on Y **for various values of thrust uncertainty, initial amplitudes** $(\delta_x = 1e5\ km, \delta_y = 0\ km, \delta_z = 1e5\ km)$

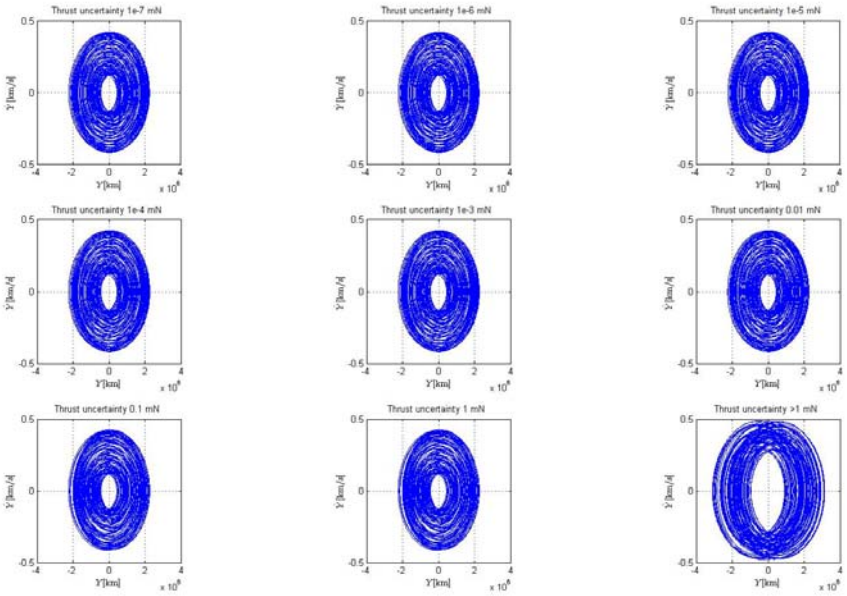

Figure 4.22 State space $(Y - \dot{Y})$ for various values of thrust uncertainty, initial amplitudes $(\delta_x = 1e6\ km, \delta_y = 0\ km, \delta_z = 1e6\ km)$

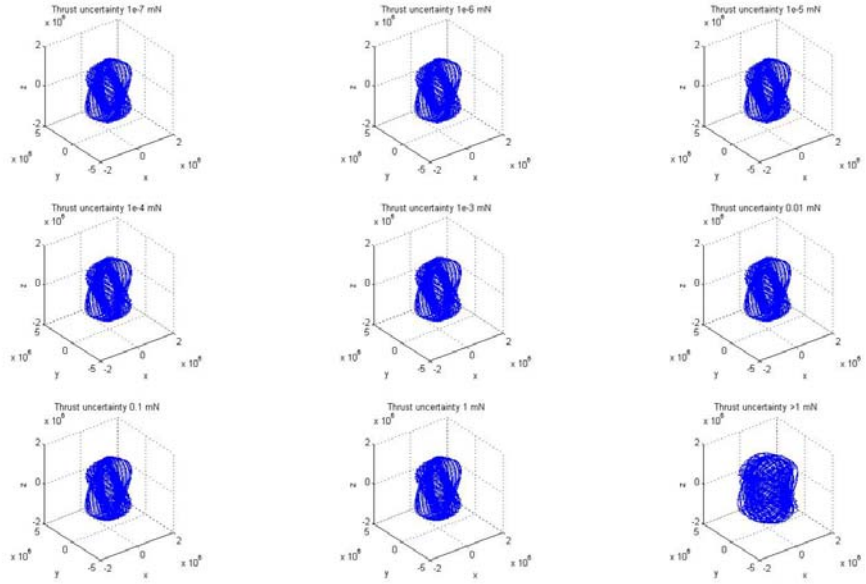

Figure 4.23 3D trajectory for various values of thrust uncertainty, initial amplitudes $(\delta_x = 1e6\ km, \delta_y = 0\ km, \delta_z = 1e6\ km)$

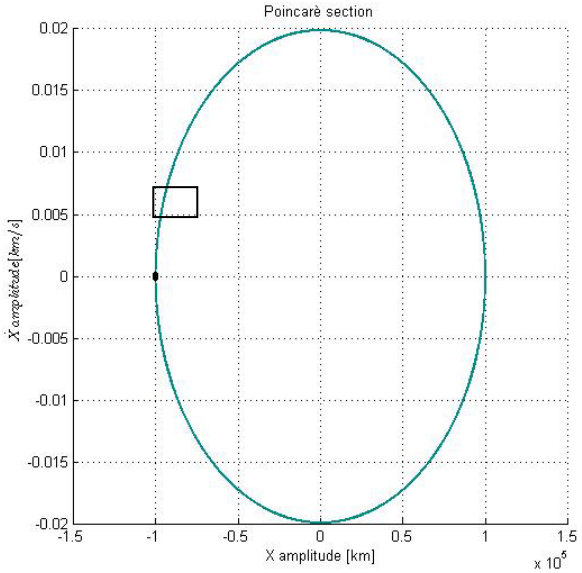

Figure 4.24 Poincarè section, uncertainty 1e-7 mN, initial amplitudes ($\delta_x = 1e5\ km, \delta_y = 0\ km, \delta_z = 1e5\ km$)

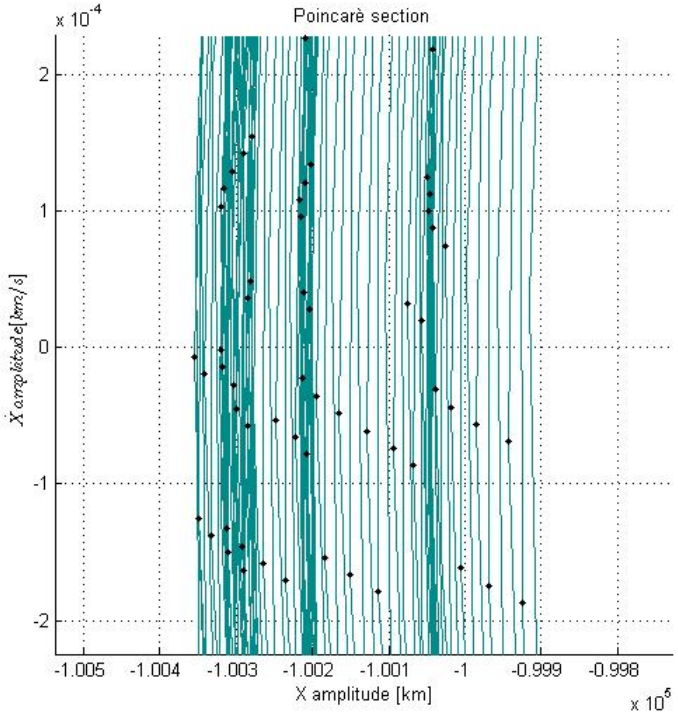

Figure 4.25 Poincarè section, zoom of figure 4.24

4.2 Discussion

It's apparent that linearization requires that orbits must have small amplitudes whereas in order that propagated orbits behave like analytical one, amplitude must be high. These two constrains are evidently in contrast.
Like periodic orbits around natural equilibrium point, periodic orbit around AEP are obtained only for amplitudes higher enough that nonlinear contribution isn't negligible.

Nevertheless periodic orbit can be achieved taking into account some aspect: due to the high sensitivity of the problem to all parameters it is important that libration trajectories are modeled accurately. The integration of equations of motion must be very precise (high order numerical integrators like Runge Kutta 7-8 should be employed). Also precise force modeling is required including secondary gravity potential field, multiple 3-body perturbation effects and solar radiation pressure. Furthermore a targeting approach is generally adopted, making use of a differential corrector (DC) to achieve orbit goals.

Finding a periodic orbit around an AEP is thus laborious since the first approximation gives initial conditions that once employed in a propagator that make use of all force and perturbations don't allow a periodic motion.
A target sequence that has appropriate objective must be used in order to change initial conditions and achieve periodic orbit.

It is also apparent that the control strategy used is an open loop control, obviously a closed loop control must be employed to improve the trajectory design.

5 AEPs stable regions and Software validation

In this chapter regions where AEPs are stable are presented with the thrust necessary for a 1000 kg spacecraft to transform a non-equilibrium point into an AEP for various three body problem.
Also some orbits of various type are propagated and results are compared with tadpole and horseshoe orbit and benchmark orbit obtained by Morimoto (16) to validate the developed computational tools. Lastly results output by the tool are inputs in the commercial orbit propagator STK, developed by AGI, to obtain finer solution thanks to finer numerical models implemented in the mentioned software.

5.1 Search for AEP

To find stable, periodic AEPs for which the required thrust is less than some fixed value, a three dimensional grid has been build, and for each point thrust required, stability and periodicity has been checked.
These checks are performed in the following way:

- ***Thrust required***
  First acceleration needed to cancel gravity pull and centrifugal acceleration is found in the synodic rectangular reference frame. Then by multiplying the norm of these accelerations by the total spacecraft mass the thrust required is obtained.

- ***Stability***
  The real part of the **A** matrix eigenvalues (§3.2.1) is checked; to achieve oscillatory motion the real part should be zero; actually, it turns out that the real part is not exactly zero, anyway whenever the magnitude is very low compared to the propagation time the motion is marginally stable. So the check is performed in this way:

  $$0.999 \le e^{\sigma t} \le 1.001$$

  thus

  $$\ln(0.999) \le \sigma t \le \ln(1.001) \rightarrow -0.001 \le \sigma t \le 0.00099$$

This must hold for large propagating time, anyway missions on AEPs expend fuel. The time chosen is about 10000 days, clearly is extremely high with respect to actual missions lifetime but it is a conservative choice. Hence the previous equations can be rewritten as

$$\frac{-0.001}{3600 \cdot 24 \cdot 10000} \leq \sigma \leq \frac{0.00099}{3600 \cdot 24 \cdot 10000}$$

$$-1.16 \cdot 10^{-12} \leq \sigma \leq 1.15 \cdot 10^{-12}$$

Accordingly the check can be:

$$\left|\mathrm{Re}(\boldsymbol{\lambda})\right| < 10^{-12}$$

where

$$\boldsymbol{\lambda} = \{\lambda_1 \quad \lambda_2 \quad \lambda_3 \quad \lambda_4 \quad \lambda_5 \quad \lambda_6\}^T$$

$$\lambda_{j,j+1} = \sigma_j \pm i\omega_j \qquad j = 1,3,5$$

Since a double pole in zero would imply instability, an additional check is made: if the first check on stability is verified, the following must also be true

$$\mathrm{Im}(\boldsymbol{\lambda}) \neq \mathbf{0}$$

- ***Periodicity***

  To verify periodicity the ratio between imaginary part of eigenvalues must be less than some tolerance. In the present case the tolerance value was set to *1E-3*. Thus:

$$\left|\mathrm{Round}\left[\frac{\max(\omega_1,\omega_3)}{\min(\omega_1,\omega_3)}\right] - \frac{\max(\omega_1,\omega_3)}{\min(\omega_1,\omega_3)}\right| < 10^{-3}$$

  or

$$\left|\mathrm{Round}\left[\frac{\max(\omega_2,\omega_3)}{\min(\omega_2,\omega_3)}\right] - \frac{\max(\omega_2,\omega_3)}{\min(\omega_2,\omega_3)}\right| < 10^{-3}$$

The following graphs (from figure 5.1 to 5.17) show stability region, thrust contour and periodic points for various three body problem.

5.1.1 Stable region and thrust contour (Sun-Earth System)

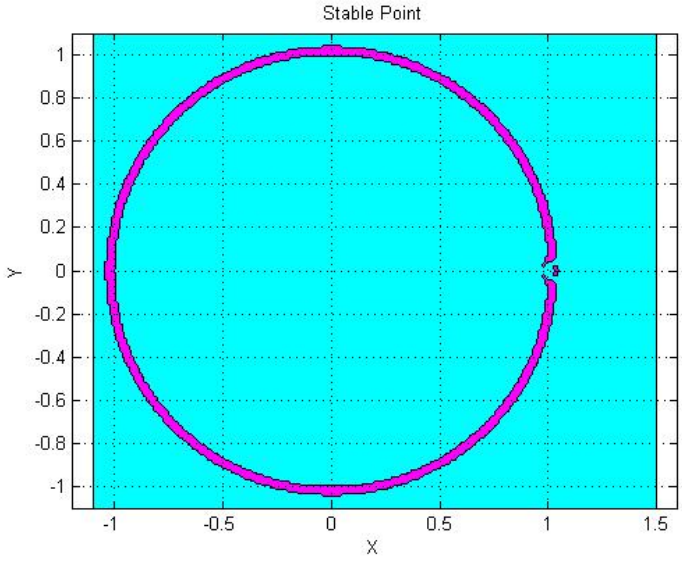

Figure 5.1 Stable point region (magenta), Sun-Earth System (z=0)

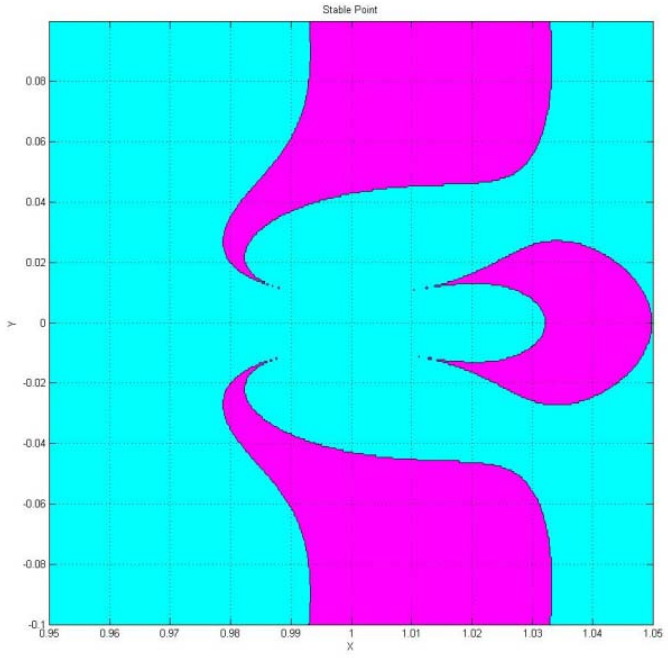

Figure 5.2 Stable point region (magenta), Sun-Earth System (0.95<x<1.05,z=0)

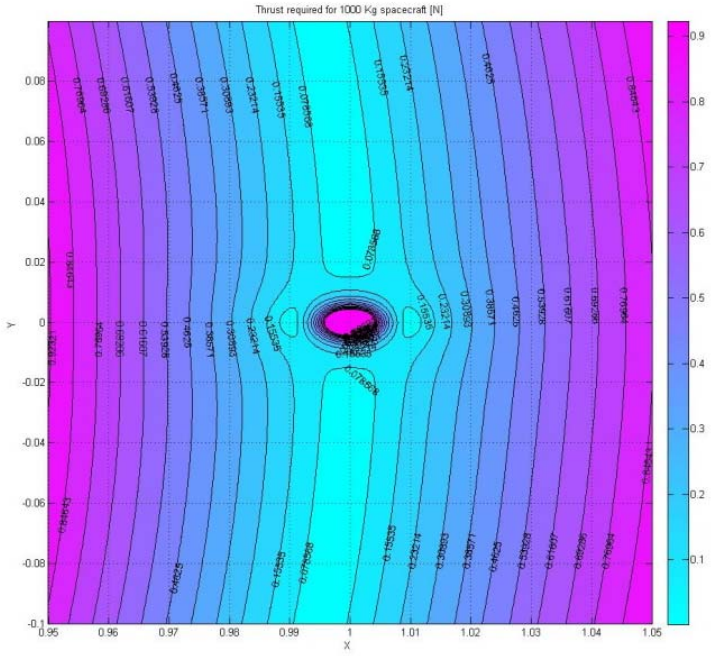

Figure 5.3 Thrust contour, Sun-Earth system (0.95<x<1.05, z=0)

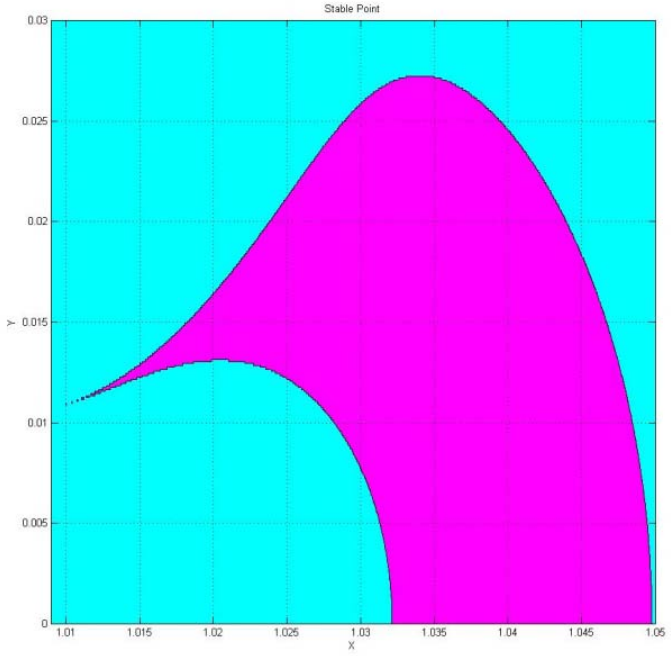

Figure 5.4 Stable point region (magenta), Sun-Earth System (1.01<x<1.05, z=0)

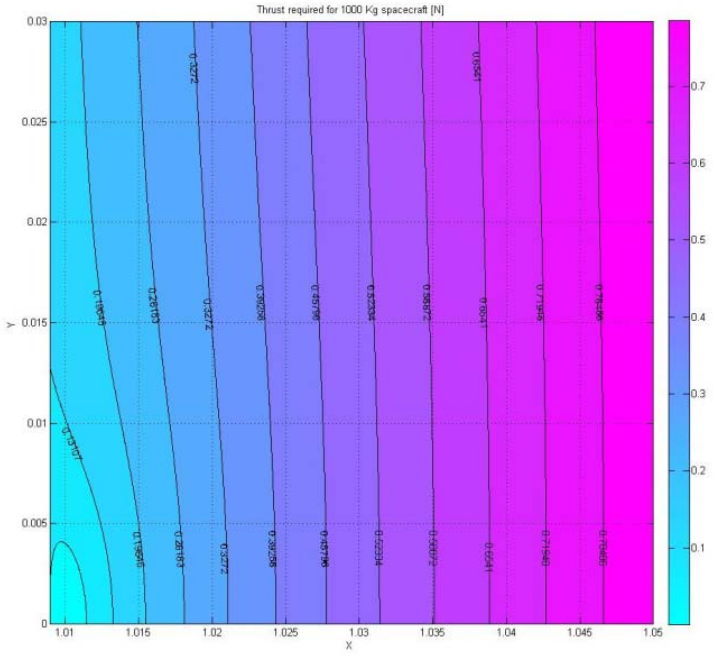

Figure 5.5 Thrust contour, Sun-Earth system (1.01<x<1.05, z=0)

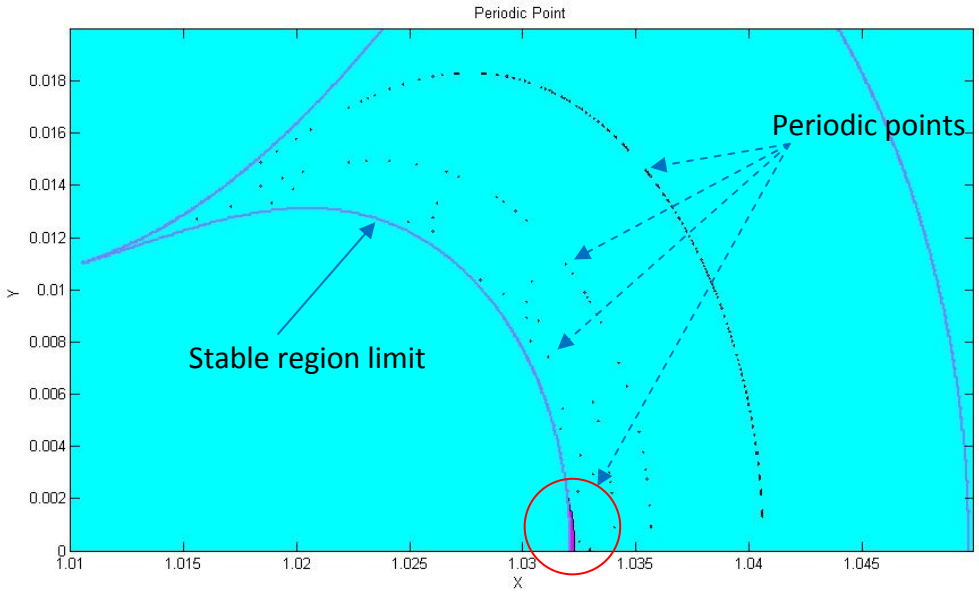

Figure 5.6 Periodic points, Sun-Earth system (z=0)

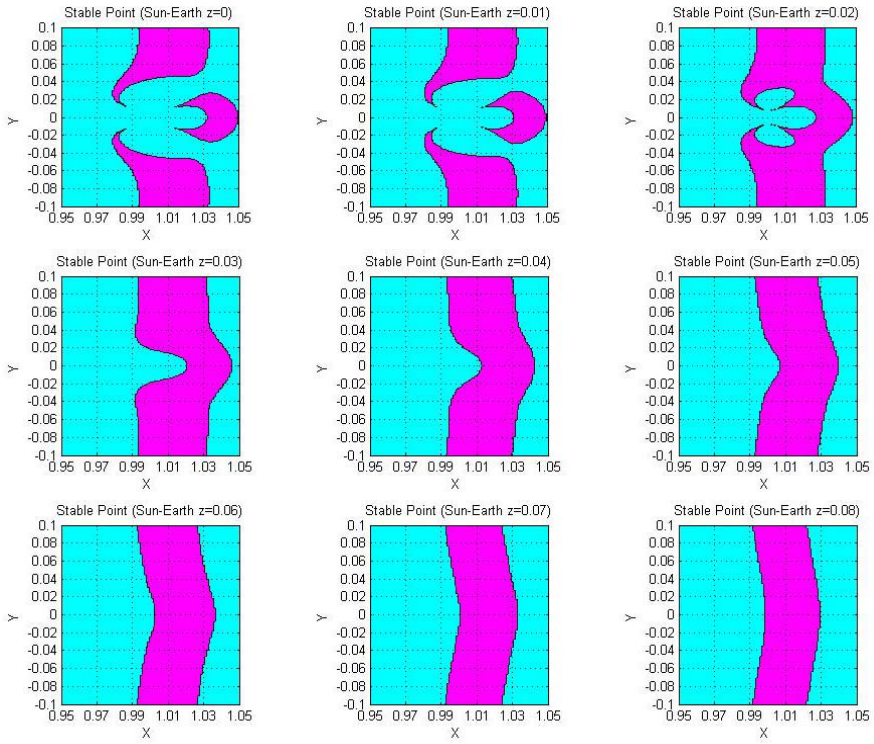

Figure 5.7 Stable point region (magenta), Sun-Earth System(0<z<0.08)

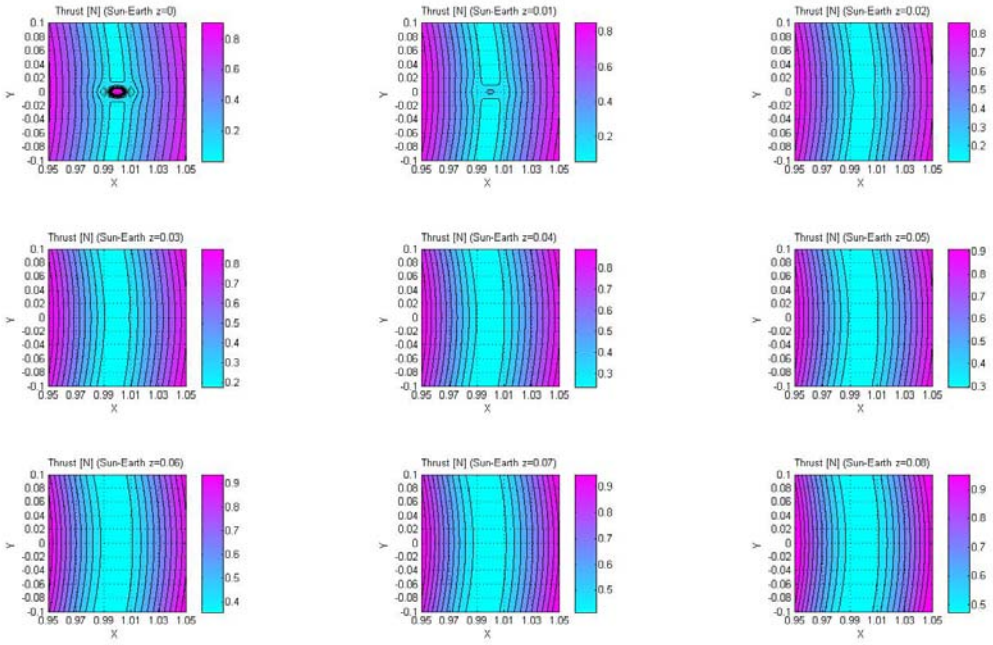

Figure 5.8 Thrust contour, Sun-Earth system (0<z<0.08)

All the graphs are computed with nondimensional approach of §3.3. In figures 5.1, 5.2, 5.4 and 5.7 stable regions are highlighted in violet, while the unstable region is cyan. Since L_2 is located at 1.01 on the X axis, in figure 5.4 is evident that the stable region is far from the Earth than L_2.
Figures 5.3 and 5.5 shows that thrust is higher near the Earth, and far from it, and as expected there are two minimum at 1.01 and 0.99 (L_2 and L_1 respectively). Figure 5.6 is obtained with a finer grid than other figures, this is due to find those points where orbits can be periodic. These are not points, but actually, regions, in fact these regions are so small that at this scale they seem points. The only region that is visible is that highlighted in the red circle. It is evident that the periodic condition is very restrictive since a only a small portion of the stable region allow this type of motion. Figures 5.7 and 5.8 shows the stable regions and thrust contours as function of z. The range of z reported is $0 \leq z \leq 0.08$, this because this range is the most interesting because as figure 5.7 shows, is clear that for $z = 0.02$ the two stable regions coalesce, and in this case, stable points can be found also for $x < 1.01$. The only, and obvious thing, that figure 5.8 shows, is that by increasing z also the thrust magnitude is increased.

5.1.2 Stable region and thrust contour (Earth-Moon System)

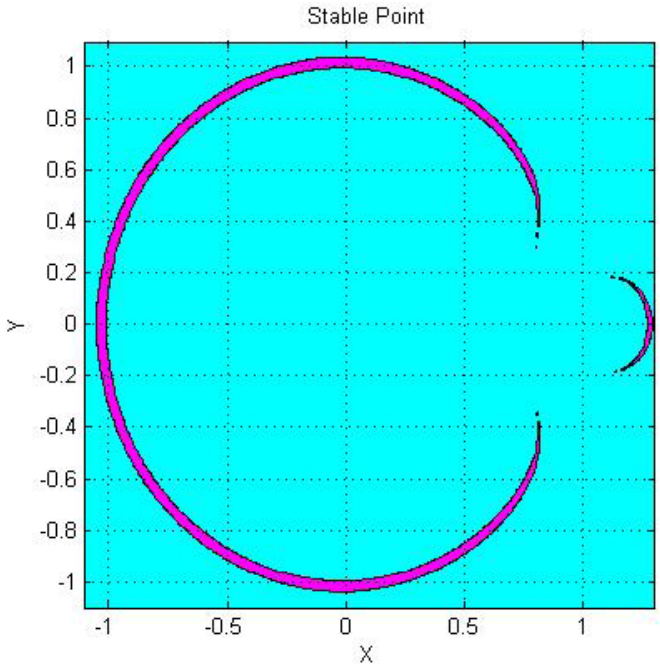

Figure 5.9 Stable point region (magenta), Earth-Moon System (z=0)

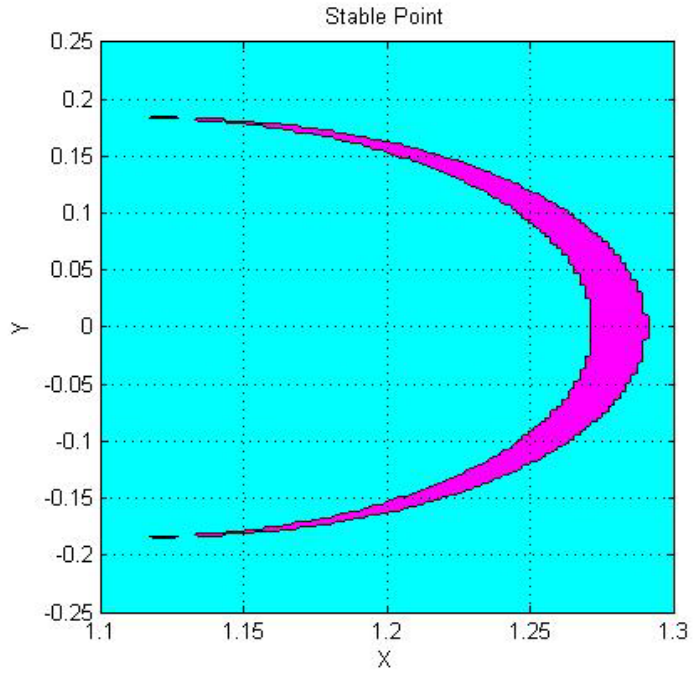

Figure 5.10 Stable point region (magenta), Earth-Moon System (1.1<x<1.3, z=0)

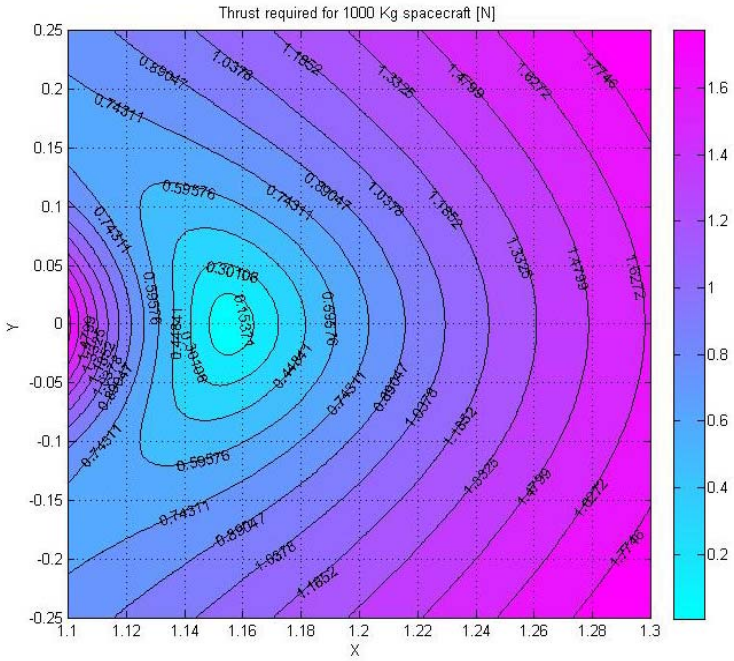

Figure 5.11 Thrust contour, Earth-Moon system (1.1<x<1.3, z=0)

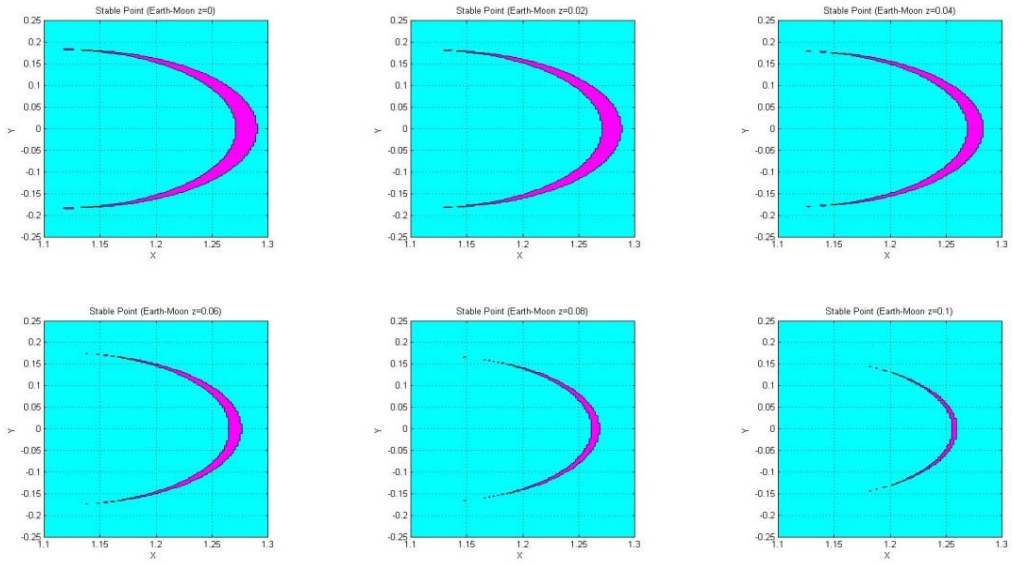

Figure 5.12 Stable point region (magenta), Earth-Moon System(0<z<0.1)

All the things said about Sun-Earth system are still valid, anyway for Earth-Moon mass ratio, it's apparent that the stability region (fig. 5.9 & 5.10) and the thrust contours (fig. 5.11) are quite different: near the less massive primary (x=1), there is only one region, and by increasing z, this region thins (Figure 5.12). In figure 5.11 as expected there is a minimum on thrust at $x = 1.156$ (L_2), in this case the contour shows that the thrust is also strongly dependant by y direction.

5.1.3 Stable region and thrust contour (Sun-Jupiter System)

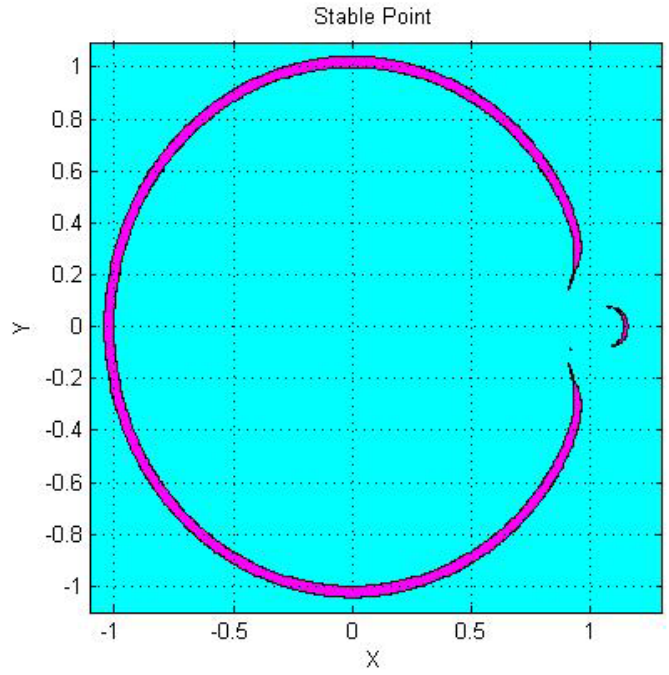

Figure 5.13 Stable point region (magenta), Sun-Jupiter System (z=0)

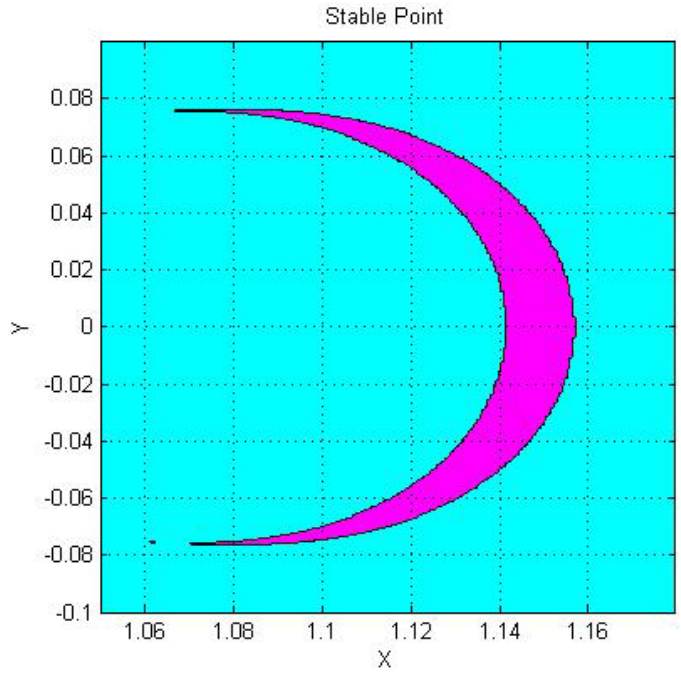

Figure 5.14 Stable point region (magenta), Sun-Jupiter System (1.06<x<1.16, z=0)

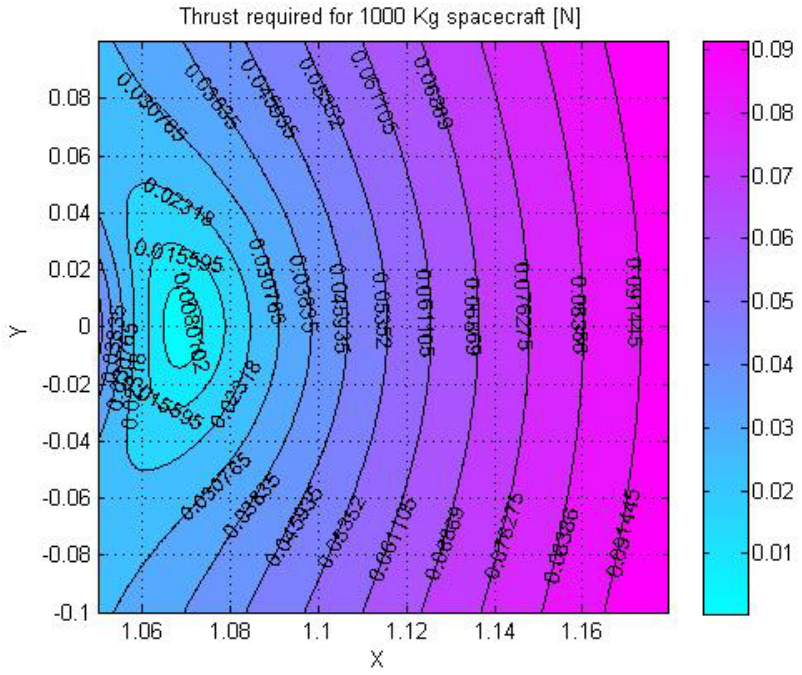

Figure 5.15 Thrust contour, Sun-Jupiter system (1.06<x<1.16, z=0)

Analyzing the pictures from 5.13 to 5.15 it's evident that the Sun-Jupiter system, is qualitatively identical to Earth-Moon system.

5.1.4 Stable region and thrust contour (Sun-Ceres System)

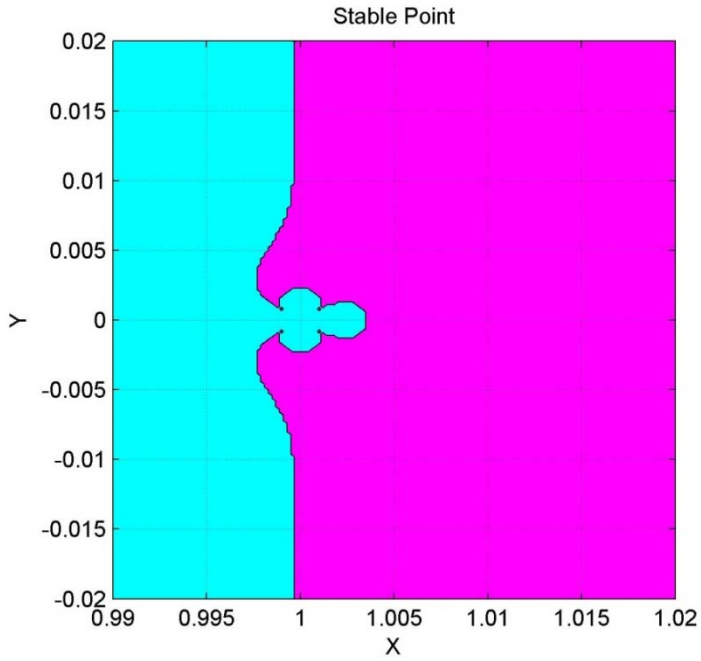

Figure 5.16 Stable point region (magenta), Sun-Ceres system (1.06<x<1.16, z=0)

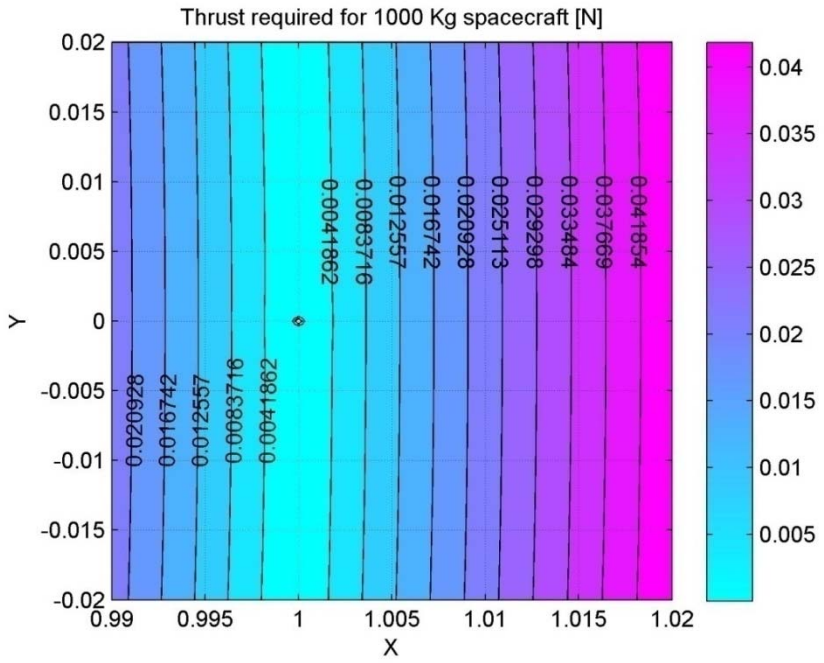

Figure 5.17 Thrust contour, Sun-Ceres system (0.99<x<1.02, z=0)

Pictures 5.16 and 5.17 shows the stable region and thrust contour for a system with the mass of second primary very small compared to that of the first primary. In this case the Sun-Ceres system is considered. The first thing that emerges is that the stability region "try to enclose" the less massive primary. In figure 5.17 the location of L_2 and L_1 aren't visible, this is due because of the scale (since L_2 is at ~1.0005 and L_1 is at ~0.9995).

5.1.5 Thrust comparison

In all analyzed systems it is clearly seen that as $\bar{\mu}_2$ increases, L_2 moves to the right and the minimum thrust zone move consequently. This fact can be also seen in picture 5.18 where qualitative, adimensional thrust contour are shown for various values of $\bar{\mu}_2$. In order get some insight, various values of $\bar{\mu}_2$ for various TBP are listed in table 5.1.

Table 5.1 values of $\bar{\mu}_2$function for the TBP considered.

	Sun-Earth	Earth-Moon	Sun-Mars	Sun-Jupiter	Jupiter-Europa	Sun-Saturn	Sun-Ceres
$\bar{\mu}_2$	3e-6	0.012	3.2e-7	9.5e-4	2.5e-5	2.8e-4	4.7e-10

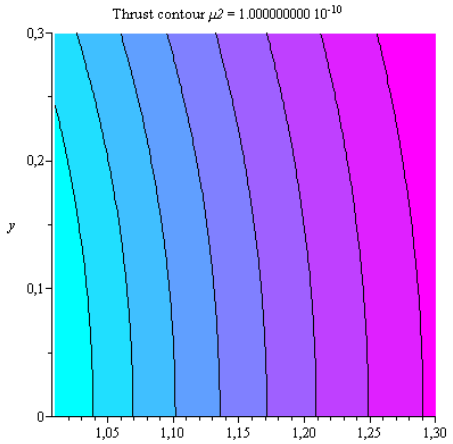

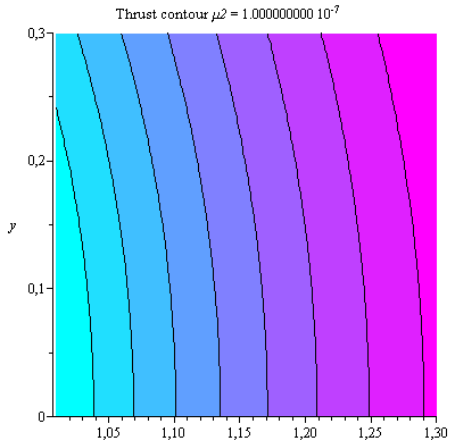

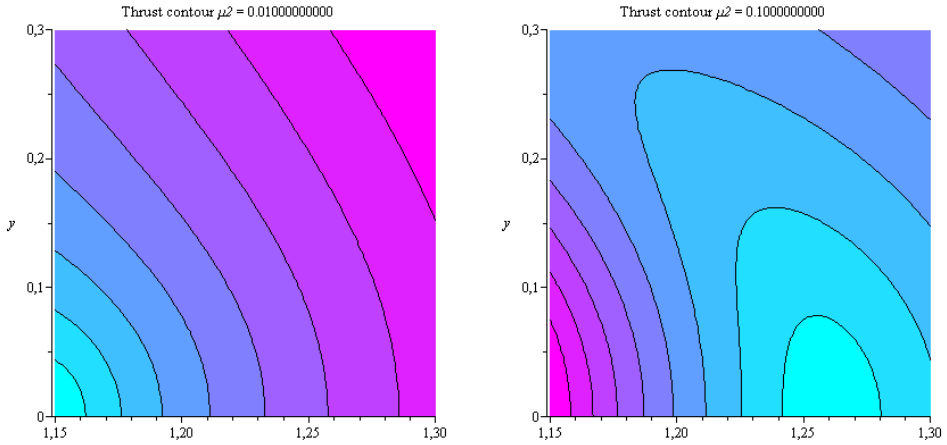

Figure 5.18 qualitative thrust contour, it should be noted that the in all picture the minimum thrust value move to the right, this effect is more visible in the third and fourth pictures.

Quantitative value of thrust are visible in figures 5.5, 5.11,5.15 and 5.17. for convenience, in table 5.2 are reported maximum values obtained from the pictures.

Table 5.2 values of μ_2 function for the TBP considered.

	Sun-Earth	Earth-Moon	Sun-Jupiter	Sun-Ceres
Thrust for 1000 kg spacecraft	0.8 N	1.7 N	0.1 N	0.045 N

Is to be noted that the values in table 5.2 are only indicative of the thrust magnitude. It is apparent that, in principle, since this values are very low, an electric thruster could be employed (e.g. ion thruster). In the case of "high thrust" such as the one required in the Earth-Moon system, a couple of Hall effect thruster could be employed.

5.2 Tadpole and horseshoe orbits

Before verifying that orbits around AEPs are correctly propagated, orbits around the triangular points were analyzed in order to possibly debug the software.
The motion of an object located in proximity of L_4/L_5 is generally referred as *tadpole orbit* because of the elongated shapes of the orbits. Orbit encompass both L_4 and L_5 are referred as *horseshoe orbit*.

Solution obtained for different starting points are plotted in the following graphs (from 5.19 to 5.23). The same solution has been illustrated in Murray (10) and in Taylor (19).

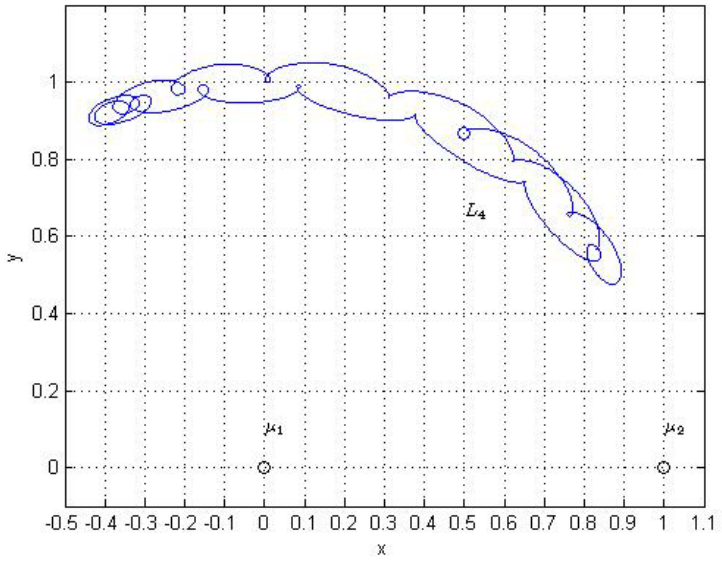

Figure 5.19 Tadpole orbit librating about L_4 equilibrium point ($x_0=1/2-\mu_2, y_0=\sqrt{3}/2$) for $\mu_2=0.001$. Starting conditions are $x=x_0+0.0065$, $y=y_0+0.0065$, $z=0$, $\dot{x}=\dot{y}=\dot{z}=0$. Orbit Is followed for 15 orbital periods (30π)

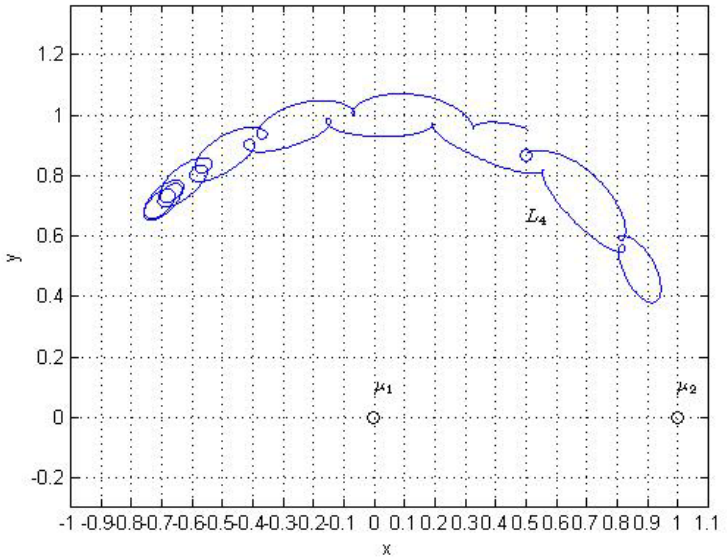

Figure 5.20 Tadpole orbit librating about L_4 equilibrium point ($x_0=1/2-\mu_2, y_0=\sqrt{3}/2$) for $\mu_2=0.001$. Starting conditions are $x=x_0+0.008$, $y=y_0+0.008$, $z=0$, $\dot{x}=\dot{y}=\dot{z}=0$. Orbit Is followed for 15.5 orbital periods (31π)

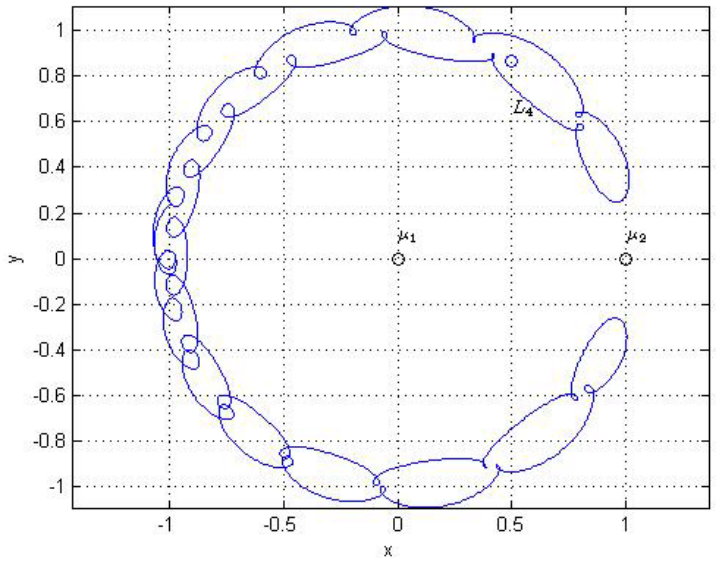

Figure 5.21 Horseshoe orbit librating about L_4 equilibrium point ($x_0=1/2-\mu_2, y_0=\sqrt{3}/2$) for $\mu_2=0.001$. Starting conditions are $x=-0.97668$, $y=0$, $z=0$, $\dot{x}=0$, $\dot{y}=-0.06118$, $\dot{z}=0$. Orbit Is followed for 30 orbital periods (60π)

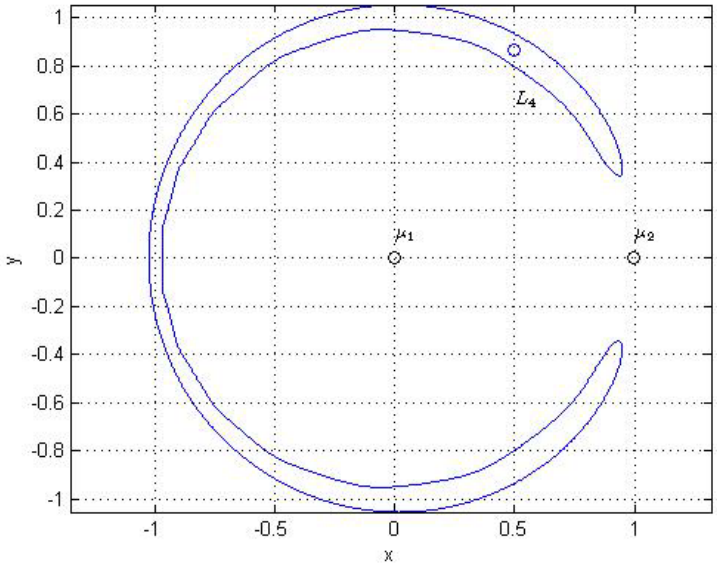

Figure 5.22 Horseshoe orbit librating about L_4 equilibrium point ($x_0=1/2-\mu_2, y_0=\sqrt{3}/2$) for $\mu_2=0.001$. Starting conditions are $x=-1.02745$, $y=0$, $z=0$, $\dot{x}=0$, $\dot{y}=0.04032$, $\dot{z}=0$. Orbit Is followed for 30 orbital periods (60π)

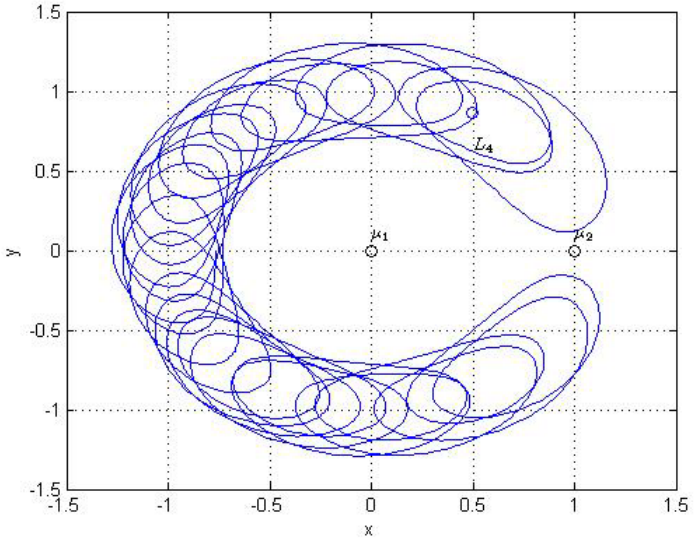

Figure 5.23 Horseshoe orbit librating about L_4 equilibrium point ($x_0=1/2-\mu_2, y_0=\sqrt{3}/2$) for $\mu_2=0.001$. Starting conditions are $x=-0.76665$, $y=0$, $z=0$, $\dot{x}=0$, $\dot{y}=-0.5123$, $\dot{z}=0$. Orbit Is followed for 30 orbital periods (60π)

5.3 AEP Benchmark orbits

In the following section some results are shown, the same results are found in "**Periodic orbits with low thrust propulsion in the restricted three body problem"** Morimoto (8). The Sun-Earth system is considered. All the orbits considered are obtained with constant control acceleration. It's to be noted that the values of points coordinates could slightly differ from the one used by Morimoto, this because the values here presented are computed by the software.

Tables from 5.3 to 5.6 shows AEPs coordinates, constant acceleration required, period and thrust needed for a 1000 kg spacecraft for four orbits used as benchmark. In the same table results obtained by Morimoto are presented.

5.3.1 First Orbit

The initial perturbed position is:

$\delta_x = 0$ [*Km*]

$\delta_y = 15$ [*Km*]

$\delta_z = 15$ [*Km*]

Table 5.3 First benchmark orbit.

	Current Results	***Morimoto Results***
Equilibrium Point coordinates		
x	1.03223 [---]	1.03223 [---]
y	0.0 [---]	0.0 [---]
z	0.0 [---]	0.0 [---]
Constant control acceleration		
a_x	$-5.3999 \cdot 10^{-7}$ [Km/s^2]	$-5.38 \cdot 10^{-7}$ [Km/s^2]
a_y	0.0 [Km/s^2]	0.0 [Km/s^2]
a_z	0.0 [Km/s^2]	0.0 [Km/s^2]
Orbit Period (Periodic type: *x:z* 1:1)		
T_x	365.7 [*days*]	365.25 [days]
T_y	5720.7 [*days*]	n/a
T_z	365.5 [*days*]	365.25 [days]
Thrust required (for 1000 Kg spacecraft)		
F_x	-539.99 [*mN*]	n/a
F_y	0.0 [*mN*]	n/a
F_z	0.0 [*mN*]	n/

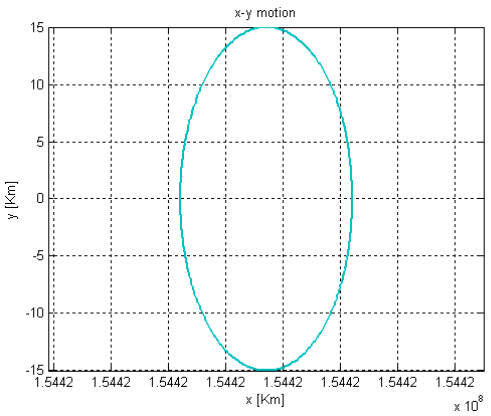

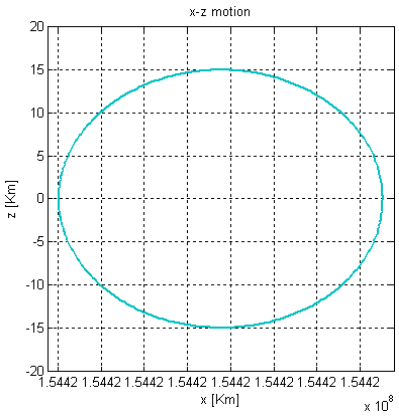

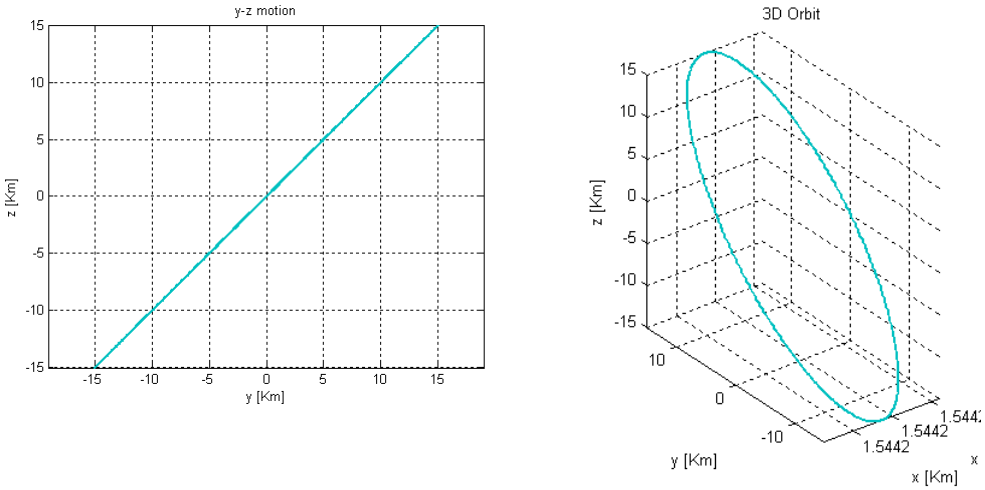

Figure 5.24 Periodic Orbit analytical solution

5.3.2 Second Orbit

The initial perturbed position is:

$\delta_x = 4.8 \ [Km]$

$\delta_y = 15 \ [Km]$

$\delta_z = 15 \ [Km]$

Table 5.4 Second benchmark orbit.

	Current Results	*Morimoto Results*
Equilibrium Point coordinates		
x	1.0405952 [---]	1.040731[---]
y	0.0 [---]	0.0 [---]
z	0.0 [---]	0.0 [---]
Constant control acceleration		
a_x	$-6.85049 \cdot 10^{-7}$ [Km/s^2]	$-6.86 \cdot 10^{-7}$ [Km/s^2]
a_y	0.0 [Km/s^2]	0.0 [Km/s^2]
a_z	0.0 [Km/s^2]	0.0 [Km/s^2]
Orbit Period (Periodic type: *y:z* 1:1)		
T_x	399.7 [*days*]	n/a
T_y	756.8 [*days*]	756 [days]
T_z	378.3 [*days*]	378 [days]
Thrust required (for 1000 Kg spacecraft)		
F_x	-685.05 [*mN*]	n/a
F_y	0.0 [*mN*]	n/a
F_z	0.0 [*mN*]	n/a

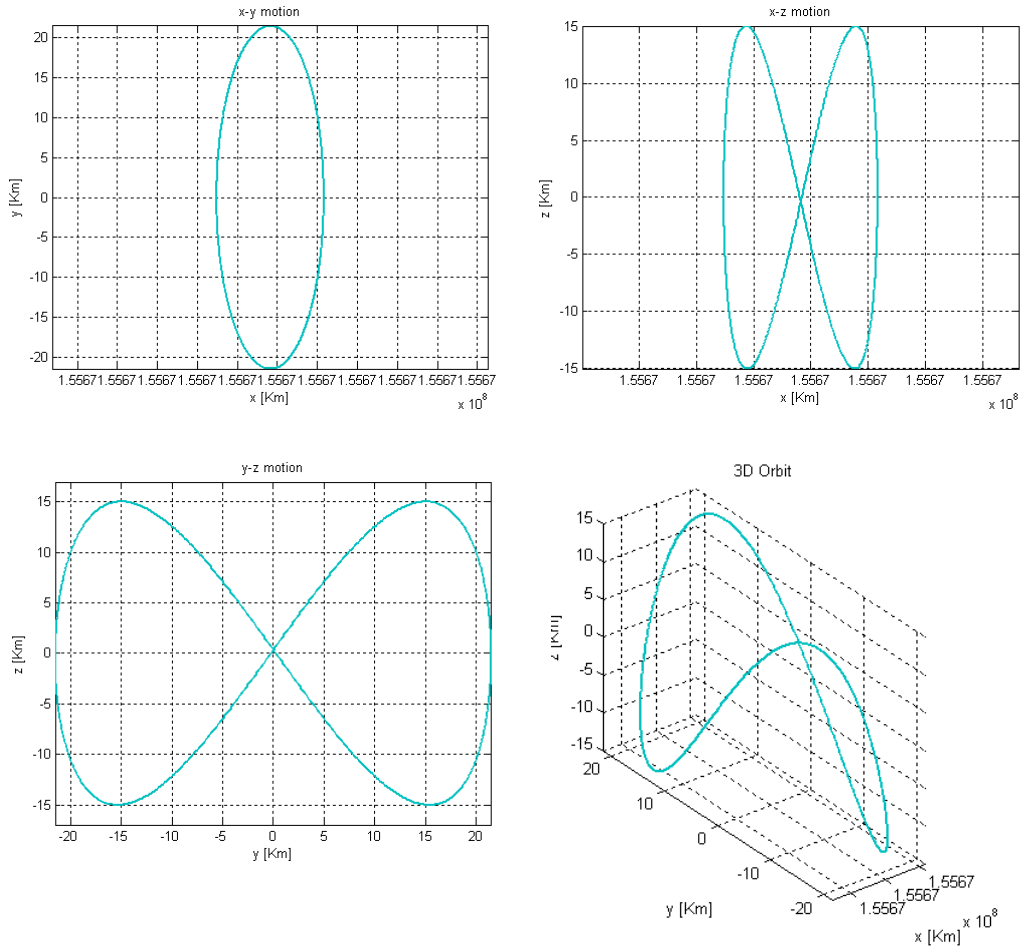

Figure 5.25 Periodic Orbit analytical solution

5.3.3 Third Orbit

The initial perturbed position is:

$\delta_x = 0 \ [Km]$

$\delta_y = 15 \ [Km]$

$\delta_z = 15 \ [Km]$

Table 5.5 Third benchmark orbit.

	Current Results	*Morimoto Results*
Equilibrium Point coordinates		
x	1.03567 [---]	1.035799 [---]
y	0.0 [---]	0.0 [---]
z	0.0 [---]	0.0 [---]
Constant control acceleration		
a_x	$-6.0044 \cdot 10^{-7}$ [Km/s^2]	$-6.01 \cdot 10^{-7}$ [Km/s^2]
a_y	0.0 [Km/s^2]	0.0 [Km/s^2]
a_z	0.0 [Km/s^2]	0.0 [Km/s^2]
Orbit Period (Periodic type: *y:z* 1:3)		
T_x	379. [*days*]	n/a
T_y	1115.1 [*days*]	1115 [days]
T_z	371.6 [*days*]	372 [days]
Thrust required (for 1000 Kg spacecraft)		
F_x	-600.44 [mN]	n/a
F_y	0.0 [mN]	n/a
F_z	0.0 [mN]	n/a

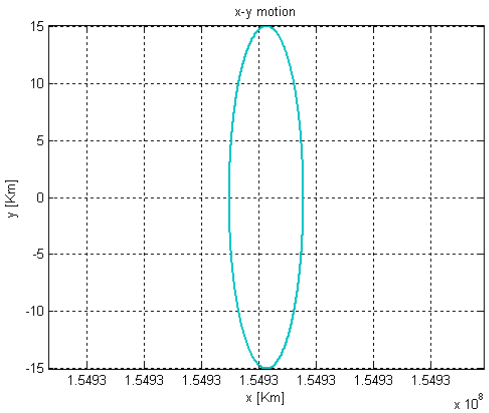

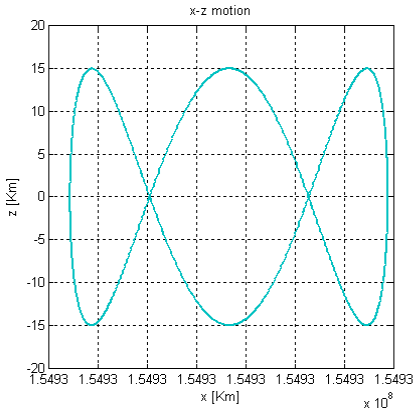

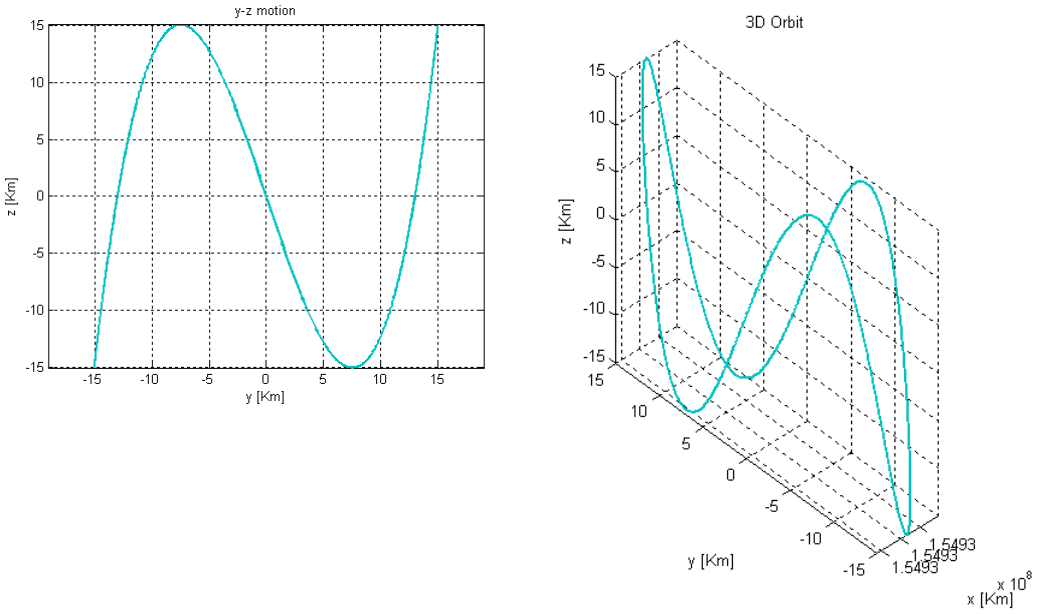

Figure 5.26 Periodic Orbit analytical solution

5.3.4 Fourth Orbit

The initial perturbed position is:

$\delta_x = 6 \ [Km]$

$\delta_y = 15 \ [Km]$

$\delta_z = 15 \ [Km]$

Table 5.6 Fourth benchmark orbit.

	Current Results	Morimoto Results
Equilibrium Point coordinates		
x	1.03406 [---]	1.03418 [---]
y	0.0 [---]	0.0 [---]
z	0.0 [---]	0.0 [---]
Constant control acceleration		
a_x	$-5.7225 \cdot 10^{-7}$ [Km/s^2]	$-5.73 \cdot 10^{-7}$ [Km/s^2]
a_y	0.0 [Km/s^2]	0.0 [Km/s^2]
a_z	0.0 [Km/s^2]	0.0 [Km/s^2]
Orbit Period (Periodic type: *y:z* 1:4)		
T_x	373.06 [*days*]	n/a
T_y	1475.95 [*days*]	1477 [days]
T_z	368.933 [*days*]	369 [days]

Thrust required (for 1000 Kg spacecraft)		
F_x	-572.25 [mN]	n/a
F_y	0.0 [mN]	n/a
F_z	0.0 [mN]	n/a

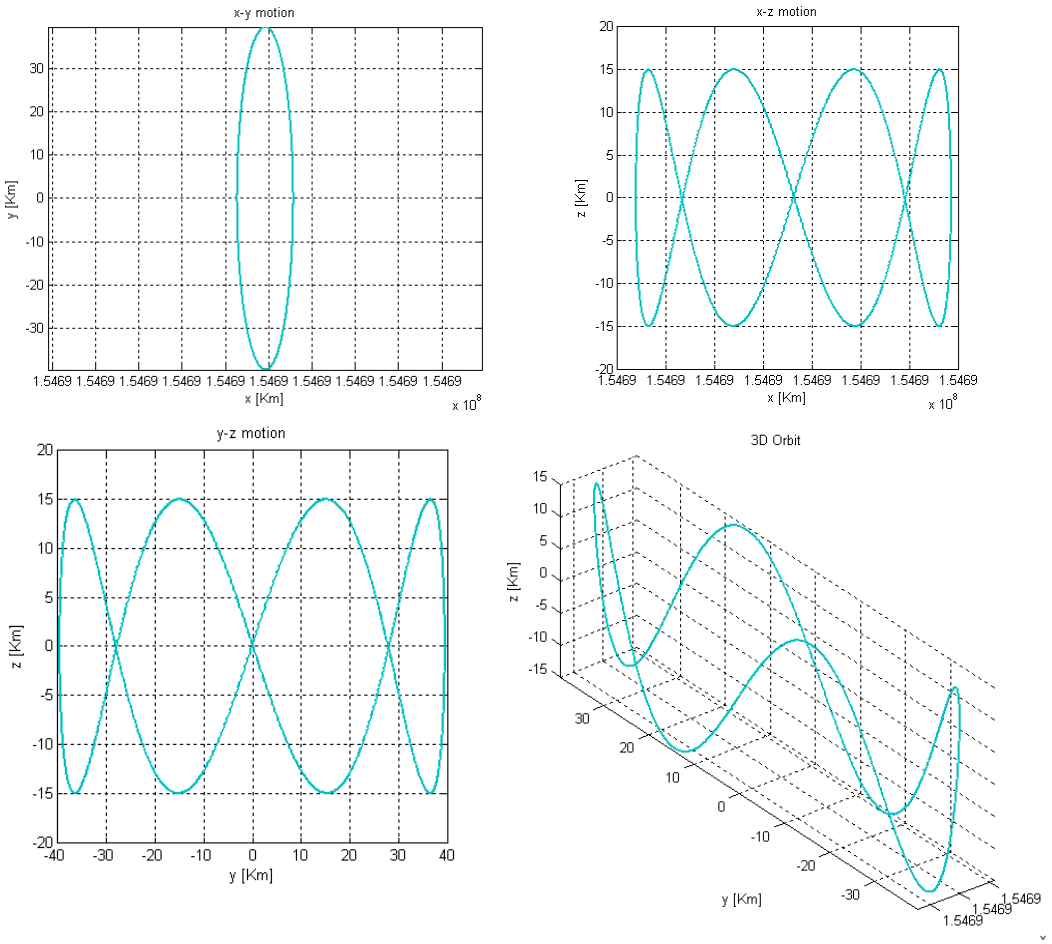

Figure 5.27 Periodic Orbit analytical solution

Pictures from 5.24 to 5.25 shows orbit trajectory for the four benchmark orbits.

5.4 STK analysis: Sun-Earth constant control acceleration

In order to verify that the theory and software developed are able to provide results that can then be used as a starting point for more detailed analysis, a model was built with Astrogator. This is a specialized analysis module for interactive orbit maneuver and spacecraft trajectory design. With this tools is possible to model from low to high accuracy all the problem.

The system analyzed is Sun-Earth, in this case a constant control acceleration AEP is considered.

Point coordinates	
x	154406406 [Km]
y	0.0 [Km]
z	0.0 [Km]
Orbit Period (Periodic type: *x:z* 1:1)	
T_x	365.7 [$days$]
T_y	5720.7 [$days$]
T_z	365.5 [$days$]
Constant control acceleration	
a_x	$-5.37\cdot10^{-7}$ [Km/s^2]
a_y	0.0 [Km/s^2]
a_z	0.0 [Km/s^2]

Initial orbit amplitudes are:

$\delta_x = 3\cdot10^5$ [km]

$\delta_y = 0$ [km]

$\delta_z = 0$ [km]

With these data the initial condition in the synodic reference frame are:

Initial conditions obtained from software			
X_0	154706406 [km]	$\dot{X}_0$	0 [km/s]
Y_0	0 [km]	$\dot{Y}_0$	-0.11944 [km/s]
Z_0	0 [km]	$\dot{Z}_0$	0 [km/s]

As already noted in §4.2, an accurate model must be used, so the following disturbance effects are modeled:

- Earth Gravity field, geopotential coefficients up to degree 4.
- Sun third body perturbation
- Moon third body perturbation
- Mars third body perturbation
- Venus third body perturbation
- Spherical SRP

The only approximation retained is that the primaries orbits are circular and coplanar. The engine is modeled with a constant I_{sp} and constant acceleration. The direction of thrust is that of Earth-Sun in the synodic system.
To numerically integrate the trajectory a Runge Kutta 8-9 method is employed.

Clearly from the introduction of all these new perturbation and from all that has been said in §3, in order to achieve a periodic orbit a shooting method with differential corrector must be employed. Astrogator is able to perform this kind of operation, so a target sequence was build.

Since the problem is symmetric it's clear that when spacecraft cross *XZ* plane, his velocity in *x* and *z* direction must be *0*. Thus with a DC approach is necessary to modify initial V_y and *X* position in order to make the spacecraft velocity V_x and V_z equal to *0* when the spacecraft cross the *XZ* plane.

The new initial conditions in the synodic reference frame are:

Initial conditions obtained from software			
X_0	154813915 [*km*]	$\dot{X}_0$	0 [*km/s*]
Y_0	0 [*km*]	$\dot{Y}_0$	-0.14643 [*km/s*]
Z_0	0[*km*]	$\dot{Z}_0$	0 [*km/s*]

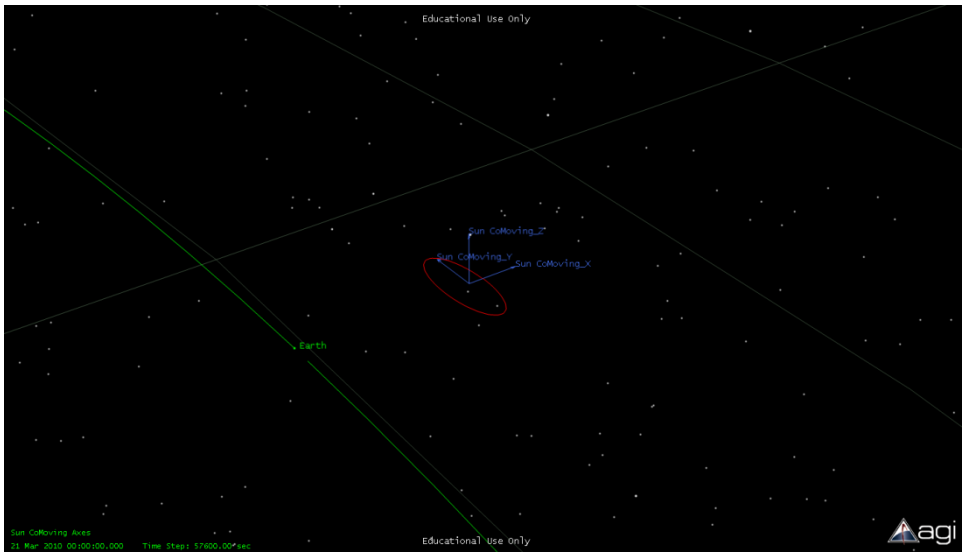

Figure 5.28 Spacecraft trajectory viewed in the synodic frame (red line). Earth orbit (green line) and synodic frame centered on the AEP. Orbit propagated for two XZ plane crossing (period: 639 days).

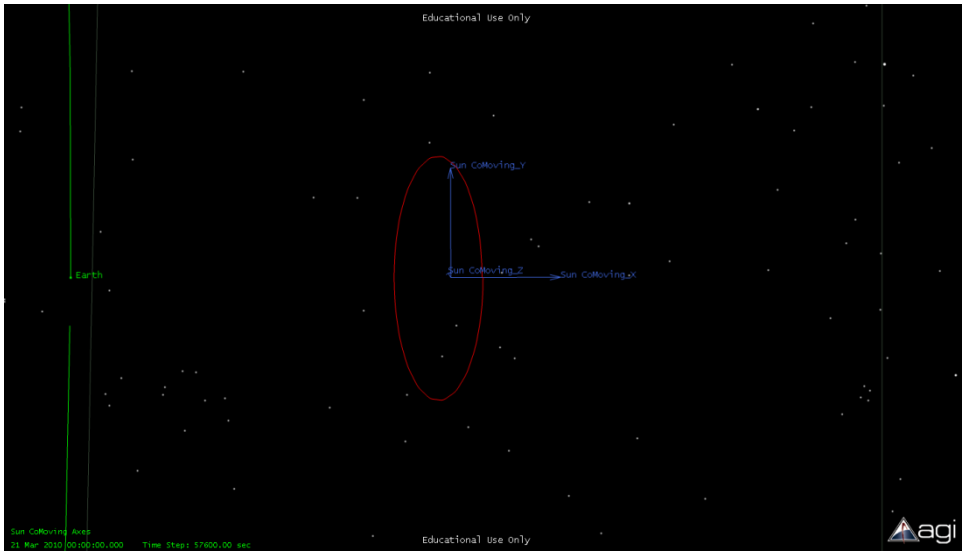

Figure 5.29 Spacecraft trajectory viewed in the synodic frame (XY plane)

With these new initial conditions, the final state is equal to the initial one, but the mean distance from the AEP is increased as can be seen from Figure 5.30 and 5.31; this also imply that the period of the new orbit is greater than the old one.

The main discrepancies with analytical orbit are, as told, the mean distance from the AEP and the period of the orbit. While analytical orbit

have a mean distance from AEP of 4.72E5 km and has a period of about 365 days, the propagated orbit has a mean distance of 1.11E6 km, and its period is about 640 days .

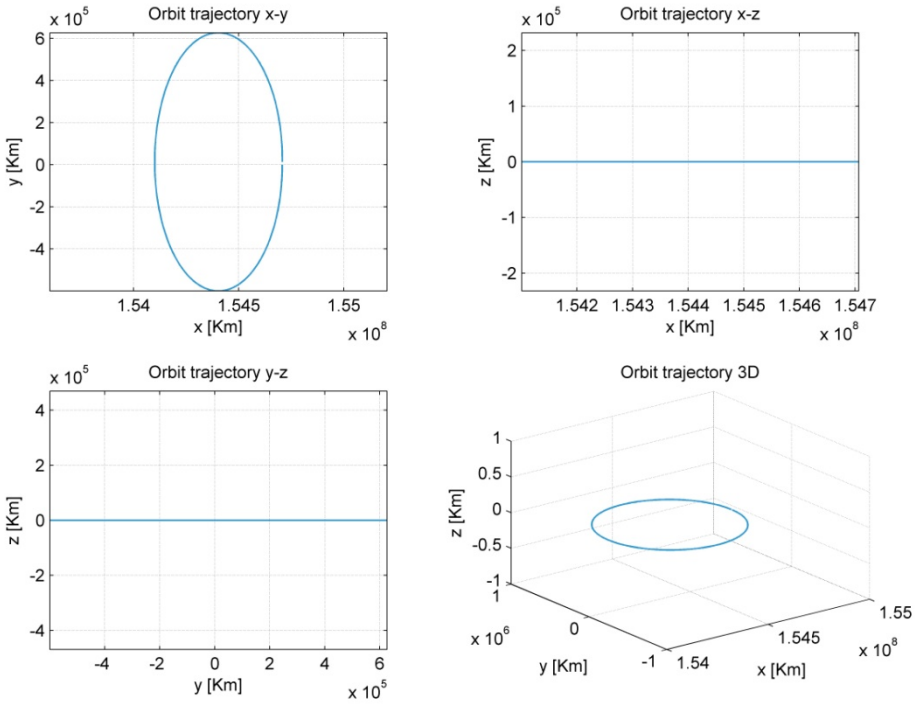

Figure 5.30 Analytical solution

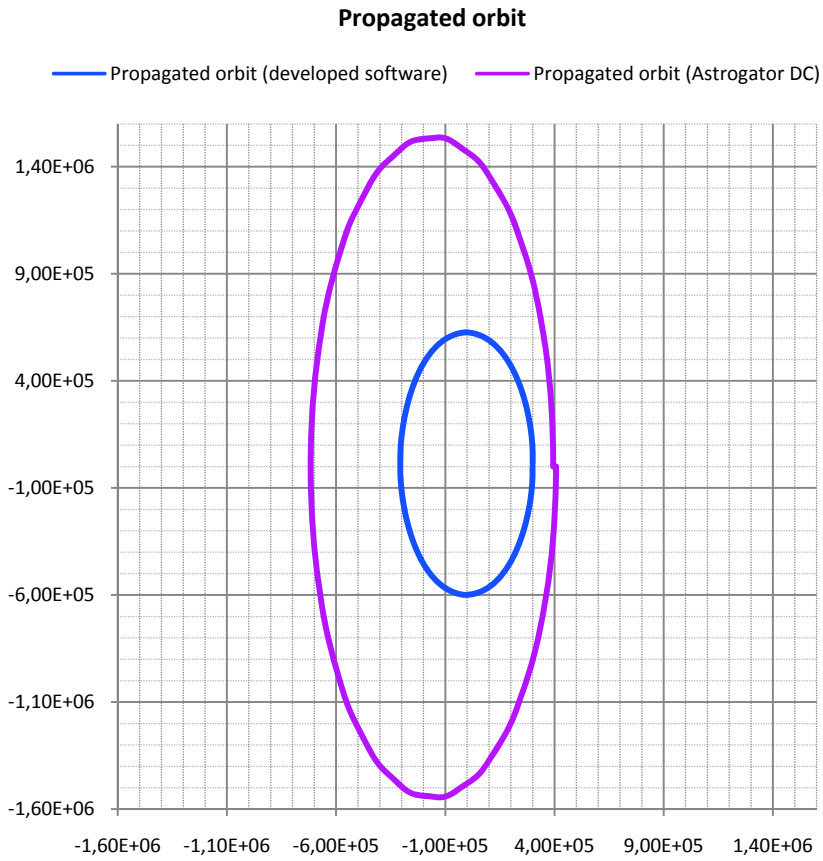

Figure 5.31 Propagated orbit (XY plane)

Till now nothing has been said about spacecraft fuel mass, but is evident that fuel consumption cannot be limited like at natural equilibrium point, where only a sort of station keeping maneuvers are needed. The graph in Figure 5.32Figure 5.32 Spacecraft mass & thrust history shows the total mass, fuel mass and thrust required versus time. For the simulation a dry mass of 200 kg and a 800 kg fuel mass were supposed.

Clearly the orbit can be maintained as long as a thrust can be developed. Thus it is important to verify when fuel run out. In the specific case propagating for 1060 days the fuel run out and the orbit isn't periodic anymore, this can be seen in Figure 5.33

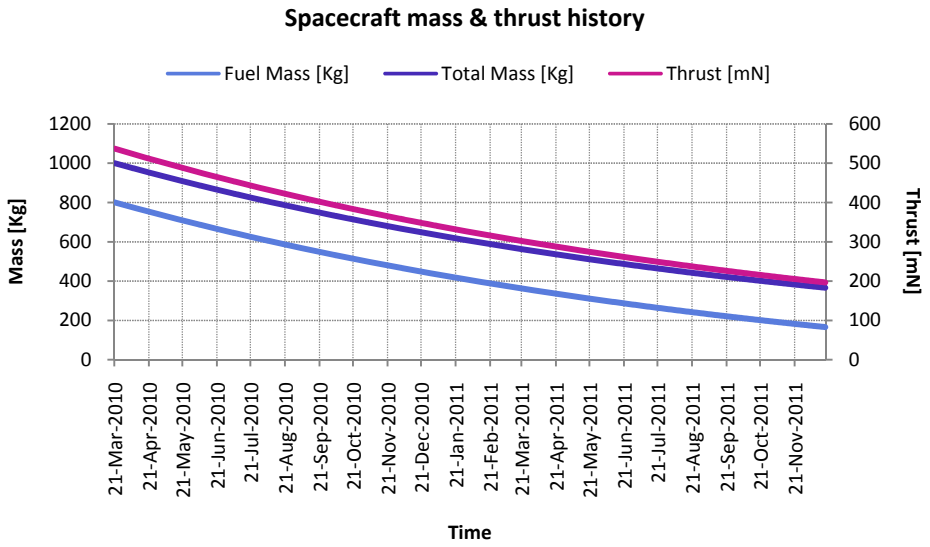

Figure 5.32 Spacecraft mass & thrust history

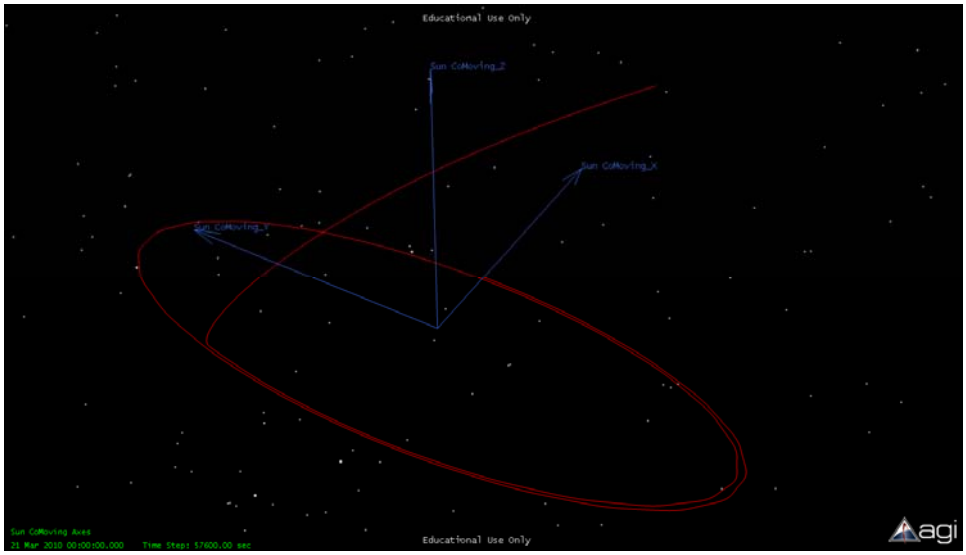

Figure 5.33 Spacecraft propagated for four XZ plane crossing, fuel ran out during this maneuver so the spacecraft leave its periodic orbit .

5.4.1 Conclusion

In this chapter regions of stability for AEPs, obtained with a constant control acceleration, were computed. It turns out that these stable regions are slightly farer from the less massive primary than L_1/L_2. Furthermore a spacecraft can achieve a periodic motion only in small sub-regions. Anyway, as demonstrated in §3.4, those limits are not so restrictive, since with the aid of variable control accelerations it is possible to obtain stable periodic motion also out of this regions. The main constraint is the continuous control acceleration, but as seen in §5.1.5, an ion engine or Hall effect thruster could be employed to develop such small continuous thrust.

The benchmarks have shown that the tool developed is able to give coherent results. Lastly, though with a specific example, it was shown how, starting from an output obtained from the tool developed and using it as input into software that is able to model the problem much better (STK), it is possible to achieve a better mission analysis.

6 Real missions: possible scenarios discussion

Few are the mission where satellites have flown around natural equilibrium points, and none have flown around AEPs* as stated in §2.1.1. Since the use of "active" control acceleration not only turns any point into an artificial equilibrium point but also increases the stable region and theoretically allows periodic motion, it is reasonable to assume that applications similar to those proposed for the natural equilibrium points can be foreseen for AEPs.

In this chapter natural and artificial equilibrium points are compared in order to determine the possible benefit and drawback of using AEPs instead of NEP. Lastly , scenarios considered worthy of interest will be proposed. These scenarios are treated as concepts and not analyzed in detail to be further investigated if needed.

6.1 Natural versus Artificial Equilibrium Points

Almost all space missions involving natural equilibrium points are about L_1 or L_2, this because L_1 in the Sun-Earth system is an ideal site for a solar observatory while L_2, as mentioned, is suitable for telescopes that need great thermal stability and also allow near 100% sky coverage since Sun, Earth and Moon are always behind it and locked in the same region. In the Earth-Moon system L_2 is a good location for a communication link to the back side of the moon. Is unlikely to find any use for the Sun-Earth L_3 point since it remains hidden behind the Sun at all times.
Since collinear points are unstable a periodic correction action is needed to keep a spacecraft nearby those points.
The triangular point (L_4/L_5) demonstrate better stability than the collinear point and are excellent places to observe space weather. With both the Sun and Earth in view, a spacecraft could track solar storms and watch them evolve as they move toward Earth. These positions have been also studied as possible sites for artificial space stations in the distant future, but a considerable constraint is the high energy needed to reach these

* AEPs are still now analyzed by a theoretical point of view

points (see §2.1.1 and pictures2.3). Since L_4 and L_5 are stable points, a natural object tends to librate about them, most remarkable examples are the "Trojans" and "Greek" asteroids located respectively in L5 and L4 of the Sun-Jupiter system. These asteroids moves on tadpole orbits. Also the first known "Trojan" of mars is Eureka , an asteroid captured from the asteroids belt.

At first glance, the major benefit of AEPs stays in that the region where spacecraft can be placed is much wider than that due to natural equilibrium points; furthermore AEPs may be made stable and periodic motion may be obtained by tuning the control; the evident drawback is that a control action must be supplied to maintain the orbit, and obviously the effort needed to perform this kind of control is significantly higher than that required to control a spacecraft near a natural equilibrium point. For example it has been shown in §5.1.5 that the thrust for Sun-Earth system is of the order of *0.4-0.7 N*, while for the Sun-Jupiter the thrust is of the order of *0.05-0.1 N*. Also the higher the mass of the spacecraft the higher is the thrust required.

Up to now the dimensions of periodic orbit about natural equilibrium points were very large, about 10^5 km of amplitudes, this is because to force two frequencies to be equal with the Lindstedt Poincarè method (18) there is a constrain on the minimum value that amplitudes can have. For example, Richardson (4) showed that in the Sun-Earth system, the minimum value of A_x for the motion about L_1 or L_2 is approximately 200˙000 km.
Table 6.1 show amplitudes values for past missions.

Theoretically there isn't such a constraint on AEP orbits amplitudes, but recalling the analysis results discussed in §4.1.2, a limit on amplitudes exists for this kid of orbits, and this limits is technological: no engine could perform a precise thrust control to keep the uncertainty within a acceptable range whenever amplitudes are small. Obviously this is true in the model adopted, improvement of that could lead to orbits with small amplitudes.

Table 6.1 Amplitudes values for past libration points missions (Sun-Earth system)

Mission	Location Type	Amplitudes (A_x, A_y, A_z) [km]
ISEE-3	L_1 Halo	175 000, 660 670, 120 000
WIND	L_1-Lissajous	10 000, 350 000, 250 000
SOHO	L_1-Lissajous	206 448, 666 672, 120 000
ACE	L_1-Lissajous	81 775, 264 071, 157 406
MAP	L_2-Lissajous	n/a , 264 000, 264 000
Genesis	L_1-Lissajous	25 000, 800 000, 250 000

It is clear that AEPs open a wide range of new opportunities for missions, having in mind some constraints.
In the following paragraph the effect of fuel consumption is analyzed.

6.1.1 Fuel consumption

Since orbiting about an AEP require a constant control acceleration, a continuum thrust generator is needed; as the thrust level are limited, either a low thrust engine or a solar sail may represent the practical solution; generally the thrust direction is not aligned with the Sun-Spacecraft line consequently the a good choice is a low thrust engine*. Fuel consumption become an important parameter for mission design. The amount of fuel expended directly depends on the required thrust level, the time of thrusting and the fuel mass flow rate.

Once the acceleration required to keep spacecraft in an artificial equilibrium point has been determined, the dry and fuel masses can be determined, given the total mass and time of flight.

To do this, engine data must be supplied and then the following computation could be performed:

* Actually an hybrid combination of low thrust engine and solar sail could be adopted (15)

Inital Data

$$\begin{cases} a_x, a_y, a_z \\ m_{tot} = m(0) \\ I_{sp} \\ g = 9.81 \ \dfrac{m}{s^2} \end{cases}$$

$$F_{(t_k)} = m_{(t_k)} \sqrt{\left(\left(a_{x(t_k)} \right)^2 + \left(a_{y(t_k)} \right)^2 + \left(a_{z(t_k)} \right)^2 \right)}$$

$$\dot{m}_{(t_k)} = \frac{F_{(t_k)}}{I_{sp} g}$$

$$m_{p(t_k)} = \dot{m}_{(t_k)} \cdot dt$$

$$m_{(t_{k+1})} = m_{(t_k)} - m_{p(t_k)}$$

$$m_{dry} = m_{tot} - \sum m_p$$

$$m_{fuel} = \sum m_p$$

The next graphs (Figure 6.1, Figure 6.2 and Figure 6.3) show the fuel mass required for a spacecraft of total mass of 1000 kg that orbits for 365 days making use of constant control acceleration. The engine I_{sp} is assumed to be 3000s, such a value can be provided by ion engine or high power Hall effect thruster*. The qualitative behavior of this pictures is the same as the thrust contours presented in Figure 5.5,Figure 5.11and Figure 5.15. The conclusion that can be made looking at all those pictures is that, for the same time of flight and total mass, the higher the initial thrust required the higher is the fuel mass needed. The analysis in §5.4, even if specific, presents a graph of the thrust and spacecraft masses versus time. The qualitative behavior shown in Figure 5.32 is expected for all AEPs obtained with constant control acceleration.

* For the Sun-Earth system or Earth-Moon, where thrust can reach value as high as 0.7-1.6 N an Hall effect thruster such BUSEK BHT-20K can be adopted, instead for Sun-Jupiter system where thrust are of order of 0.1 N engine like QuintiQ T6 gridded ion thruster can be used.

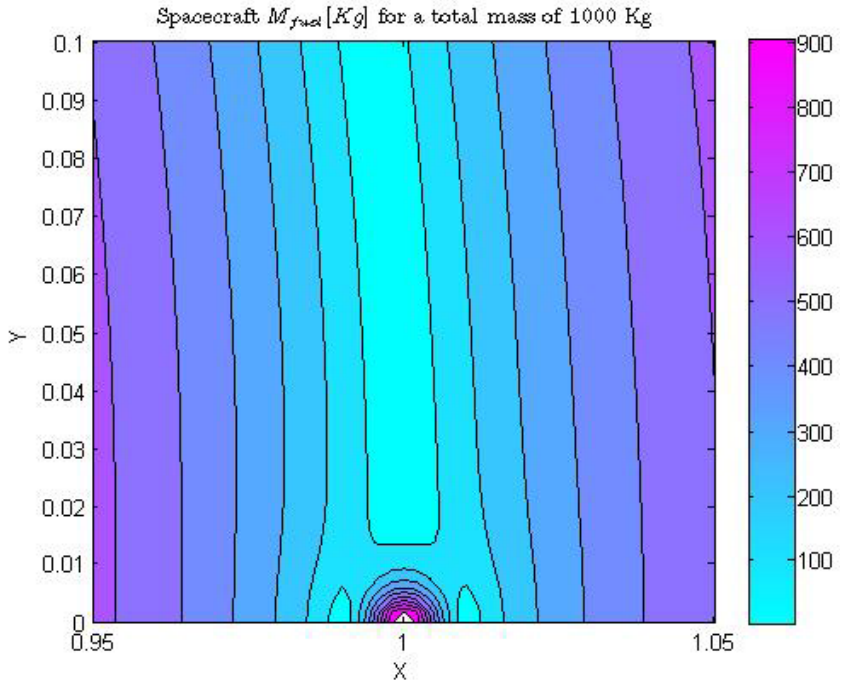

Figure 6.1 Sun-Earth system, fuel mass expended function of position (Mission time:365 days, Engine I_{sp}:3000s)

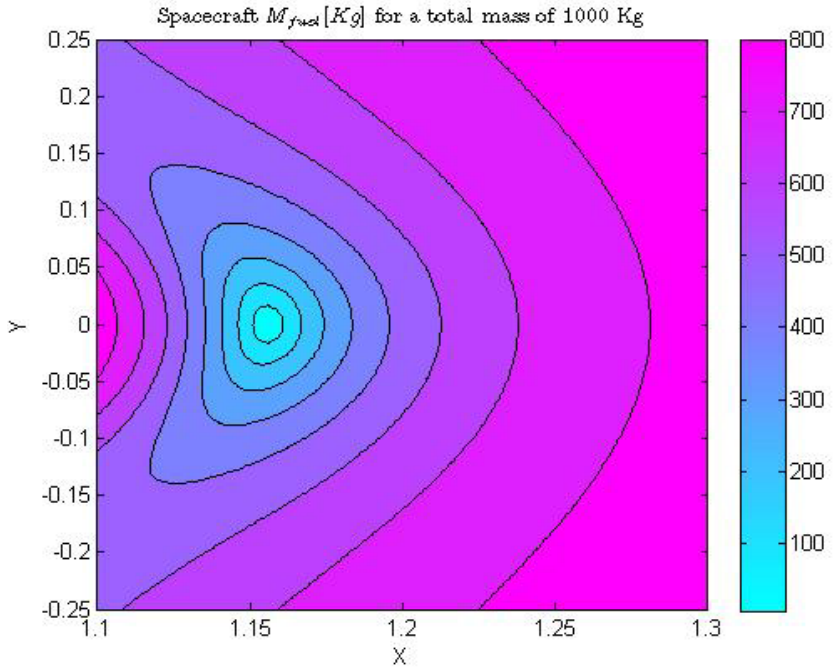

Figure 6.2 Earth-Moon system, fuel mass expended function of position (Mission time:365 days, Engine I_{sp}:3000s)

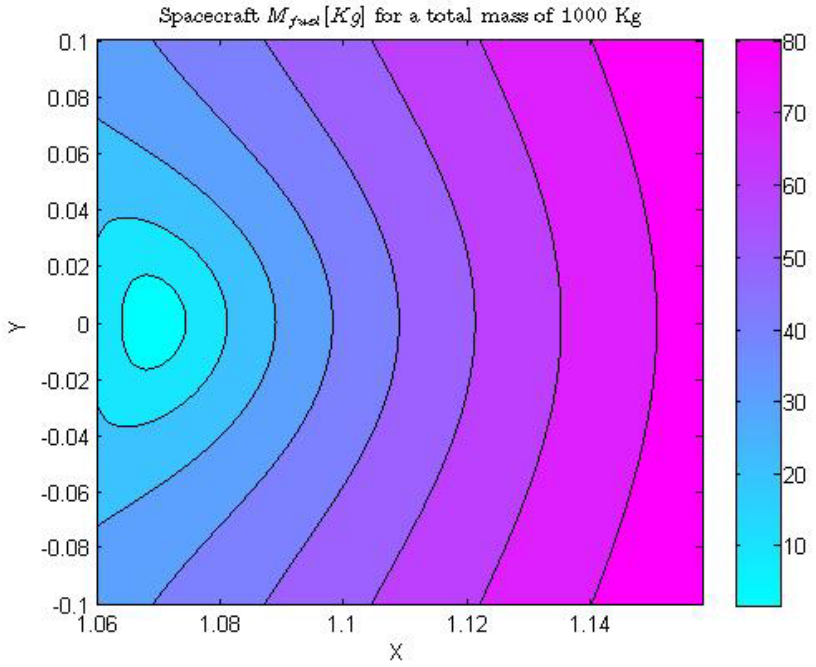

Figure 6.3 Sun-Jupiter system, fuel mass expended function of position (Mission time:365 days, Engine I_{sp}:3000s)

Those graphs (6.1, 6.2 and 6.3) highlight that while the fuel mass required is almost acceptable for Sun-Earth system, it is evident that for the Sun-Jupiter system the fuel consumption is so low that longer mission could also be possible. From the engine lifetime point of view, a typical gridded ion engine has lifetime of 10000 hours or more, that is more than 416 days of continuous thrust. Thus while for a mission in the Earth-Sun system only one or two engine are needed, for a Sun-Jupiter mission with three or four years of mission lifetime, many more engine must be used.

6.2 Possible scenarios

In the few next chapter some possible scenarios are considered, it is pointed out that, since AEP are still under study, no practical application were proposed till now, thus the following scenarios may not be the best applications for AEPs.
The mission analyzed are:

- Observation & ground communications for the less massive attractor
- Space observation
- Relay missions
- Mission on asteroids
- Formation Flying

6.3 Observation & ground communication missions of the less massive attractor

One possible type of missions is the study of the less massive planet surface. Observation mission can make use of optical or electromagnetic equipments. Since the distance between the spacecraft and the planet is larger than that of a satellite orbiting the planet itself and also since the type of track on the planet is bounded between two parallels, like in Figure 6.4, optical system may not be the best choice. A further possibility is to make use of ground penetrating radar (GPR) or Interferometric synthetic aperture radar (In SAR) or any other remote sensing tools that operate by electromagnetic waves. Moreover communication satellite could be set developed, used for mobile applications such as communications to ships, vehicles, planes; but even in this case it's probable that spacecraft on classical Keplerian orbit might work best for this type of applications.

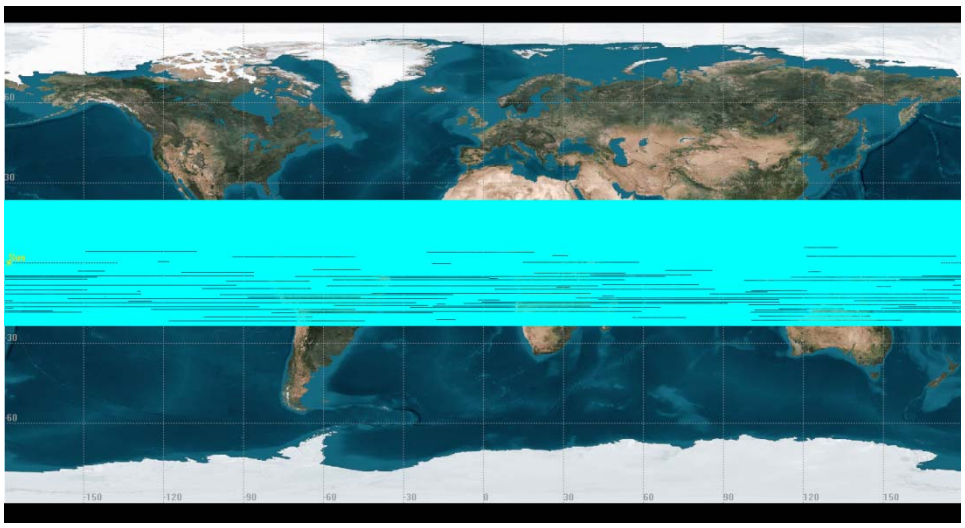

Figure 6.4 Example of ground track of a spacecraft orbiting around AEP computed by the simulation of §5.4

6.3.1 Distance from secondary

As far as surface observation missions are concerned, the minimum and maximum distance from the surface is an important information: it can be either imposed by the selected on board payload or drive the selection of the applicable scientific payloads. Figure 6.5 shows the minimum distance achievable for a stable but not necessarily periodic point, obtained with constant acceleration. Of course this gives only an idea of the minimum distance, actually with variable control acceleration stable and periodic points nearer to the secondary can be obtained.

As stated these are not the true minimum distances, because these values are obtained searching the space for stable points, and then was selected the point that is nearer to the secondary. Of course if a more refined grid is used to perform this search it's possible to find a lower value, but those reported in table are still a good approximation. Also once an orbit is achieved around one of this point, distance may vary in function of the orbit amplitude. However, since as stated in §4.1.1, the amplitude of the orbit cannot be too high, the variations of distance due to the amplitudes are small and have tiny effect on the values of the distances reported in Figure 6.5

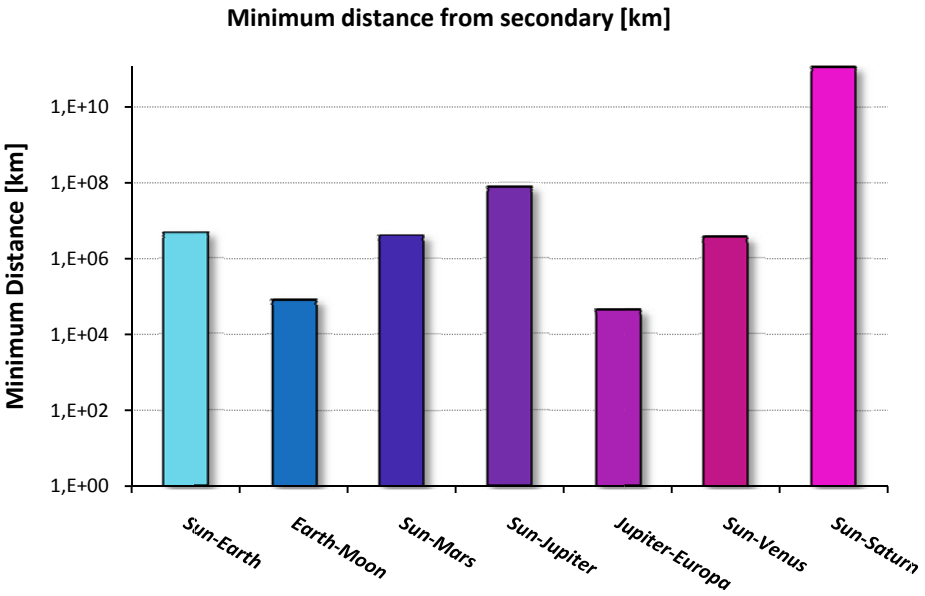

Figure 6.5 Minimum distance from the less massive primary

In order to better understand the advantages of using variable control acceleration let's make some example.

Consider the Sun-Earth system, the stable region in the plane x-y is shown in Figure 6.6, as can be seen in figure 6.7 the nearest point to the Earth, computed with a fine gird, that is stable and that allow periodic motion, obtained with constant control acceleration, is at . The distance of this point to the Earth is of .

If now a variable control acceleration is used, at a point of coordinates (the distance of this point to the Earth is) a periodic orbit can be generated.

Figure 6.8 shows analytic solution, Figure 6.9 show propagated orbit (four periods) and Figure 6.10 show the acceleration required versus time.

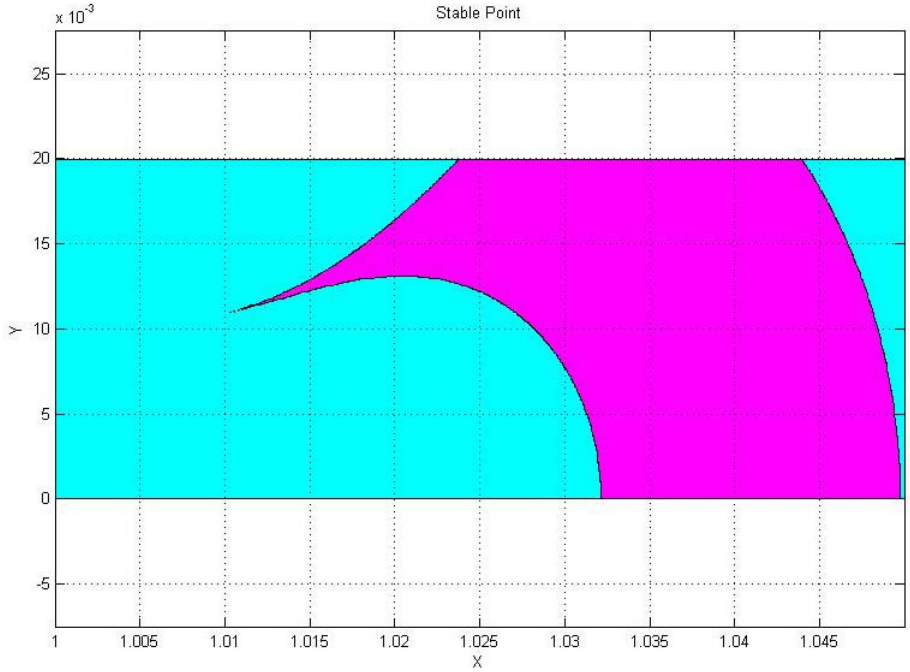

Figure 6.6 Stable point region (magenta), Sun-Earth system (z=0)

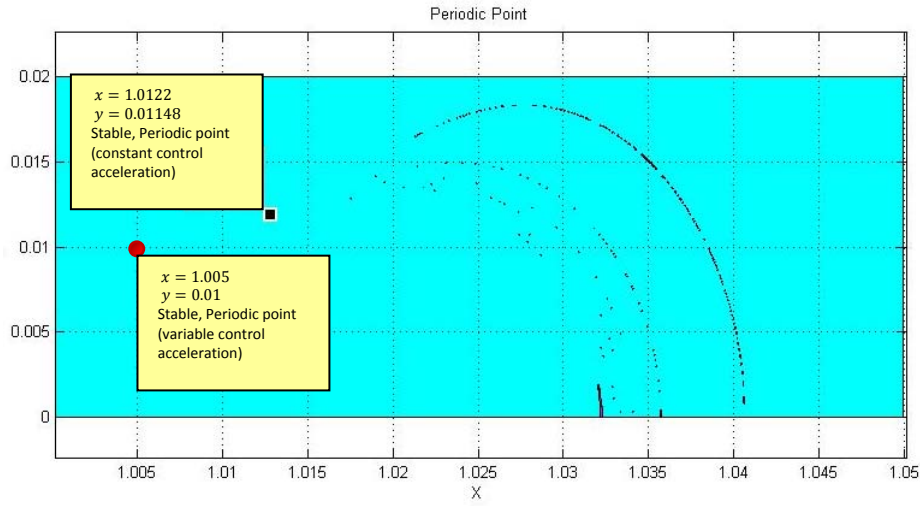

Figure 6.7 Periodic point region, Sun-Earth system (z=0)

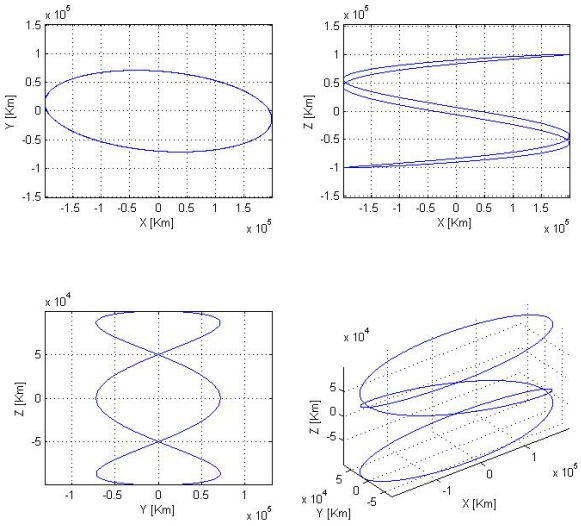

Figure 6.8 Analytical solution, $\delta_x = \delta_z = 1e5\ km,\ \delta_y = 0\ km$

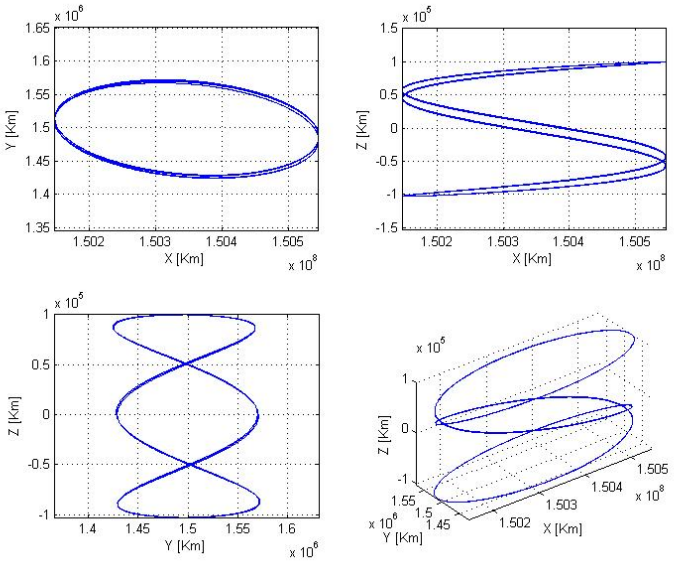

Figure 6.9 Numerical solution, $\delta_x = \delta_z = 1e5\ km,\ \delta_y = 0\ km$

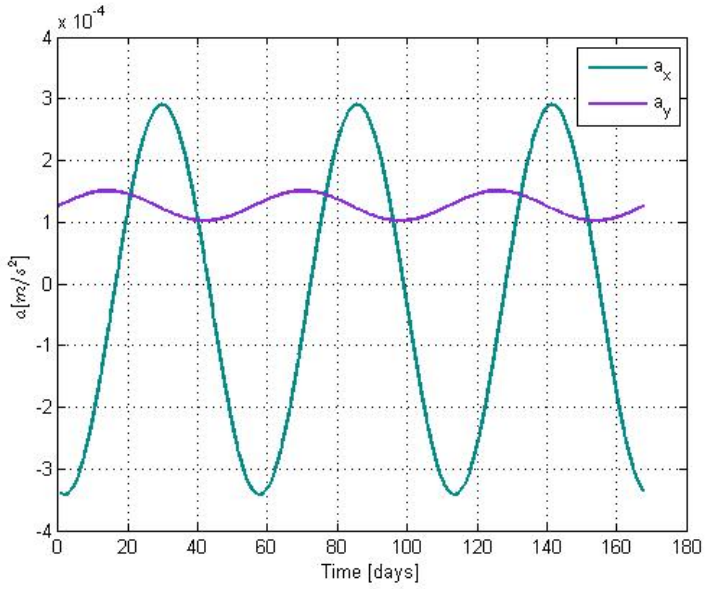

Figure 6.10 Acceleration profile

6.4 Space observation missions

As stated in §2.2, for space observation missions, L_2 in the Sun-Earth system is a favorable location because spacecraft obtain nearly an unobstructed view of the galaxy and also is unhindered by the atmospheric and geomagnetic disturbance. One possible application is to place a spacecraft in any point of the stable region, since Sun, Earth and Moon are locked in a fixed position with respect to the spacecraft, their influence on it is minimal, and the satellite still has almost 100% sky available for observations.
In principle, it could be possible to position the spacecraft anywhere in order to gain advantage of visibility at that specific point or communications.

Another possible application is the study of magnetic field in the Sun-Jupiter system, in this case the Jovian magnetosphere extend to approximately 80 Jovian radius, thus $\sim 56 \cdot 10^6\, km$, that is ~ 0.07in nondimensional units. Figure 6.11 shows this limits as blue line in the stability region. Is clear that L_2 is just inside the region, but if data are to be collected out of the line joining the two primaries, as before, variable

acceleration can be adopted in order to generate periodic orbit somewhere in the magnetotail zone.

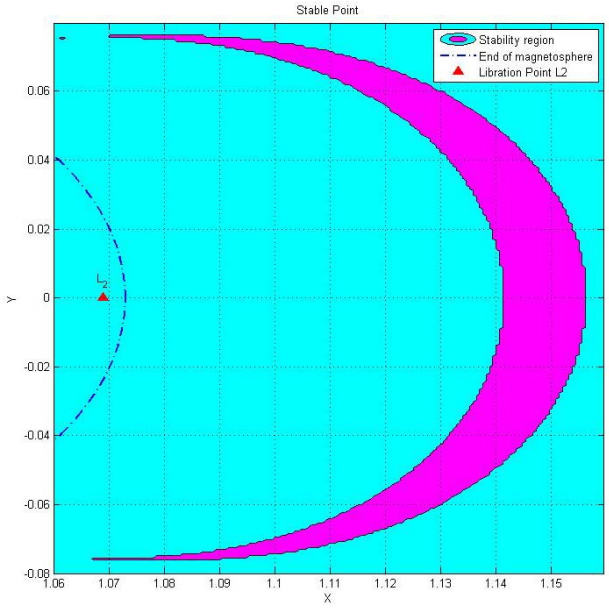

Figure 6.11 Stability region in the Sun-Jupiter System (magenta) and approximate end of Jovian magnetosphere (blue line)

A further application may also be the analysis of the solar wind near Mercury. Also there is the possibility to make observation of asteroids, positioning a spacecraft in the farthest region of the Sun-Mars problem.

6.5 Relay missions

One possible application is to use a spacecraft in an AEPs in order to build a communication network. Radio stations that cannot communicate directly due to distance, terrain or other difficulties sometimes use an intermediate radio relay station to relay the signals. AEPs can be exploited in order to relay data from any object on the surface and objects around the surface of a planet to other planet.

As an example, a rover located on a planet does not have a continuous line of sight with the Earth, thus can transmit data only during certain

time intervals, usually rovers are accompanied by a satellite that orbit the planet so that, in addition to making various types of analysis, the satellite sends the data to the Earth. However even the satellite does not have continuous line of sight. One possible use of AEPs is to place a satellite into a position from which it can always see the Earth, and operate as a relay between rover/satellite and Earth stations. The spacecraft can be placed on a large periodic orbit near L_2 , in this way the thrust required will be low and accordingly the fuel consumption will be tiny. Figure 6.12 and 6.13 shows the just mentioned configuration but, depending on the missions, many other architecture are available and AEPs allow the spacecraft to be positioned in a wider region than natural equilibrium points.

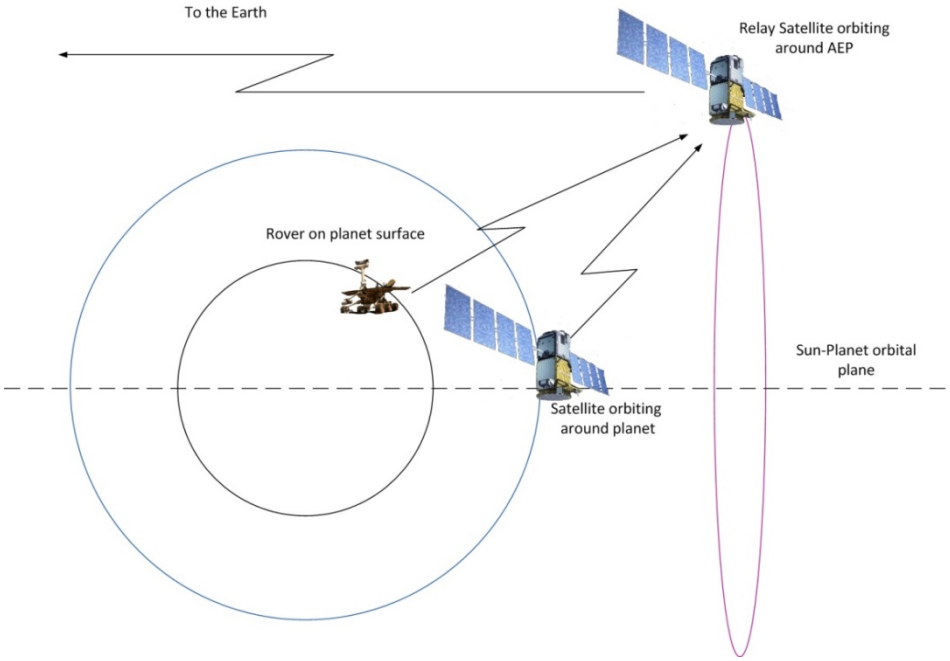

Figure 6.12 Relay satellite orbiting around AEP near L_2 (Top view x-y of synodic reference frame)

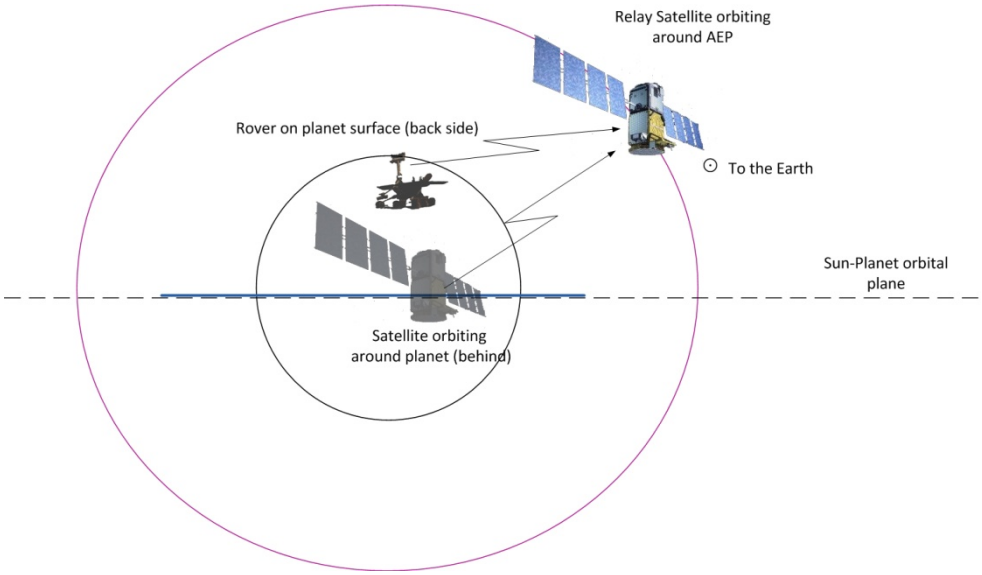

Figure 6.13 Relay satellite orbiting around AEP near L_2
(Front view y-z of synodic reference frame)

6.6 Missions on asteroids

A CRTBP can be obviously set up for Sun-asteroid systems too; the main feature of such system is that mass ratio is significantly low $O(10^{-10})$, therefore stable region are wider than that for Sun-planet systems; moreover the required thrust level for AEPs generation and control is smaller (order of $20 - 40\ mN$ §5.1.4).
For example the minimum distance in the Sun-Ceres system is about 1.7E6 km, that is the same order of magnitude in the Sun-Earth system but the thrust required is of the order of tens mN (as can be seen in Figure 5.17) while for the Sun-Earth system the thrust is one order of magnitude greater.

6.7 Formation flying missions

Spacecraft formation flying (SFF) has the potential to enhance imaging/interferometry missions by distributing mission task to many small spacecraft(20).

Formation flying near natural libration points is even more challenging with its own unique problems of stability, formation reconfiguration, high power consumption to maintain satellites relative positions and unstable characteristics of dynamics near collinear points.

The same things said for natural equilibrium points apply to AEPs.
One possible configurations is to put one or more small spacecrafts in a small periodic orbit near the ISS, so that tasks such as inspection of the station, or some kind of support can be achieved.

In Figure 6.14,Figure 6.15 and Figure 6.16 stable region, thrust contour and zones that allow periodic motion in the Earth-ISS system are shown. It is evident that a spacecraft on the y axis (shown in Figure 6.14 as yellow circle), would have low fuel consumption since the thrust required in that zone is limited $O(10 - 100\, mN)$.

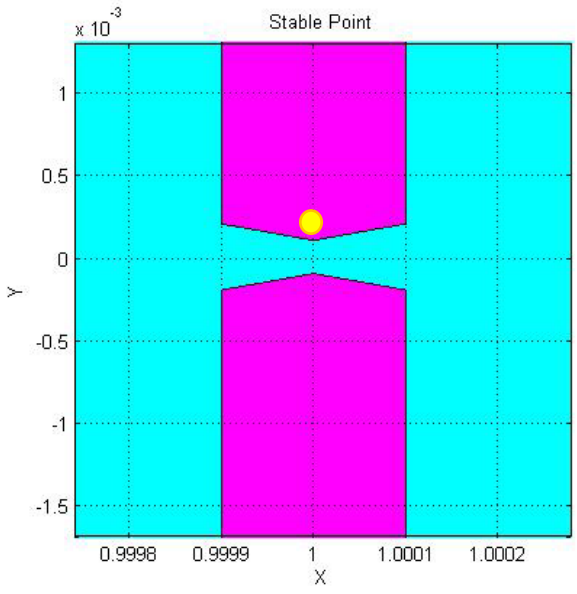

Figure 6.14 Stable region (magenta) in the Earth-ISS system, and a possible location for a spacecraft (yellow circle)

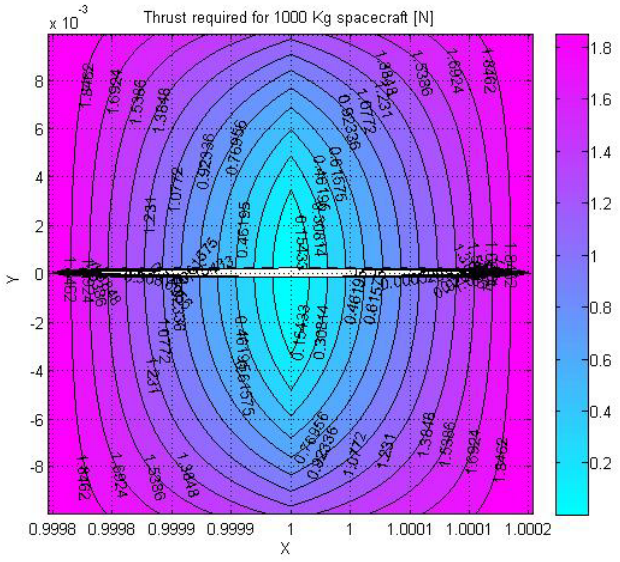

Figure 6.15 Thrust contour in the Earth-ISS system

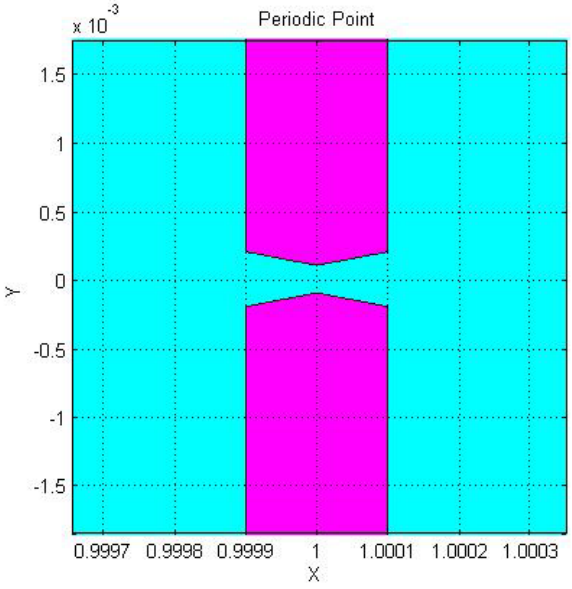

Figure 6.16 Regions that allow periodic motion (magenta) in the Earth-ISS system

A simple example of an application of this type is now reported.
Consider a point whose coordinates in the synodic frame are:

$x = 1$

$y = 0.003$

$z = 0$

Such a point will be at about 20 km from the station.

Amplitude should be small, but the model adopted prevent a correct solution with this kind of data. Anyway, in order to see which are the limitation a periodic orbit with $\delta_x = \delta_z = 5\ km$ and $\delta_y = km$ is chosen.

Analytic solution is shown in Figure 6.17.

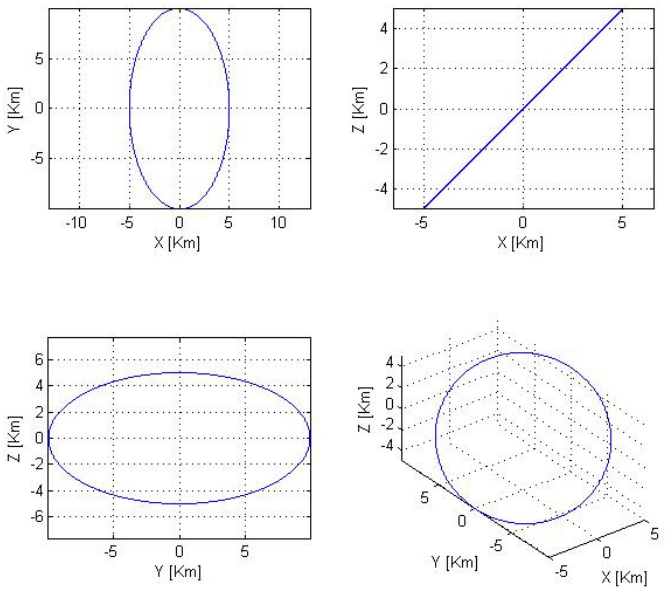

Figure 6.17 Analytic solution (Earth-ISS)

The numeric solution is obtained with assuming that the engine can provide a thrust with an accuracy of *0.1 mN*. Is clear that with such high accuracy a poor results are obtained, however form the thrust point of view, the maximum value of thrust is of about *36 mN* and, as Figure 6.19 shows, the fuel consumption is quite low.

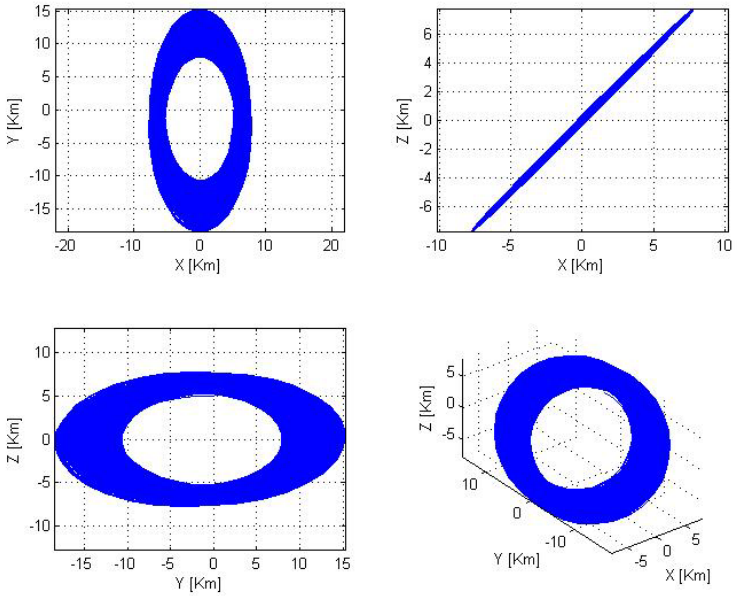

Figure 6.18 Numeric solution (Earth-ISS)

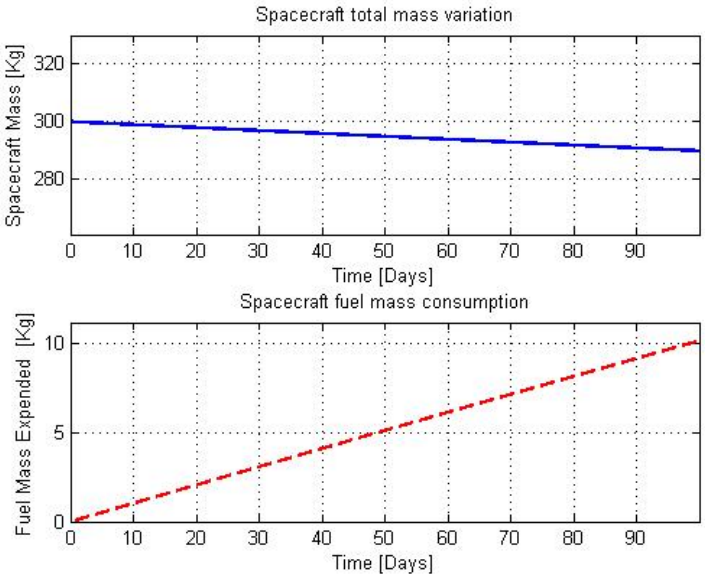

Figure 6.19 Mass versus time (Earth-ISS)

From this example is apparent that the main limit of the model adopted is the inability to generate periodic orbit with small amplitude. However,

if a more accurate model will be developed in the near future, it is possible that missions like the one just described can be realized.

7 Conclusions and future developments

The computation of AEP in the synodic frame of the CRTBP, was achieved with the aid of a control thrust. Analytical model for variable acceleration was also developed, but only for the specific case of AEPs that lie on the line joining the two primaries. The main limits of the model were identified.

Using constant control acceleration is possible to transform a non-equilibrium point into an artificial equilibrium point. On these points local stability of motion was analyzed by means of linearization of equations of motion. As seen, in areas where points are marginally stable and then oscillatory motion is allowed, it was possible to identify those points where the motion can also be periodic.

The behavior in presence of variable control acceleration was also analyzed, both analytically and numerically. The first approach was used to investigate in depth the case of AEPs that lie on the line joining the two primaries; this was done in order to verify that adding degrees of freedom to the problem could be exploited in order to generate stable periodic point even in region where this wouldn't normally be possible. Once this was proved, the more general problem where a generic point has to be turned into a stable, periodic AEP was addressed: a numeric procedure has been settled to identify a polynomial model for the variable acceleration needed to turn an unstable into a stable, periodic point.
A numerical optimization was used, but a posteriori analysis shows that thanks to the problem features, a different approach could be followed: the problem can be faced as a classical control problem where the eigenvalues must be assigned. Thus a pole placement technique could be employed. In this way the control would have been the fluctuation on the constant control acceleration applied.

The theoretical model adopted has two main limits of validity: orbits with large amplitudes cannot be correctly described because of the problem linearization; orbits must have large amplitudes, since for small amplitudes the uncertainty on thrust would be such that no actual engine could be employed.

With these limits in mind is however possible to develop detailed analysis, using the output obtained from the linearized model as input for a more accurate numerical model. As seen, since the problem exhibits extreme sensibility to various parameters, a very precise model of perturbations and high accuracy numerical integration is needed in order to obtain periodic orbit (§4.2).

In fact, following these devices it was possible to develop a more realistic mission design (even if still retaining some simplifications) with a commercial software (STK).

Another important aspect considered was the fuel consumption, and it was shown that missions near the Earth can last one or two years. For some other TBP such the Sun-Jupiter system, consumption are quite small and longer mission are possible*.

Some concept scenarios considered worthy of interest were treated, however it is hard to say if these kind of application can be truly useful, since a careful comparison among the alternatives (Classical Keplerian orbits or periodic orbits about natural equilibrium points) was not carried on.

In the next future the main feature to be investigated are the possibility of realizing periodic orbits with small amplitude. Also analytical model for variable control acceleration should be improved. A more efficient control approach to the variable acceleration may be developed. The analysis of the transfer trajectory to AEPs should be considered. Last, but not least, concrete applications of the theory should be investigated.

* It should noted anyway that for such system the transfer segment was not analyzed and it can heavily influences the mission lifetime.

References

1. *Low energy interplanetary transfers using invariant manifolds of L1,L2 and halo orbits.* **Lo, M.W. and Ross.** Monterey,California : s.n., 1998. Space Flight Mecanics Meeting.

2. *The Interplanetary Transport Network.* **Ross.** 3, 2006, Americanscientist, Vol. 94.

3. **K.C.Howell.** Three dimensional, periodic, 'halo' orbits. *Celestial Mechanics adn Dynamical Astronomy.* 1984, Vol. 32, 1.

4. **D.L.Richardson.** Analytic construction of periodic orbits about the collinear points. *Celestial Mechanics and Dynamical Astronomy.* 1980, Vol. 22, 3.

5. **R.W.Farquhar.** The control and use of libration-point". *NASA Technical Reports Server (NTRS), Document ID:19680021946.* [Online] 1968. http://naca.larc.nasa.gov/search.jsp.

6. *Solar Sail parking in the restricted three body system.* **C. McInees, A. McDonald, J. Simmons, E. McDonald.** 2, 1994, Jurnal of Guidance, Control and Dynamics, Vol. 17.

7. *Artificial Equilibrium Points in the Low-Thrust Restricted Three-Body Problem.* **M. Morimoto.** 5, 2007, Juranl of Guidance, Control and Dynamics, Vol. 30.

8. *Periodic orbits with low thrust propulsion in the restricted three body problem.* **Morimoto, M.** 5, 2006, Jurnal of Guidance, Control and Dynamics, Vol. 29.

9. *Artificial halo orbits for low-thrust propulsion spacecraft.* **C. McInnes, S.Baig.** 4, 2009, Celestial Mechanics and Dynamical Astronomy, Vol. 104.

10. **C.D., Murray and S.F., Dermott.** *Solar System Dynamics.* s.l. : Cambridge press, 1999.

11. **Curtis, H.D.** *Orbital Mechanics for Engineering Students.* s.l. : Elsevier, 2005.

12. **Hirsch, Morris W., Smale, Stephen and Devaney, Robert L.** *Differential Equations, Dynamical Systems & An Introduction to Chaos.* s.l. : Elsevier, 2004.

13. **Lawrence, J.D.** *A catalog of special plane curves.* s.l. : Dover, 1972.

14. **Quarteroni, Alfio, Sacco, Riccardo and Saleri, Fausto.** *Numerical mathematics.* s.l. : Springer, 2000.

15. *Artificial Three-Body Equilibria for Hybrid Low-Thrust Propulsion.* **McInnes, C. and Baig, S.** 6, 2008, Journal of Guidance, Control and Dynamics, Vol. 31.

16. *Periodic orbits with constant control acceleration in the restricted three body problem.* **Morimoto and Yamakawa.** 2008, The university Electro-Communications,Japan.
17. **Farquhar, R. W.** *Station-keeping in the vicinity of collinear libration points with an application to a lunar communications problem.* s.l. : Nasa Technical Reports server, 1966. Accession Number: 67A27543; Document ID: 19670048814; Report Number: AAS PAPER 66-132.
18. **Strogatz, S.** *Nonlinear Dynamics and Chaos.* s.l. : Westview press, 2000.
19. *Horseshoe periodic orbits in the restricted problem of three bodies for a sun-jupiter mass ratio.* **Taylor, D.B.** 1981, Astronomy and Astrophysics.
20. *Spacecraft formation flying near sun-earth L2 lagrange point: trajectory generation and adaptive output feedback control.* **Wong, Hong and Kapila, Vikram.** 2005, American Control Conference.
21. *Solar sail equilibiria in the elliptical restricted three body problem.* **C. R. Mc Innes, Hexi Baoyin.** 3, 2006, Journal of Guidance, Control and Dynamics, Vol. 29.
22. *Solar Sail Orbits at Artificial Sun-Earth Libration Points.* **McInnes, C. and Baoyin, Hexi.** 6, 2005, Journal of Guidance, Control and Dynamics, Vol. 28.
23. **Vallado, David A.** *Fundamentals of Astrodynamics and Applications.* s.l. : Microcosm Press, 2007.
24. **Mengali, Giovanni.** *Meccanica del volo spaziale.* s.l. : Edizioni Plus, 2001.
25. **Gòmez, G., et al.** *Dynamics and Mission Design Near Libration Points, Volume I : Fundamentals : The Case of Collinear Libration Points.* s.l. : World Scientific Publishing Company, 2001.
26. **Gòmez, G., et al.** *Dynamics and Mission Design Near Libration Points, Vol. III, Advanced Methods for Collinear Points.* s.l. : World Scientific Publishing Company , 2001.
27. **Gerard Gomez, Martin W. Lo, Josep J. Masdemont.** *Dynamics and Mission Design Near Libration Points, Vol. IV: Advanced Methods for Triangular Points.* s.l. : World Scientific Publishing Company , 2001.
28. **Gomez, G., et al.** *Libration Point Orbits and Applications.* s.l. : World Scientific Publishing Company, 2003.
29. **Gòmez, G., et al.** *Dynamics and Mission Design Near Libration Points, Vol. II: Fundamentals: The Case of Triangular Libration Points.* s.l. : World Scientific Publishing Company, 2001.